Universidade do Minho
Escola de Engenharia

Andreia Joana Costa Vasconcelos

Protein matrices for wound dressings

Novembro de 2010

Andreia Joana Costa Vasconcelos **Protein matrices for wound dressings**

UMinho | 2010

Universidade do Minho
Escola de Engenharia

Andreia Joana Costa Vasconcelos

Protein matrices for wound dressings

Tese de Doutoramento em Engenharia Têxtil

Trabalho efectuado sob a orientação do
Professor Doutor Artur Manuel Cavaco-Paulo

Novembro de 2010

To my father

The research described in this thesis was financially supported by Fundação para a Ciência e Tecnologia by means of a PhD grant (SFRH/BD/41603/2007).

Acknowledgments

It has been a long path during which I had the privilege of knowing and working with many talented people that directly and indirectly contributed to the accomplishment of the work described in this thesis. To them, I would like to deeply express my gratitude.

My first acknowledgments are made to my supervisor Prof. Artur Cavaco-Paulo, which gave me the privilege of being a part of a fantastic research group. For all the support, guidance and patience during these years and for the opportunity to grow up as a researcher attending several scientific meetings and conferences, where I had the opportunity to present my work. For the opportunity to participate in a European project (Lidwine) where I've met extraordinary people whose experience had enriched me.

To the Portuguese Foundation for Science and Technology for the financial support during my PhD.

To Dr. Giuliano Freddi that welcome me on Silk Research Institute, Milan, for the personal and professional growth that my staying there represented.
To Ilaria and Francesca from the same institute that open the doors of their homes to me.

To Drª Ana Paula Pêgo from INEB and, Drª Andreia Gomes from Minho University for all the help with the cellular assays.

I would like to express my sincere thanks to my former and present colleagues at the Laboratório de Investigação em Acabamentos, far all the help and good moments.

During these years I've known extraordinary people that I have the luck to call friends. I want to express my admiration and gratitude to them:
To Carla Joana, Zille and Florentina, the persons that help grow up as a person and as a researcher.

To Carla Manuela my sincere gratitude for all the help, especially during these last months, with the fast and efficient corrections of my thesis and, for all the suggestions that she has made during this work. Must of all I have to thank Carla Manuela for her friendship, her fantastic laugh that makes me feel so good and for being such as strong pillar in our lab.
To Raquel for her friendship, for helping me during the difficult periods with wise advices, for her sweetness. She has been my “safe place” during this last year. I wish that one day I can do for her the same that she’s being doing for me…

Finally to my family, my mother, Filomena, the person I admire the most. She is the greatest and best example I could wish for. The way my mother faces the problems and can rise through difficulties is an enormous inspiration for me. To my sisters, Sara and Rita and, to my nephew and niece, Afonso and Maria for the feeling of unconditional love.

Abstract

Protein matrices for wound dressings

Fibrous proteins such as silk fibroin (SF), keratin (K) and elastin (EL) are able to mimic the extracellular matrix (ECM) that allows their recognition under physiological conditions. The impressive mechanical properties, the environmental stability, in combination with their biocompatibility and control of morphology, provide an important basis to use these proteins in biomedical applications like protein-based wound dressings. Along time the concept of wound dressings has changed from the traditional dressings such as honey or natural fibres, used just to protect the wound from external factors, to the interactive dressings of the present. Wounds can be classified in acute that heal in the expected time frame, and chronic, which fail to heal because the orderly sequence of events is disrupted at one or more stages of the healing process. Moreover, chronic wound exudates contain high levels of tissue destructive proteolytic enzymes such as human neutrophil elastase (HNE) that need to be controlled for a proper healing.

The aim of this work is to exploit the self-assemble properties of silk fibroin, keratin and elastin for the development of new protein materials to be used as wound dressings: i) evaluation of the blending effect on the physical and chemical properties of the materials; ii) development of materials with different morphologies; iii) assessment of the cytocompatibility of the protein matrices; iv) ultimately, study the ability of the developed protein matrices as wound dressings through the use of human chronic wound exudate; v) use of innovative short peptide sequences that allow to target the control of high levels of HNE found on chronic wounds.

Chapter III reports the preparation of silk fibroin/keratin (SF/K) blend films by solvent casting evaporation. Two solvent systems, aqueous and acidic, were used for the preparation of films from fibroin and keratin extracted from the respective silk and wool fibres. The effect of solvent system used was studied by evaluating the physical-chemical properties of the resulting films. It was shown that SF and K are able to establish intermolecular interactions when mixed and, that the mechanical properties and the biological degradation can be tuned by the blend composition.

In Chapter IV, SF/K films were further used to serve as a platform for the release of HNE inhibitors peptides. Bowman-Birk inhibitor (BBI) based peptide was incorporated onto the SF/K films that were consequently incubated with porcine pancreatic elastase (PPE) as a model for HNE, to monitor the decrease in activity. The results indicated that swelling properties, degradation and release rates are dependent on the amount of keratin present

in the blend. Furthermore, no cytotoxicity was observed in the presence of mouse fibroblasts, which makes these SF/K films suitable candidates for interactive wound dressings with a specific goal – controlling high levels of HNE.

The next step of the work, Chapter V, reports for the first time blends of silk fibroin with elastin (SF/EL) for the production of scaffolds. These were prepared by lyophilization technique and crosslinked with a natural and low toxic agent, genipin. The crosslink allows the control of the scaffolds morphology, such as pore size and porosity, which in turns, modulates the *ex vivo* degradation rates, by a human chronic wound exudate, and the release rates of model compounds. In addition, no cytotoxicity was observed for SF/EL samples, with and without genipin, by human skin fibroblasts. Thus, the high porosity observed for SF/EL scaffolds, allowing the growth and cellular attachment, together with their biocompatibility provide fitting characteristics for wound dressings.

Chapter VI, describes the design of two elastase inhibitors peptides based on the reactive site-loop of the BBI protein in order to control the high levels HNE. To a known peptide sequence, modifications were made at both N- and C-terminal. Inhibition kinetics analysis indicated that these peptides are competitive inhibitors for HNE and PPE and, that the inhibitory potency can be regulated by the introduced modifications. Additionally, these peptides showed no toxicity with human skin fibroblasts and, were also effective in reducing the HNE activity found in a human chronic wound exudate, which allow them to be applied to those wounds.

The motivation for this thesis was to combine the excellent properties of silk fibroin with other proteins. Blending allows modulating the physical-chemical properties of the resulting materials such as mechanical strength, swelling, morphology, degradation and release rates. Silk fibroin is widely characterized in the literature for the production of biomaterials, but this work is the first that successfully evaluates the blends silk fibroin/keratin (SF/K) and silk fibroin/elastin (SF/EL) for their application as wound dressings.

Resumo

Matrizes proteicas para compressas de feridas

Proteínas fibrosas como a fibroína da seda, a queratina e a elastina têm a vantagem de conseguir imitar a matriz extracelular, permitindo o seu reconhecimento em condições fisiológicas. As excelentes propriedades mecânicas destas proteínas, a estabilidade química juntamente com a biocompatibilidade e controlo da morfologia, são importantes pressupostos para o uso destas proteínas em aplicações biomédicas. Um exemplo é o tratamento de feridas com compressas baseadas nestas proteínas. As compressas usadas nas feridas sofreram grandes mudanças ao longo do tempo, partindo das tradicionais baseadas em mel e fibras naturais, que eram usadas apenas para cobrir e proteger as feridas de factores externos, até às compressas interactivas do presente. As feridas podem ser classificadas em agudas, que curam no tempo previsto e crónicas, que não cicatrizam porque o processo de cura é interrompido. Estas feridas podem ainda ser diferenciadas pelo tipo de exudado que produzem. Nas feridas crónicas, o exudado contém níveis elevados de enzimas proteolíticas como a elastase humana dos neutrófilos (HNE) e as metaloproteases de matriz (MMP), que precisam de ser controlados para um melhor processo de cicatrização.

O objectivo deste trabalho é explorar as excelentes propriedades da fibroína, queratina e elastina para o desenvolvimento de novos materiais proteícos para serem usados como compressas. Para tal estudou-se: i) avaliação do efeito das misturas nas propriedades físicas e químicas dos materiais; ii) desenvolvimento de materiais com diferentes morfologias; iii) avaliação da toxicidade dos materiais; iv) avaliação das propriedades dos materiais desenvolvidos usando um exudado obtido de feridas crónicas; v) desenvolvimento de péptidos inibidores para controlar os elevados níveis de HNE nas feridas crónicas.

No Capítulo III é descrita a preparação de membranas baseadas na mistura fibroína e queratina (SF/K) por evaporação de solvente. Foram utilizados dois sistemas de solventes, aquoso e ácido, para a preparação dos filmes a partir da fibroína e queratina extraídas das respectivas fibras têxteis, seda e lã. Estudou-se o efeito dos solventes usados nas propriedades físico-químicas das membranas resultantes. Verificou-se que a fibroína e a queratina estabelecem interacções intermoleculares e, as propriedades mecânicas e a degradação podem ser moldadas através da composição da mistura.

No Capítulo IV, as membranas desenvolvidas foram posteriormente utilizadas para a libertação de inibidores da elastase. Péptidos baseados na proteína inibidora Bowman-Birk (BBI) foram incorporados nas membranas de fibroína e queratina verificando-se que

após incubação com a elastase há uma diminuição da actividade da mesma. Os resultados demonstram que as propriedades de inchamento, degradação e libertação dependem da quantidade de queratina presente na mistura. Adicionalmente, os materiais não apresentam toxicidade na presença de fibroblastos de ratinho. Os resultados indicam que estas membranas são candidatas adequados para o uso em compressas interactivas com uma actividade específica – controlar os elevados níveis de HNE.

O próximo passo do trabalho, Capítulo V, reporta pela primeira vez, o desenvolvimento de estruturas esponjosas baseadas na mistura de fibroína e elastina (SF/EL). Estes materiais foram preparados por liofilização e fixados com um agente de fixação natural e de baixa toxicidade, a genipina. Este passo de fixação permite controlar a morfologia dos materiais como o tamanho dos poros e porosidade, que têm influência directa na degradação pelo exudado e na libertação de compostos modelo. Observou-se também, que as estruturas esponjosas não apresentam toxicidade para fibroblastos humanos de pele, mesmo depois da fixação com genipina. Consequentemente, a biocompatibilidade demonstrada juntamente com a porosidade observada nestes materiais, que permitem a adesão e crescimento de células, são características importantes para o uso destes em compressas para feridas.

O Capítulo VI descreve o desenvolvimento de dois péptidos inibidores da elastase baseados no centro activo da proteína BBI de forma a controlar os elevados níveis de HNE presentes nas feridas crónicas. Foram introduzidas modificações nos terminais C e N de uma sequência conhecida. Estudos cinéticos de inibição indicam que estes péptidos são inibidores competitivos para a elastase de diferentes fontes, humana e porcina, e que a capacidade inibitória depende das modificações introduzidas. Adicionalmente, os péptidos não são tóxicos na presença de fibroblastos humanos de pele sendo eficazes na redução da actividade da elastase presente num exudado de uma ferida crónica. Estes resultados indicam que os péptidos desenvolvidos podem ser usados no tratamento das mesmas.

A motivação deste trabalho partiu das excelentes propriedades da fibroína, queratina e elastina. O desenvolvimento de novos materiais baseados em misturas destas proteínas permite moldar as propriedades finais como a força mecânica, inchamento, morfologia, degradação e libertação de compostos. O uso da fibroína em biomateriais está vastamente descrito na literatura. Contudo, este trabalho descreve pela primeira vez, com sucesso, o uso das misturas fibroína/queratina e fibroína/elastina para a sua aplicação em compressas para feridas.

Table of contents

List of abbreviations

2-D - Two-dimensional

2-Me - 2-mercaptoethanol

3-D - Three-dimensional

∆H - Enthalpy variation

µg - Micrograms

µL - Microliters

α_1-PI - α_1-Protease inhibitor

$t_{1/2}$ - Half-life time of an enzyme

A - Alanine

$A_{C=O}$ - Area of C=O stretching

AFM - Atomic Force Microscopy

Ala - Alanine

ALP - Alkaline phosphatase

A_{N-H} - Area of N-H bending

ASCs - Adipose-derived stem cells

ATR - Attenuated total reflectance spectroscopy

ATCC - American Type Culture Collection

Asp - Aspartic acid

Arg - Arginine

***B. mori* -** *Bombyx mori*

BBI - Bowman-Birk inhibitors

BMP-2 - Bone morphogenetic protein-2

CAM - Chorioallantoic membrane

CG - Cathepsin G

CM/PL - Compression-molded/particulate leaching

CS - Chondroitin sulphate

Cys - Cysteine

DAPI - 4,6-diamidino-2-phenylindole

DMEM - Dulbecco's Modified Eagle's Medium

DMSO - Dimethylsulfoxide

DNA - Deoxyribonucleic acid

Dox - Doxorubicin

DSC - Differential scanning calorimetry

DTT – D,L-Dithiothreitol

ECACC - European Collection of Cell Cultures

ECM - Extracellular matrix

EDTA - Ethylenediaminetetraacetic acid

EGF - Epidermal growth factors

EGDE - Ethylene glycol diglycidyl ether

ELPs - Elastin-like polymers

EL - Elastin

ESI - Electrospray Ionization

F-actin - Filamentous actin

FBS - Fetal bovine serum

FITC-BSA - Fluorescein isothiocyanate-Bovine serum albumin

FT-IR - Fourier transform infrared

G – Glycine

GAGs - Glycosaminoglycans

GDE - Glycerol diglycidyl ether

GE - Genipin

Glu - Glutamic acid

Gly - Glycine

HA - Hyaluronic acid

HFIP - 1,1,1,3,3,3-hexafluoro-2-propanol

HGTPs - High glycine-tyrosine proteins

His - Histidine

hMSCs - Human mesenchymal stem cells

HNE - Human neutrophil elastase

HPLC - High performance liquid chromatography

HRP - Horseradish peroxidase

HSPs - High sulfur proteins

HT_{50} - Half healing time

IFPs - Intermediate filament proteins

IGF-I - Insulin growth factor I

IC_{50} - Half maximal inhibitory concentration

Ile - Isoleucine

K - Keratin

LbL - Layer-by-layer

LCST - Lower critical solution temperature

LDV - Leucine-aspartic acid-valine

Leu - Leucine

Lys - Lysine

MEFs - Murine embryonic fibroblasts cells

Met - Methionine

mM - Milimolar

MMPs - Metalloproteinases

MMP-9 - Gelatinase

MNEI - Monocyte/neutrophil elastase inhibitor

MTS-3-(4,5-dimethylthiazol-2-yl)-5-(3-carboxymethoxyphenyl)-2-(4-sulfophenyl)-2H-tetrazolium

NGF - Nerve growth factor

Nle – Norleucine

ORC - Oxidized regenerated cellulose

PA6 - Polyamide 6

PBS - Phosphate buffered saline

PCU - Poly(carbonate)-urethane

PDB - Protein data bank

PDLLA - Poly(D,L-lactic acid

PEG - Polyethylene glycol

PEO - Poly(ethylene oxide)

PET - Poly(ethylene glycol terephthalate

pHA - Polarized hydroxyapatite

PHEMA - Poly 2-hydroxyethylmethacrylate

Phe - Phenylalanine

PI9 - Protease inhibitor 9

PLA - Poly(lactic acid)

PLGA - Poly(lactide-co-glycolic acid)

PMN - Polymorphonuclear elastase

PPE - Porcine pancreatic elastase

Pro - Proline

PS - Penicillin/Streptomycin

PTH - Parathyroid hormone

PU - Polyurethane

PVA - Polyvinyl alcohol

RCL - Reactive centre loop

RFU - Relative fluorescence units

RGD - Arginine-glycine-aspartic acid

SD - Standard deviation

SDS - Sodium dodecyl sulfate

Ser - Serine

SEM - Scanning electron microscopy

SF - Silk fibroin

SELPs - Silk-elastin like polymers

SLPI - Secretory leukocyte protease inhibitor

Suc-(Ala)$_3$-*p*NA - Succinyl-Ala-Ala-ala-*p*-nitroanilide

TCPS - Tissue culture polystyrene

Thr - Threonine

Tyr - Tyrosine

TCA - Thricloroacetic acid

Tg - Glass transition temperature

UHSPs - Ultra-high sulfur proteins

uPA - Urokinase-type plasminogen activator

UV - Ultra-violet

Val – Valine

List of figures

List of tables

List of equations

Introduction to the thesis format

This thesis is divided into seven chapters, with four of them being experimental research. According to a philosophy that has been implemented in our laboratory, the thesis format is based on published or submitted papers, including the introduction chapter. The contents of each chapter are summarized below.

Chapter I

The first chapter of this thesis is based on a review paper and presents a comprehensive overview on the novel protein-based biomaterials based on silk fibroin, keratin and elastin. Their physical, chemical and biological properties are discussed for their application on the context of wound dressing materials. The type of wounds and wound healing process are also reviewed.

Chapter II

Chapter II describes the materials and methods used along the work. The main objective was to complement the information given in each of the following experimental chapters.

Chapter III to VI

The chapters included within this section are based on the series of related papers that resulted from research work already published or submitted for publication.

Chapter III describes the development of silk fibroin/keratin films and their physical-chemical characterization.

Chapter IV reports the application of the silk fibroin/keratin films as platforms for the release of elastase inhibitors.

Chapter V illustrates the development of new scaffolds based on silk fibroin and elastin and their application as wound dressing materials.

Chapter VI describes the design of new elastase inhibitors and the type of inhibition mechanism.

Chapter VII

This thesis ends with Chapter VII, which is the summary and conclusions of the research work under the scope of this thesis.

CHAPTER I

Fibrous proteins-based wound dressings

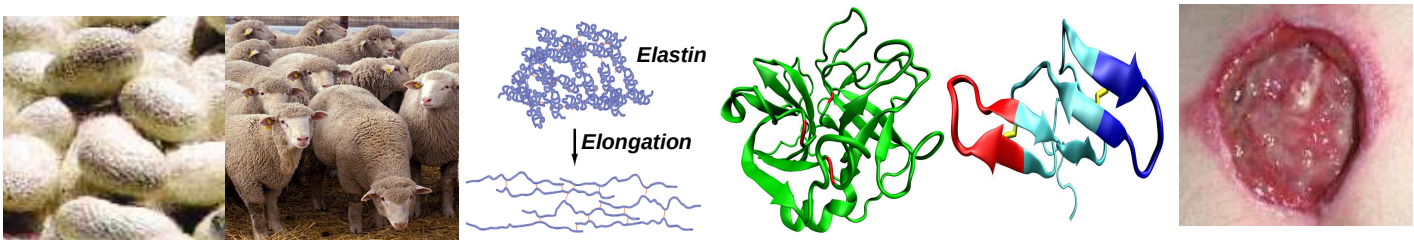

CHAPTER I

Fibrous protein-based wound dressings: a review

Abstract

Wound dressings have experienced continuous and significant changes over the years based on the knowledge of the biochemical events associated with chronic wounds. The development goes from natural materials used to just cover and conceal the wound, to interactive materials that can facilitate the healing process addressing specific issues in non healing wounds.

Recently the wound dressing research is focusing on the replacement of synthetic polymers by natural protein materials to delivery bioactive agents to the wounds. This review provides an overview on the novel protein-based wound dressings such as silk fibroin keratin and elastin. The processing methods, physical, chemical and biological properties of these biomaterials will be discussed. The different types of wounds and the effective parameters of healing process will be reviewed. A special attention will be given to human neutrophil elastase (HNE), a destructive proteolytic enzyme present in a chronic wound environment.

This chapter is based on the following publication: **Andreia Vasconcelos**, & Artur Cavaco-Paulo, Protein-based wound dressings: a review, *Submitted*

---

1. Introduction

Fibrous proteins such as silk fibroin, keratin and elastin are characterized by high mechanical strength and represent architectural functions in nature. They often possess relatively homogeneous secondary structures via self-assembly. The ability of these proteins to self-assemble into various physical states was exploited for the development of new biomaterials. These have shown to undergo materials with improved mechanical strength, control of morphology and surface modifications options, allowing their application in controlled delivery systems and tissue engineering. Furthermore, wounds treated with these materials have shown to promote the healing by enhanced cellular proliferation, growth and differentiation and, reduced inflammation when applied to *in vivo* models.

1.1. Silk fibroin-structure and properties

Silks are naturally occurring protein polymers produced by a wide variety of insects and spiders [1-3]. The diverse functions of silks range from web construction and prey capture (spider webs), safety lines (draglines) to reproduction (cocoons) [4-6]. Silk in its natural form is composed by a filament core protein, silk fibroin, and a glue-like coating consisting of sericin proteins.
The most widely studied silks are cocoon silk from the silkworm *Bombyx mori* and dragline silk from the spider *Nephila clavipes* [3, 7]. Silk fibroins from these species are characterized as natural block copolymers composed of hydrophobic blocks with highly preserved repetitive sequences consisting of short side-chains amino acids such as glycine and alanine and, hydrophilic blocks with more complex sequences that consist of larger side-chain as well as charged amino acids [4, 8]. The hydrophobic blocks tend to form β-sheet crystals through hydrogen bonding and hydrophobic interactions which are the basis for the high tensile strength of silk fibroins [9, 10]. These ordered hydrophobic blocks combine with the less ordered hydrophilic blocks to give elasticity and toughness of silk fibroin [3, 11]. In general, silks represent a unique family of structural proteins that are biocompatible, degradable and mechanically superior, are amenable to

aqueous or organic solvent processing and can be chemically or biologically modified to suit a wide range of biomedical applications.

Silk fibers from the domesticated silkworm *B. mori* are 10-25 µm in diameter and consist of two proteins: a light chain (≈ 26 kDa) and a heavy chain (≈ 390 kDa) which are present in a 1:1 ratio and are linked by a single disulfide bond that holds the fibroin together [12]. These proteins are coated with a family of hydrophilic proteins, sericin (20-310 kDa) which counts for 25% of the silk cocoons mass [2, 12-14]. The amino acid composition of silk fibroin from *B. mori* consists mainly of glycine (Gly) (44%), alanine (Ala) (29%) and serine (Ser) (11%) [15]. The crystalline domains in the fibers consists of Gly-X repeats, with X being Ala, Ser, threonine (Thr) and valine (Val) [16].

In the solid state, silk fibroin can assume two polymorphs including the glandular state prior to crystallization/spinning (silk I) and, the spin silk state which consist of the β-sheet secondary structure (silk II) [2, 7, 17]. The silk I structure is water soluble and, upon exposure to heat, physical spinning and organic solvents easily converts to silk II structure [18]. The β-sheet structures (silk II) are asymmetrical with one side occupied by hydrogen side chains from glycine, and the other occupied by the methyl side chains from the alanine that populates the hydrophobic domains. The β-sheets are arranged so that the methyl groups and hydrogen groups of opposing sheets interact to form the intersheet stacking in the crystals (Figure 1.1). Strong hydrogen bonds (inter- and intra-chain) and van der Waals interactions generate a structure that is thermodynamically stable [12, 19]. The silk II is water insoluble as well in several solvents including mild acid and alkaline conditions and several chaotropes. For a better elucidation of readers a resume of the main structural properties of the studied proteins will be provided (Table 1.1.).

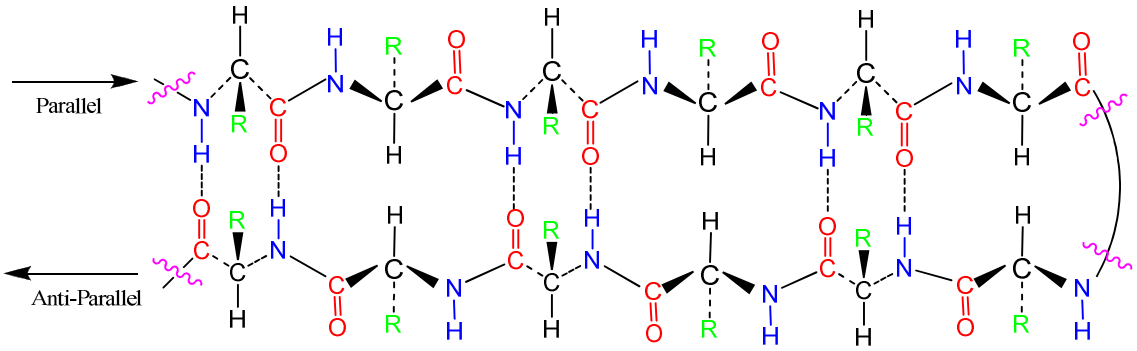

Figure 1.1. Silk fibroin β-sheet crystals.

1.1.1. Silk fibroin-based biomaterials

Silk fibers from *B. mori* have been primarily used in biomedical applications as sutures [20] and, during decades of use, silk fibers proven to be effective in many clinical applications. Nevertheless, immunological reactions observed to virgin silk suture have been attributed to the sericin protein [21]. It has been showed that sericin is a potential allergen causing a type I allergic reaction [22, 23]. In this way, removal of sericin from silk is necessary to prepare non-allergic and non-cytotoxic silk-based materials. However, a recent study using sericin/gelatin blends for the fabrication of films and sponges, reported cytocompatibility using feline fibroblasts cells and, low immunogenicity [24].

Methods to extract and regenerate silk fibroin have been developed. The studies that will be described wherein report the use of sodium carbonate (Na_2CO_3, boiling, 60 min) and autoclaving (120 ℃, 30 min) for the removal of sericin. The most common and used method for the extraction of fibroin from degummed (without sericin) silk fibers is dissolution in a concentrated solution of lithium bromide (LiBr 9 M, 60 ℃, 4 h) [25-50]. A ternary solvent system of calcium chloride/ethanol/water ($CaCl_2$-CH_3CH_2OH-H_2O, 80 ℃, 2 h) in a 1:2:8 molar ratio had also been used by some authors [36, 51-59]. Deriving from these methods, regenerated fibroin can be further dissolved in 1,1,1,3,3,3-hexafluoro-2-propanol (HFIP, $(CF_3)_2CHOH$) [53, 60-62] and formic acid (HCOOH) [15, 51, 52, 57, 63]. After filtration and dialysis, the regenerated fibroin solutions will be further used to prepare silk-based biomaterials.

Silk films can be prepared by solvent casting or layer-by-layer (LbL) deposition of solutions [15, 26, 33-35, 38, 40, 41, 46-48, 57, 59, 60, 62, 64-67]; SF sponges or scaffolds can be formed after lyophilization, porogens or gas foaming [25, 27, 31, 32, 36, 45, 53, 56, 58, 61, 63, 68-71]; SF hydrogels are formed via sol-gel transitions, sonication, vortexing or the presence of acid and/or ions [49]; SF nanofibers are prepared by electrospinning [28, 36, 43, 44, 59] and SF micro/nanospheres have been prepared by water/oil emulsion, spray-drying, lipid vesicles, salt leaching and sonication [72-76]. The different morphologies of SF can be observed in Figure 1.2. To be further used, it is necessary to induce β-sheet crystallization so that silk-based materials became water insoluble and slower degraded. This can be achieved through the use of organic solvents such

as methanol and formic acid, mechanical stress, high concentrations of salts and thermal treatment [51, 52, 77, 78]. Water-based annealing procedure and very slow drying have shown to induce the formation of β-sheet crystal of SF materials [79, 80]. Recently, it was reported that blending with other molecules induces the crystallization of SF. Studies made on SF/keratin blends indicated that addition of keratin induces the β-sheet formation most likely due to the high polarity of keratin protein that act as a organic solvent [81]. In another study, blending SF with hyaluronic acid (HA) enhances higher levels of β-sheet formation in the presence of methanol or water [82]. Accordingly to the US Pharmacopeia, a degradable material is defined as one that "loses most of its tensile strength within 60 days" post-implantation *in vivo*. By this definition, silk is classified as non-degradable. However, based on the literature, fibroin is proteolytically degradable over longer time periods [6, 37].

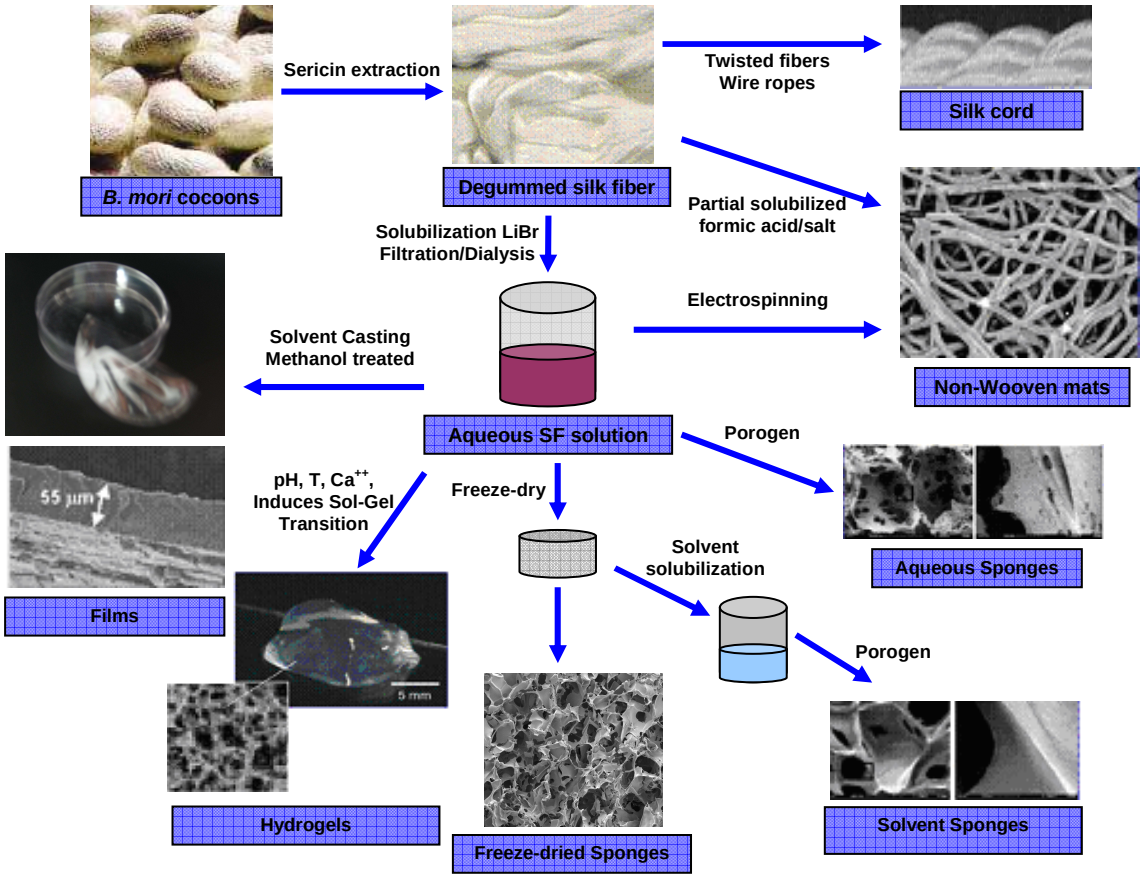

Figure 1.2. Silk fibroin processing into different morphologies adapted from [83]: (silk cords by twisting [6]; non-woven silk mats [84]; non-woven silk fibers [85]; aqueous- and solvent-based porous sponges [53]; hydrogels [86] and films [15, 87]).

1.1.2. Silk fibroin films

Silk fibroin films have been cast from aqueous or organic solvent systems as well as after blending with other polymers. Silk films possess oxygen and water vapor permeability depending on the content of silk I and silk II structures [88, 89]. Mechanical and degradability properties of the films are also affected by these silk structures [89]. Research has shown the importance of surface topography and texture in controlling the shape, orientation and gene expression of adherent cells [47, 66]. Gupta et al. extended the versatility of silk fibroin further in developing patterned films cast directly from fibroin solubilized in an ionic liquid. In addition, these films were found to support normal keratinocytes proliferation and differentiation [66].

The controlled release of active compounds from SF films has been extensively evaluated [40]. It was found that the release is affected by the amounts of β-sheet crystals. Furthermore, the methanol treatment performed to induce the crystallization of the films does not affect the activity of the compounds as shown by the study performed by Uebersax et al., where nerve growth factor (NGF) is continuously released from SF films up to 3 weeks without loss in the NGF bioactivity [41]. The utility of SF films to promote long-term adenosine release from adenosine kinase deficient embryonic stem cells was investigated [90, 91]. These studies demonstrate that SF constitutes a suitable material for the direct differentiation of embryonic stem cells and for cell-mediated therapeutic release of adenosine. In a recent study, SF films were used for the stabilization of enzymes or therapeutic proteins [48]. Glucose oxidase, lipase and horseradish peroxidase (HRP) were entrapped in silk films over 10 months with significant activity retained. This study demonstrates that SF films can be used for the stabilization of enzymes without the need for cryoprotectants, emulsifiers, covalent immobilization or other technique. The biomedical applications of SF films could be broadened by surface modifications with RGD (arginine-glycine-aspartic acid) or specific growth factors. As shown by Sofia et al. and Chen et al. RGD coupling (via carbodiimide chemistry) to SF films promotes the attachment, spreading, proliferation and differentiation of human osteoblasts, fibroblasts and bone marrow stromal cell [60, 92]. This is most likely due to an increase in cell density that promotes cell-cell interactions [92].

The surface of SF films was modified with parathyroid hormone (PTH), involved in the induction of bone formation, and it was showed that adhesion of human osteoblasts on SF films was promoted by surface modification [60]. Immobilization of bone morphogenetic protein-2 (BMP-2) in SF films, by carbodiimide reaction, enhanced osteogenic differentiation of human bone marrow stromal cells [93]. Overall, these studies demonstrated that the diversity of amino acid residues present in fibroin facilitates surface modification and immobilization of adhesion ligands and growth/morphogens factors. This allows selective modifications of SF biomaterials to encode specific functions. The *in vitro* inflammatory response was first reported by Santin et al. It was demonstrated that interactions of fibroin with the humoral components of the inflammatory system were comparable with those of controls, i.e., no added inflammatory response was observed [35]. Meinel et al. studied the inflammatory response of SF films (with or without covalently bonded RGD) *in vitro* and *in vivo* [62]. It was reported that cell proliferation *in vitro* was enhanced on SF or SF-RGD in comparison to controls (collagen and TCPS). *In vivo*, the inflammatory reaction and foreign body response to SF and SF-RGD is similar or less with that of controls.

The structure and properties of SF films can be further modified by blending with other natural and synthetic polymers such as polyethylene glycol (PEG) [33, 94, 95], polyacrylamide [96], cellulose [97, 98], polyallylamine [99], chitosan [100, 101], polyethylene oxide (PEO) [87], collagen [102], gelatin [67] and tropoelastin [26]. Generally, the blend systems showed better properties when compared to the pure components like, improved mechanical strength [26, 59, 65, 94, 96, 99] and thermal stability [65, 96], controlled release [49] and improved cellular attachment and proliferation [26, 99, 102]. Blend systems can also introduce changes in the morphology of the resulting film SF blended with cellulose and chitosan resulted in the formation of microporous [59, 98] and, addition of PEO to SF leads to films with a highly regular patterned microstructure [87].

There is considerable research in the development simple and versatile methods to assemble robust, biocompatible and functional biomaterial coating that directs cells outcomes. The self-assembly of SF to form coatings is dominated by hydrophobic and some electrostatic interactions. Therefore, both hydrophilic and hydrophobic materials could be coated. In general, the thickness of the coating is linearly correlated with the number of layers, which in turns depends on the SF

and salt concentrations used in the process. Coatings of SF have been studied to provide interfaces for biomaterials, Petrini et al. coated the surface of 2D and 3D polyurethane (PU) scaffolds in order to modify their surface [90]. After methanol treatments, SF-coatings showed good stability in physiological-like conditions and promote the adhesion and growth of human fibroblasts cells. The effect of SF coating at 2D poly(carbonate)-urethane (PCU) substrates on attachment, proliferation, metabolism and extracellular matrix (ECM) synthesis of four strains of human fibroblasts was reported by Chiarini et al. [103]. SF-PCU improved cell attachment by 2.2 fold in comparison to uncoated PCU films. At the same time, SF coating significantly affected the metabolism of fibroblasts and enhanced the extracellular assembly of collagen Type I, the major ECM contribution from fibroblasts. The last, seeded on SF-coated substrates did not secrete appreciable levels of cytokines which are implicated in inflammation reaction and tissue repair during wound. In a similar study, SF-coating on 3D PU scaffolds showed that cell attachment, proliferation and cellular metabolism is similar to the 2D PU substrates [104]. The surface modification of poly(D,L-lactic acid) (PDLLA) by SF coating improved the interactions between osteoblasts cells and PDLLA films [105]. Using the same substrates, SF coating was performed by carbodiimide chemistry and physical entrapment. The results showed that the SF coating via entrapment, presented higher osteoblasts viability and proliferation on the PDLLA films than the carbodiimide reaction [106]. Wang et al. employed an all-aqueous stepwise (layer-by-layer) deposition technique to assemble nanoscale thin films SF coating on a number of substrates [38]. The assembled films were stable under physiological conditions and supported human bone marrow stem cells adhesion, growth and differentiation. Furthermore, it was found that film thickness is linear to the number of SF layers. Thus, the release of drugs from these types of coatings can be controlled by the number of layers and secondary structure. Nanolayer coatings of SF to retain model compounds such as rhodamine B and azoalbumin have been prepared using the same procedure [107] and, it was found that higher crystallinity and thickness leads to the suppression of the initial burst release and prolonged the duration of the same. Multilayer SF coatings are also an effective system for the release of heparin, paclitaxel and clopidrogel [67]. Paclitaxel and clopidrogel were successfully released from SF-coatings inhibiting the proliferation of smooth muscle and endothelial cells. Heparin release was demonstrated by the promotion

of human aortic endothelial cell proliferation [67]. SF coating performed on poly(lactide-co-glycolic acid) (PLGA) and alginate microspheres stabilized the same from degradation, providing mechanically stable shells with a diffusion barrier that significantly delays the release from the microspheres [42]. When a chemical crosslinking of SF coating is employed, zero-order release kinetics can be achieved [54]. Recently, solid adenosine powder coated with SF was investigated for local and sustained delivery of the anticonvulsant adenosine from encapsulated reservoirs [29]. An increase in the thickness of the coating and crystallinity delayed adenosine burst release, decrease average daily release rate and increased the duration of the same.

These reports demonstrate that SF coatings generate biomaterials with controlled morphological and structural features for several applications such as drug delivery and tissue engineering.

1.1.3. Silk fibroin sponges/scaffolds

Silk-based porous sponges are attractive biomaterials for tissue engineering applications, cell attachment, proliferation and migration and, for nutrient and waste transport. SF sponges have been formed using porogens (sodium chloride (NaCl) or sugar), gas foaming and lyophilization. Solvent-based sponges can be prepared by dissolving aqueous derived SF, after freeze drying, in HFIP [53], or by adding small amounts of organic solvents (ethanol, methanol (CH_3OH), dimethylsulfoxide (DMSO, $(CH_3)_2SO$)) into aqueous SF solution before lyophilization [68].

Aqueous-based SF sponges can be prepared using salt crystals as porogens with control of pore sizes from 490-900 µm, by manipulating silk concentration and the size of salt crystals [61]. Due to partial solubilization of salt, aqueous-based sponges have rougher surface morphology than solvent-based ones. Higher porosity and better mechanical strength is obtained from aqueous-based sponges depending on SF concentration [61]. Furthermore, enzymatic degradation is faster for aqueous-based sponges [61, 108]. The same behavior is observed *in vivo*. Solvent and aqueous-derived SF sponges were implanted in rats. All scaffolds were tolerated by the animals with a mild immune response. Moreover, aqueous-

based sponges degraded completely between 2 and 6 months whereas solvent-based sponges persisted beyond 1 year [32].

The principal feature of the sponge materials is the cellular attachment and proliferation on the porous structures. SF-based sponges have shown to promote the adhesion, proliferation and differentiation of human dermal fibroblasts [71], human cervical cells [25], human mesenchymal stem cells [69, 109] and chondrocyte cells [31]. Silk sponges had been used successfully in the healing of critical size femur defect in rats [110]. Aqueous and solvent-based SF sponges were used for bone tissue engineering and, trabeculae bone-like structures were observed with higher organization for aqueous-derive SF sponges [111]. SF-sponges seeded with chondrocytes cells also supported a cartilage tissue engineering [112] yielding a frictional coefficient similar to that of native cartilage [113]. Additionally, SF micromolded sponges supported a significant enhancement in cell attachment, spreading, mitochondrial activity and proliferation, in comparison to tissue culture plates as controls [114], showing, once again, how matrix surface and topography is important for cellular interactions [63].

SF sponges have also been used for the incorporation of compounds. Vepari and Kaplan reported the immobilization (via carbodiimide chemistry) of horseradish peroxidase (HRP) enzyme gradients to prepare new functional scaffolds [115]. SF sponges loaded with BMP-2 induced human bone marrow stromal cells to undergo osteogenic differentiation when the seeded sponges were cultured for 4 weeks [116]. Uebersax et al. reported that the release of insulin growth factor I (IGF-I) from silk sponges promoted chondrogenic differentiation of human bone marrow mesenchymal stem cells [117]. Adenosine release via silk-based implants to the brain has been developed for the refractory epilepsy treatments [118, 119]. SF sponges loaded with adenosine demonstrated therapeutic ability, including the sustained release of adenosine, manipulated by slow degradation of silk, biocompatibility and the delivery of predetermined doses of adenosine [118].

The properties of SF sponges had also been exploited by blend systems. Improved mechanical properties can be achieved by blending SF with PEG [95] and chitosan [120]. Furthermore, degradation studies on SF/chitosan sponges showed that the blend sponges maintained the porous structures till 6 weeks of degradation in phosphate buffered saline (PBS) at 37 ℃ [56]. Silva et al. reported that crosslinking of SF/chitosan sponges with genipin promoted the formation of

stable structures that favored adhesion, proliferation and matrix production on chondrocyte-like cells [45]. SF/collagen sponges retained the excellent mechanical properties of SF-based sponges and, when heparin was loaded into the sponges, these become blood compatible due to the slow release of heparin [55]. In a different study, Lu et al. showed that growth of fibroblasts and vascular smooth muscle cells is improved in the SF/collagen relatively to pure SF sponge [58].
SF sponges blended with calcium alginate beads, loaded with drugs, resulted in a prolonged release without initial burst when compared to calcium alginate beads without SF [70]. Recently, a green process avoiding the use of organic solvents and harsh chemical processes was used for the preparation of SF/gelatin sponges. Addition of gelatin induces conformational changes to SF, which resulted in the formation of porous structures during lyophilization [27].

1.1.4. Silk fibroin-based wound dressings

Pure SF and blend systems had been applied in the development of new wound dressing materials. Yeo et al. reported the effect of polyvinyl alcohol (PVA)/Chitosan/SF (PCS) sponges on the wound healing in rats [121]. PCS-sponges covered an excised wound and, it was observed that PCS absorbed the exudate gaining flexibility and softness. The histopathological inspection of the wound showed an increase of vascular ingrowth and the absence of inflammatory cells after 12 days of implantation. Moreover, it was found that accelerated wound healing is obtained with PCS-sponges in comparison with control and the pure components or in various combinations [121]. Silk fibroin films were used in full-thickness wounds of mice [122]. It was reported that the area of the wound was reduced by 10% and the healing time of the wounds dressed with SF films was 7 days shorter when compared to control, DuoActive, a conventional hydrocolloid dressing. Furthermore, a higher collagen regeneration and reduced inflammation was obtained with SF films. When compared to lyophilized porcine dermis (Alloask D), which is used as a dressing for burns, ulcers and decubitus, the promotive effects of the wounds with SF films were similar or slightly better [122]. In another study, SF/alginate (SF/AA) sponges were applied to the same type of wounds [123]. It was reported that the half healing time (HT_{50}) was dramatically reduced by SF/AA sponges in comparison to control or pure SF and alginate. The same trend

was observed on the significant increase of re-ephitelialization and in the number of proliferative cells. These results indicate that SF and alginate act synergistically for the promotion of wound healing [123]. Polarized hydroxyapatite (pHA) and SF composite dressing gel were also tested on the epidermal recovery from full-thickness porcine skin wounds [124]. It was found that the blend with polarized hydroxyapatite showed higher promotive effects, re-ephitelialization and matrix formation that pure SF or the blend without polarized hydroxyapatite. Tsubouchi et al. patented a wound dressing material containing silk fibroin and sericin [125]. The dressing was applied to a corium-flayed mouse and it was observed that the SF/sericin dressing inhibited edematization and functioned as a wound dressing material. Silk wound dressings that selectively sequester targeted proteases from wound sites were patented by Mcdevitt and Tyrell [126]. It was found that silk wound dressing effectively removes human neutrophil elastase from the wound site, protecting from proteolytic degradation thus, accelerating the healing. More recently, the properties of electrospun silk mats have bee evaluated for wound dressing applications [127]. Electrospun silk materials exhibited absorption, water vapor transmission, oxygen permeability and enzymatic degradation suitable for full-thickness wound sites. Electrospun silk mats loaded with epidermal growth factors (EGF) increased the time of wound closure to 90% [128]. Altman et al. reported the potential of SF/chitosan scaffold as a delivery vehicle for human adipose-derived stem cells (ASCs) in a murine soft tissue wound model [129]. It was found that scaffolds with seeded cells enhance wound healing and show differentiation into fibrovascular, endothelial and epithelial components of restored tissue when compared to non seeded scaffolds and control. The feasibility of SF films to construct artificial skin substitutes for wound healing was demonstrated through cytocompatibility evaluation. No cytotoxicity or adverse influence on the adhesion and cell cycle was observed. Therefore, SF films provide a framework for reparation after trauma in clinical applications [130].

Overall, the healing properties presented by the SF-based materials are related to the physical properties of SF such as water absorption and vapor permeability. The ability to absorb wound exudate forms a flexible dressings that sticks to the wound, preventing excessive flow cell-proliferating substances, exudate and proteins. At the same time, smooth regeneration of the skin is accelerated,

because the flexible dressings moves when the skin moves without stimulating the wound

1.2. Keratin-structure and properties

Keratin is the major structural fibrous protein providing outer covering such as hair, wool, feathers, nails and horns of mammals, reptiles and birds [131]. Keratin proteins are self-assembled into fibers in the follicle by a high proliferative process controlled by more than 30 growth factors and cytokines [132-136]. After extrusion through the skin, the fiber is formed into a highly stable structure formed by covalent, ambient oxygen catalyzed disulfide crosslinking and non covalent interactions (Figure 1.3), which can occur between separate polypeptide chains (intermolecular) but also, between different points of the same polypeptide chain (intramolecular).

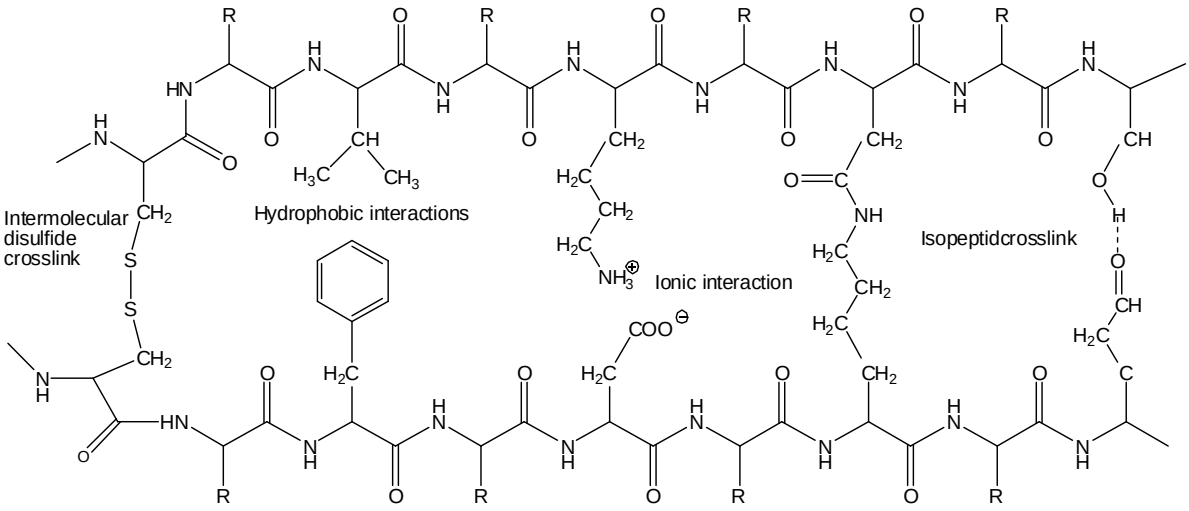

Figure 1.3. Possible interactions between keratin protein chains [137].

Keratin fibers, such as wool and human hair, consist of two major morphological parts: the cuticle layer which is composed of overlapping cells that surround the cortex, the inner part of the fiber. The cortex comprises spindle-shaped cortical cells that are separated from each other by a cell-membrane complex (Figure 1.4.), which consists of non-keratinous proteins and lipids [137-141].

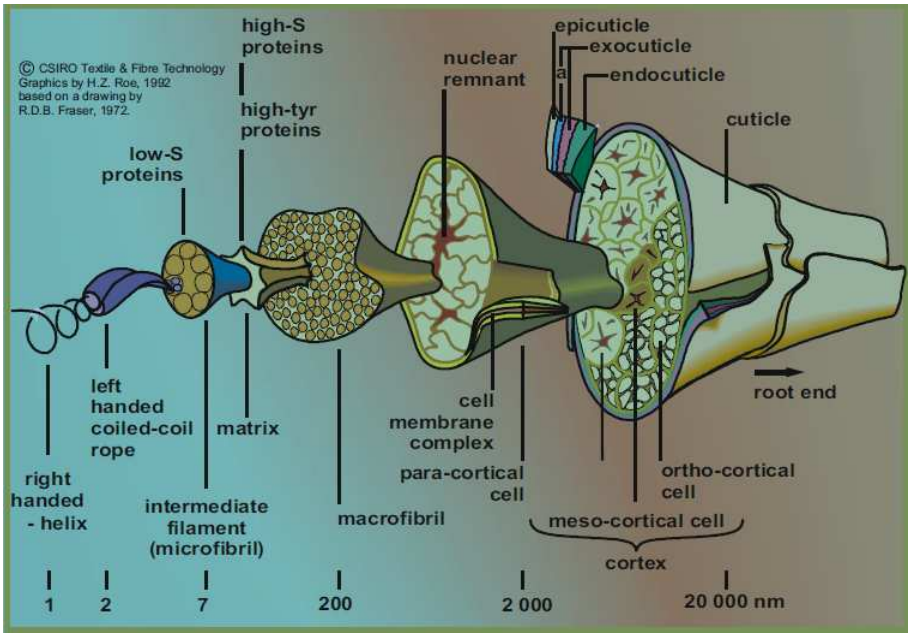

Figure 1.4. Schematic diagram of a wool fiber showing the independent structures found in the cortical cells reprinted from CSIRO Textile & Fibre Technology.

The cuticle cells comprise 10% of the total weight and are laminar with a rectangular shape forming a sheath of overlapping scales surrounding the cortex [139, 142, 143]. They are composed of three distinct layers showed in Figure 1.4. The outer resistant surface membrane is named epicuticle; the next layer is the exocuticle which is subdivided into two main layers (A and B) that differ in their cysteine content; the endocuticle is the cuticular layer nearest the cortex [137, 140, 143, 144]. Keratin proteins can be roughly classified into two groups: the intermediate filament proteins (IFPs) and the matrix proteins. The most abundant are the IFPs also known as α-keratin that reside in the fiber cortex. They have a α-helical secondary structure, are low in sulfur content and have an average molecular mass in the range of 40-60 kDa. The matrix proteins or γ-keratin are globular, have a low molecular weight and are noted for the high content in either cysteine, glycine and tyrosine residues. The ones with high sulfur content can be divided in high sulfur proteins (HSPs) or ultra-high sulfur proteins (UHSPs) depending on their cysteine content and have a molecular weight in the range of 11-26 kDa. The high glycine-tyrosine proteins (HGTPs) have a molecular weight between 6 and 9 kDa [145-147].

The matrix proteins function surround the IFPs and interact with them through intermolecular disulfide bonds [141]. The formation of the crosslinked IF-matrix composite is crucial in conferring to the α-keratin their high mechanical strength, inertness and rigidity [148]. The packing of the IFPs combined with the matrix proteins form the macrofibrils within the cortex [148, 149]. There is also another group of keratin proteins, the β-keratin. These form the majority of the cuticle and their function is to protect keratin fibers from physical and chemical damage. The β-keratin is difficult to extract and do not form especially useful reconstituted structures [149, 150]. For a better elucidation of readers a resume of the main structural properties of the studied proteins will be provided (Table 1.1.).

1.2.1. Keratin-based biomaterials

Keratins are extracted from the fibers through the use of chemicals to break the disulfide bonds. The IF and matrix proteins are converted into their non-crosslinked forms by oxidation [149, 151-153] or reduction [149, 154-156], during which cystine is converted to either cysteic acid or cysteine, respectively. The free proteins extracted with denaturating solvents produce a solution that can be purified by filtration and dialysis.

Oxidative extraction [151-153] with peracetic acid (CH_3CO_3H) or hydrogen peroxide (H_2O_2), e.g., yields keratins that are hygroscopic, non-disulfide crosslinkable, water-soluble and, susceptible to hydrolytic degradation at extremes pH values due to polarization of the backbone caused by the electron withdrawing properties of the cysteic acid. These characteristics lead to biomaterials that can degrade relatively fast *in vivo*, i.e. on the order of days to weeks.

Reductive extraction [154-156] commonly uses dithiothreitol (DTT, $HSCH_2CH(OH)CH(OH)CH_2SH$) or 2-mercaptoethanol (2-Me, $HSCH_2CH_2OH$) with a protein extraction of approximately 80% [157]. Extraction with sodium disulfite ($Na_2S_2O_5$) forms cysteine and Bunte salts residues, temporally modified S-sulfo group [131, 158, 159]. With this method the keratin extracted is about 30% of the total protein content of the original wool [160]. Reduced keratins are, less polar and as a consequence less soluble in water, more stable at extreme pH and, can be re-crosslinked through oxidative coupling of cysteine groups. This results in biomaterials that persist *in vivo* for weeks to months.

The interest of using keratin as a biomaterial in medical applications is based on several key properties that contribute to the overall physical, chemical and biological behavior of these biomaterials. Extracted keratin proteins have an intrinsic ability to self-assemble and polymerize into fibrous and porous films gels and scaffolds. The spontaneous self-assembly of keratin has been studied extensively at both microscale [161-163] and macroscale levels [164]. Furthermore, the presence of cell adhesion sequences, arginine-glycine-aspartic acid (RGD) and leucine-aspartic acid-valine (LDV) on the keratin protein derived from wool and hair, makes keratin biomaterials able to support cell attachment and growth [165, 166]. These are the same sequences found in several extracellular matrix (ECM) proteins [167, 168]. The processing of keratin protein solutions into derivatives physical states such as gels, films and scaffolds start to appear in the literature in 1972 [169-171], then the first study using a keratin biomaterial appeared wherein a vascular graft coated with keratin was successfully implanted into a dog for more than 200 days without thrombosis [172]. Since then, keratin have been studied for its application in biomaterials for wound healing [173-178], bone regeneration [179], hemostasis [180] and recently in peripheral nerve repair [181, 182].

1.2.2. Keratin films

A stable aqueous solution of keratin was obtained after reductive extraction from wool fibers. The ability of this solution to self-assemble into films was described by Yamauchi et al. [183] and, the physicochemical properties and biodegradability of the solvent-cast keratin films were evaluated. Pure keratin films presented low mechanical strength but the addition of glycerol resulted in transparent films, with increased mechanical strength, flexible and biodegradable both *in vitro* (trypsin) and *in vivo* (subcutaneous implantation in mice) [183]. Furthermore, these films proven to promote and increased cell adhesion and growth when compared to collagen and glass [184]. Fujii et al. developed a new procedure for the extraction of keratin from human hair without a surfactant agent, with a protein extraction yield greater than 70% [185]. The developed films were effective on the controlled-release of alkaline phosphatase (ALP) that retains its biological activity after incorporation into keratin films [185]. The same films were further used and, gauze

was coated with the translucid keratin film. This results in improved mechanical strength of the gauzes and, when applied to human skin, a reduced allergic reaction was observed [186]. Like many natural-derived biomaterials, keratin-based ones present poor mechanical strength. As a consequence, several approaches for controlling the physical and biological properties have been studied such as, blend systems with natural [15, 187-190] and synthetic [160, 191] polymers, use of crosslinking agents [192] and new preparation techniques [158, 186, 193]. Addition of chitosan to keratin forms strong and flexible films with improved swelling properties. Furthermore, the composite film demonstrated to be a good substrate for mammalian cell culture [189]. Lee at al. first reported keratin-silk fibroin (SF) blend films. This study aimed to understand the interactions that occur between the two proteins and how they affect the overall properties of the biomaterials. The results indicated that addition of keratin induces the transition from random coil to β-sheet of the SF chains. It was consider that keratin plays a similar role of a polar solvent due to the abundant polar groups in its amino acid composition [188]. Moreover, the antithrombogenicity and biocompatibility of keratin-SF films was improved when compared to pure keratin and SF films [81]. In a different study, the properties of keratin-SF films were further studied and, it was described that keratin and SF interactions are not simply additive but the two proteins are able to establish intermolecular interactions like hydrogen bonding. Furthermore, degradation rates are controlled by blend composition. The knowledge and strength of the interactions as well the degradation rates allows the design of matrices with controlled-release properties [15]. In addition to natural biopolymers, keratin interaction with synthetic polymers has also been studied [160, 191]. The properties of keratin films blended with poly(ethylene oxide) (PEO) were described by Tonin et al. [160], it was concluded that at appropriate levels, keratin is able to inhibit PEO crystallization. Moreover, PEO interferes with the keratin self-assembly, inducing a more thermally-stable β-sheet secondary structure. The intermolecular interactions between keratin and polyamide 6 (PA6) have also been studied and, the results indicated that the addition of keratin improves the miscibility and hydrophilicity [191].

Another common technique to improve the mechanical strength is the use of crosslinking agents. Keratin films prepared by casting a reduced keratin solution, were chemically crosslinked with ethylene glycol diglycidyl ether (EGDE, $C_8H_{14}O_4$)

and glycerol diglycidyl ether (GDE, $C_9H_{16}O_5$) [192]. It was reported that keratin crosslinked films have similar mechanical properties and improved waterproof characteristics when compared to keratin-chitosan films previously described [189]. Furthermore, chemical crosslinking does not have detrimental effects on cell biocompatibility [192]. Improved mechanical properties can also be achieved by alternative fabrication techniques. Compression molding of S-sulfo keratin powder for the production of films was developed [158]. The mechanical properties of the films can be modulated by controlling the molding temperature and water content. The biocompatibility was also demonstrated by cell adhesion and proliferation onto the films [158]. Recently, Yang et al. described the use of keratin for layer-by-layer (LbL) self-assembly [193]. In this study, keratin extracted from wool is used either as a polyanion or polycation by adjusting the pH of the solution to fabricate multilayer films. Although the mechanical properties were not evaluated, it is clear that a multilayer film will possess an increased mechanical strength when compared to a unilayer film. Reichl et al. demonstrated two approaches for substrate coating: keratin precipitation with thricloroacetic acid (TCA, Cl_3CCOOH) and casting a keratin nanosuspension. The latter presented improved cell growth in comparison to uncoated polystyrene or TCA coating [194].

1.2.3. Keratin sponges/scaffolds

The ability of extracted keratin to self-assemble into three dimensional porous structures has led to their development as scaffolds for biomedical applications.

Wool keratin sponges were first reported by Tachibana et al. [165]. The sponge scaffolds were fabricated by lyophilization of an aqueous keratin solution after controlled freezing. This resulted in sponges with homogeneous porous microstructures. Additionally, the sponges exhibited cell attachment and proliferation over a long-term cultivation period of 23-43 days [165].

The diameter and interconnectivity of the scaffolds pores is important for obtaining adequate cellular infiltration and nutrient delivery. Sponges with controlled pore size and porosity were developed by Katoh et al. [159] by means of S-sulfo keratin sponges prepared by a compression-molded/particulate leaching (CM/PL) technique. The sponges presented adequate mechanical properties and were water-insoluble [159]. In another study, a reduced keratin solution was mixed with

dried calcium alginate beads. After lyophilization and leaching, a keratin sponge with high porosity and interconnectivity was obtained, in addition to cellular adhesion and growth[168].

The presence of free cysteine residues within keratin sponges allows the immobilization of bioactive agents. Lysozyme was immobilized in a keratin sponge via disulfide and thioether bonds. Disulfide-linked lysozyme was released over a 21-days period unlike lysozyme linked via thioether bonds that remains in the sponge up to two months. This study showed that the release properties from keratin sponges can be controlled by the selection of the crosslinker [195]. Functionalization of the active free cysteine residues in the keratin sponges can be achieved by chemical treatments with iodoacetic acid (ICH_2CO_2H), 2-bromoethylamine (C_2H_6BrN) and iodoacetamide (ICH_2CONH_2), to produce carboxyl-, amino- and amide-sponges. These chemically-modified keratin sponges have been shown to mimic ECM proteins and, the large presence of active groups allows further hybridization with bioactive molecules. Tachibana et al. [179] demonstrated the hybridization of keratin sponges with calcium phosphate ($Ca_3O_8P_2$). Two types of hybrids sponges were obtained by either chemically binding of calcium and phosphate or, by trapping commercially available hydroxyapatite particles within the modified keratin sponge. Both hybridized sponges supported osteoblasts cultivation and altered their differentiation pattern [179]. Keratin carboxy-sponges have also been functionalized with bone morphogenetic protein-2 (BMP-2). BMP-2 was confined within the modified keratin sponge, without protein loading into the surrounding media, which was accompanied by preosteoblasts differentiation and growth [196].

The *in vivo* biodegradation of keratin sponges, with bars shape, was assessed by subcutaneously implantation in adult rats [197]. It was showed a gradual decrease in the mass of the bars over the 18 weeks of study. On the contrary, the elastic modulus of the bars decrease abruptly indicating an internal change in the structure and shape of the keratin bars [197].

1.2.4. Keratin-based wound dressings

The above described materials are latent wound dressings due to the cellular biocompatibility demonstrated. The cells used in the mentioned studies were

NIH3T3, L929 fibroblasts, MC3T3-E1 pre-osteoblasts, epithelial and mesenchymal human cells. In general, all have showed good cellular adhesion and proliferation on keratin materials in comparison to standard controls such as tissue culture plastic or other biomaterials like collagen.

In the field of wound healing, several patents have been published using keratin materials as wound healing promoters [173-178]. Keratin powder used as an absorbent wound dressing showed the promotion of skin healing due to the release of keratin derivative peptides to the wound [176]. Crosslinked keratin powder, films and hydrogels showed significant proliferation of wound healing cell lines like microvascular endothelial cells, keratinocytes and fibroblasts. Moreover, incubation of keratin materials with lymphocytes (T cells) and activated lymphocytes showed, respectively, no proliferation and normal growth, indicating that keratin materials are non-immunogenic and, that the body's normal cell-mediated immune response is not inhibited by keratin materials. These were also applied to wounds on animals (rats) and humans, and it was observed a faster healing of the wounds treated with keratin materials and, in the human model with reduced pain [173, 174]. Water-soluble keratin peptides derived from an oxidative extraction from human hair, showed to be wound healing agents enhancing the proliferation of human dermal fibroblasts [175]. More recently, keratin derivatives obtained either by oxidative and reductive methods, were applied to burn wounds using animal and human models. The burn wounds treated with keratin materials showed a decrease in wound size and, accelerated wound healing. When applied to bleeding wounds, the keratin materials formed a physical seal of the wound site providing a porous scaffold for cell infiltration and granulation tissue formation compared to clotted blood [178]. Keratin was also effectively blended with other components to form new wound dressings. Keratin-collagen sponges were used in rats showing tissue compatibility and accelerated wound healing by stimulating cell proliferation and vascularization [198]. An analogue keratin-collagen sponge containing poly 2-hydroxyethylmethacrylate (PHEMA) was applied to burn wounds in rats. The composite showed healing promotion by allowing *in vivo* construction of tissue engineered epidermis [199]. In another recent study, keratin-gelatin used in full-thickness wounds in dogs promoted the healing due to the early presence of hair follicles, sebaceous gland and normal thickness of the epidermis [200].

The immunogenicity/inflammation is another important parameter to be evaluated for wound dressing applications. The immunogenicity response of keratin-based materials was first evaluated by Ito et al. in which polyester mesh coated with keratin was implanted into the muscle of rabbits and dogs. The acute immune response was characterized as mild [180]. Keratin films extracted from rat hair implanted into rabbits degraded after two weeks showing a weak immunological reaction [180]. Yamauchi et al. reported that keratin films implanted into subcutaneous space of mice and retrieved after 18 weeks, showed less degradation than collagen IV and poly(lactic acid) (PLA). In addition, no adhesions or “abnormal” scar tissue was observed [183]. Keratins extracted from mousse and human hair and nails showed no rejection or allergic reactions using an animal model [185, 201]. More recently, keratin discs implanted subcutaneously into mice showed no inflammation or capsule formation. Moreover, no visibly degradation occurred after three months of implantation [150]. Keratin matrices implanted in the distal femur of the sheep, to study the biocompatibility and osseointegration, showed granulation tissue surrounding and infiltrating the implants followed by new bone formation [202], exploring the ability of keratin materials to be used in the field of bone regeneration.

1.3. Elastin-structure and properties

Elastin is an extracellular matrix (ECM) protein that is known for providing elasticity to tissues and organs. As a result, elastin is most abundant in organs that need to stretch and recoil like blood vessels, elastic ligaments, lungs and skin [203-205]. Elastin is synthesized by a variety of cells including smooth muscle cells, endothelial cells, fibroblasts and chondrocytes. Elastin is an amorphous protein, with about 75% of hydrophobic amino acid residues (Gly, Ala, Val) and highly insoluble due to interchain crosslinks [206]. This protein is secreted as the precursor tropoelastin (≈ 72 kDa) that is soluble, non glycosylated and highly hydrophobic [207-209], which will be further converted into the insoluble elastin polymer. The tropoelastin molecule consist of two types of domains encoded by separate exons: hydrophobic domains with many Gly, Val, Ala and Pro residues which often occur in repeats of several amino acids, like Gly-Val-Gly-Val-Pro, Gly-Val-Pro-Gly-Val and Gly-Val-Gly-Val-Ala Pro, and hydrophilic domains with many

Lys and Ala residues that correspond to the potential crosslinking domains of tropoelastin.

The two predominant crosslinks of native elastin are desmosine and isodesmosine (Figure 1.5) each involving four lysine (Lys) residues that are crosslinked by lysyl oxidase. In the absence of this enzyme, tropoelastin tends to associate with glycosaminoglycan (GAG) due to the presence of α-amino groups in the elastin Lys residues. These residues offer positive charges for binding with negative charges of glycosaminoglycan. In the absence of lysyl oxidase, such electrostatic interaction could be important and prevent newly synthesized tropoelastin molecules from spontaneous random aggregation far from the cell surface [210, 211].

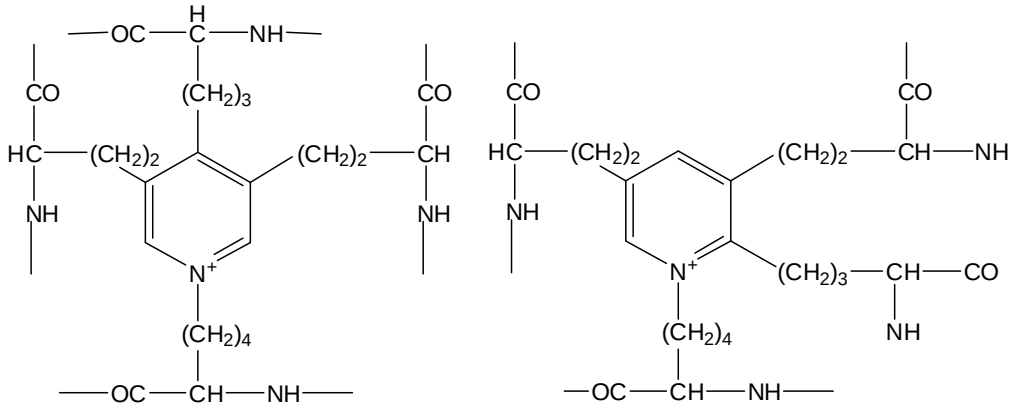

Figure 1.5. Intermolecular elastin crosslinks desmosine and isodesmosine formed from four lysine residues from two different tropoelastin molecules.

The assembly of tropoelastin into a polymeric matrix is accompanied by the elastin binding protein (67 kDa) that releases tropoelastin into a pre-formed microfibrillar network, which serves as a scaffold for tropoelastin deposition [212-215]. The lysine residues become further modified by lysyl oxidase allowing crosslinking into a stable polymeric matrix. The biophysical properties crucial for the biochemical/physiological role of elastin in the body are elasticity [216-218], glass transition [219] and coacervation [220]. Three distinct mechanisms have been proposed to explain the elasticity of elastin and, despite the differences they share the argument that the driving force for the spontaneous recoil of stretched elastin results from a predominantly entropic mechanism [221-223]. The glass transition

temperature (T_g) is an important characteristic of polymers. Below the T_g a polymer will generally behave as a rigid/brittle material and, above T_g the polymer behaves as an elastomer or a viscous fluid. The glass transition temperature of elastin depends on its water content [224, 225]. In the dehydrate state, T_g is about 200 ℃ and at 30% of hydration is around 30 ℃ [226].

A second phase transition that can occur with elastin and elastin-based materials is coacervation. This is a reversible phase separation in which a protein in solution separates from the solvent after increasing the temperature [227, 228]. The non-polar domains of elastin have been suggested to be responsible for the coacervation process through an entropic mechanism of hydrophobic association. The loss of entropy from the protein chains is compensated by the release of water [229, 230]. Elastin-based polymers lacking hydrophobic domains, e.g. those based on crosslinking domains cannot coacervate [231, 232].The onset temperature for coacervation is dependent on protein concentration, hydrophobicity (amino acid composition and distribution), pH and ionic strength of the solvent [229, 233-235]. Coacervation is a lower critical solution temperature (LCST) phenomenon which means that elastin forms ordered structures upon raising the temperature, unlike other proteins that are denaturated. It was reported that synthetic peptides based on hydrophobic sequences of elastin form fibrilar structures following coacervation [236, 237]; tropoelastin forms an open, string-like network of fibrils upon coacervation that, after overnight incubation above the coacervation temperature, the loose network became a compact aligned fibrilar structure [238]. For a better elucidation of readers a resume of the main structural properties of the studied proteins will be provided (Table 1.1.).

1.3.1. Elastin-based biomaterials

Elastin can be used in biomaterials in different forms including insoluble elastin, occurring in autografts, allografts and xenografts, decellularized extracellular matrix and in purified elastin preparations. By synthetic or recombinant techniques, repeated elastin-like sequences had also been used in biomaterials. Soluble elastin is obtained from the hydrolysis of insoluble elastin with oxalic acid (HO_2CCO_2H) or potassium hydroxide (KOH) [239, 240]. These treatments will not release tropoelastin from insoluble elastin, but will break peptide bonds yielding

soluble fragments of elastin and leaving the crosslinks intact [239, 240]. It has been shown that elastin soluble peptides influence signaling, chemotaxis, proliferation and protease release via the elastin receptor [241]. Therefore, biomaterials containing solubilized elastin may exert biological effects like increasing elastin synthesis.

The self-assembly behavior of elastin was used to obtain different biomaterials like hydrogels [242, 243], films [244], nanoparticles [245], sponges [246] and nanoporous materials [247]. These forms can be further applied in cellular orientation, small-diameter blood vessels and drug or growth factor delivery systems. Solubilized elastin has been used as a coating to improve the biocompatibility of synthetic materials such as poly(ethylene glycol terephthalate) (PET) [248]. It was showed that the elastin coating on PET promotes endothelial cell growth maintaining their phenotypic character. This composite was further applied as prosthesis in a baboon arteriovenous shunt, to study the effect on acute thrombogenicity [249] and, excellent short-term blood-contacting properties were demonstrated. Mithieux et al. reported the chemical crosslinking of recombinant human tropoelastin to construct elastic sponges, sheets and tubes [243]. It was found that the properties of the materials were similar to the native elastin. Furthermore, cells proliferated on the constructs and they were well tolerated after *in vivo* implantation. Similar results were obtained elsewhere [250, 251]. High pressure CO_2 have been used to produce porous elastin hydrogels [252, 253] and tropoelastin/elastin hydrogels [254] followed by a chemical crosslinking. When high pressure was applied it was observed an increase in the porosity, mechanical properties and swelling ratios. Additionally, due to the fabrication of large pores in the hydrogels, cellular proliferation and growth were substantially promoted.

Elastin-like polymers (ELPs) and hybrids of the same with other proteins have been extensively studied. These offer the possibility to produce an assortment of biomaterials with specific functions. Urry et al. showed that the transition temperature, T_t, of polymers based on Val-Pro-Gly-X_{aa}-Gly)$_n$ could be manipulated by the amino acid X_{aa}. As an example, a more hydrophobic amino acid resulted in a lower T_t [255]. High molecular mass polymers are favorable for the preparation of functional materials. Urry et al. prepared various elastin-like materials by polymerization of elastin penpapeptides by chemical synthesis and recombinant expression system [256-258]. These were further applied in intervertebral disc

restoring in a rabbit model [259] and filling material for urinary incontinence, urinary bladder reconstruction and prevention of post-operative tissue adhesions [260]. ELPs are attractive as polymeric carriers for drug delivery, because they undergo an inverse temperature phase transition [233, 261]. Below T_t, ELPs are structurally disordered and highly solvated. Above T_t they undertake a sharp phase transition leading to desolvation and hydrophobic aggregation of the biopolymer, which is a completely reversible process when temperature is lowered below T_t. The delivery properties of ELPs containing doxorubicin (Dox, antitumor agent) were evaluated by applying mild hyperthermia to the tumor site [262] and, cytotoxicity of uterine sarcoma cells was enhanced by 20-fold. The mechanical properties of ELPs can be further improved by chemical crosslinking [263].

Silk-elastin like polymers (SELPs) comprise a class of genetically engineered biomaterials composed of amino acid motifs from two proteins, *B. mori* silk (Gly-Ala-Gly-Ala-Gly-Ser) and elastin (Gly-Val-Gly-Val-Pro) [264]. By recombinant techniques, functional motifs can be introduced into SELPS that provides the control over gelation, crosslinking, biodegradation, biorecognition and stimuli-sensitive [265], with applications in drug [266] and gene delivery systems [267, 268]. Megeed et al. reported the controlled release of non-viral and viral genes from SELP hydrogel for cancer gene therapy. This resulted in increase transfections by a 1-3 order of magnitude, in a murine model of tumor breast cancer [267].

Elastin combined with fibrin [269] and collagen [270] has been prepared. Their potential was examined *in vivo* as a tympanic membrane [269] and a dural substitute [270]. Chemical crosslinking by carbodiimide reaction, of collagen/elastin materials improved the thermal stability [271] and decrease the enzymatic degradation rate [272]. Molecularly-defined scaffolds were obtained with collagen, elastin and chondroitin sulphate (CS) [273]. The scaffolds are biocompatible and the properties of the material are improved by the synergistic effect of each component. Incorporation of elastin on collagen-based vascular grafts increased the tensile strength and improved the viscoelastic properties [274]. Furthermore, higher contents of elastin promote cell adhesion and viability [275]. Calcification is a common problem associated to implants. The effect of collagen/elastin materials implanted in young Sprague Dawley rats, a sensitive calcification model, was evaluated [276, 277]. It was showed that collagen/elastin

reduced the calcification when compared to collagen material [276]. If solubilized elastin was used, no calcification was observed and angiogenesis was induced [277]. Electrospinning of collagen/elastin [278], collagen/elastin/gelatin [279] and poly(lactide-co-glycolide)(PLGA)/gelatin/elastin [280] resulted in scaffolds that support cellular attachment and growth. Electrospun polydioxanone-soluble elastin blends had been characterized for their used in vascular grafts [281]. Addition of elastin creates scaffolds that exhibited properties resembling that of pig artery and native human artery. Elastin was also found to be primary cause of cell-mediated immunosupression of the same materials [282].

1.3.2. Elastin-based wound dressings

Elastin-based materials have been applied as skin substitutes to treat burn or chronic wounds. Scaffolds of type I collagen coated with elastin and applied to a full-thickness wound, contributes to dermal regeneration and reduce wound contraction [283]. The same type of dressings applied to a porcine excised wound model showed reduced wound contraction, improved tissue regeneration and absence of myofibroblasts when compared to control (skin substitute without collagen/elastin) [284]. Collagen/elastin dermal substitute with seeded fibroblasts cells, applied to the last wound model, was reported by Lamme et al. [285]. Fibroblasts seeded on collagen/elastin matrix survived and proliferated, reducing the migration/proliferation of unwanted subcutaneous fibroblasts into the wound. Furthermore, the degradation of the implanted dermal substitute was retarded, indicating a protective activity of the seeded fibroblasts. In another study, collagen/elastin membranes were grafted in a rat excised wound model to serve as a template for the formation of neo-dermis [286]. The results showed that the graft becomes populated and vascularised by cells from the wound bed and margin. The grafted collagen/elastin is digested and induces the formation of a tissue-layer, whit a dermis-like texture, in which the presence of elastin is essential [286].

Clinical trials were conducted to compare the conventional treatment (split-thickness autograft) and a collagen/elastin dermal substitute in combination with an autograft. Skin elasticity was improved [287, 288] and other parameters like

rete ridges, basement membrane maturation and epidermal thickness were also improved by collagen/elastin dermal substitute [289].

The inflammatory response of collagen/elastin membrane was studied *in vitro* and *in vivo* using the chorioallantoic membrane (CAM) assay of the chick embryo as a model [290]. The results showed that the collagen/elastin membrane induces the activation of macrophages, angiogenesis and the formation of inflammatory tissue, which can result in a chronic wound. Hashimoto et al. reported the development of alginate wound dressings covalently bound hybrid laminin and elastin-derived peptides [291]. The hybrid peptides promoted the attachment of human dermal fibroblasts. When applied *in vivo*, in a rabbit ear skin defect mode, alginate dressings linked to elastin peptide showed significantly greater ephitelialization and a larger volume of regenerated tissue in comparison to alginate-laminin dressing. The proteolytic digestion of elastin induced elastic fiber deposition and synthesis when injected in the skin of nude mice [288]. This result shows the importance of soluble elastin peptides on physiological events.

The commercially available wound dressing Matriderm® composed of collagen and elastin was evaluated as a dermal substitute for the treatment of severe hand burns [292] and for the reconstruction of joint-associated defects [293]. Full range of motion was achieved in both cases with no blisters and scars. In a recent study, new SF/elastin scaffolds were evaluated using a human wound exudate [294]. Degradability of the scaffolds under wound exudate showed that when applied to the wounds, necrosis can be avoided by competition. In addition, the scaffolds supported adhesion and proliferation of human skin fibroblasts.

Table 1.1. Main properties of the studied proteins

	Silk fibroin	Keratin	Elastin
Protein	Fibrous	Fibrous	Fibrous
Secondary conformation	β-sheet	α-helix	Tropoelastin (random coil)
Molecular mass (kDa)	Light chains (≈26 kDa) Heavy chains (≈390 kDa)	IFPs (40-60 kDa) Matrix (6-26 kDa)	Tropoelastin (≈72 kDa)
Major residues	Glycine (44%) Alanine (29%) Serine (11%)	Cysteine (9%)	Glycine (32%) Alanine (24%) Proline (12%) Valine (11%)
Source	Silk fibers (silkworm, spider webs, draglines)	Wool, hair, nails, feathers	Connective tissues, ligaments
Solvents	LiBr 9 M, 60 ℃, 4 h $CaCl_2$-CH_3CH_2OH-H_2O, 80 ℃, 2 h	Reducing (DTT), Oxidant agents (H_2O_2)	HO_2CCO_2H KOH

1.4. Wounds and wound healing process

A wound, according to the Wound Healing Society, is the result of “disruption of normal anatomic structure and function” [295]. Based on the nature of the repair process wounds can be classified in acute wounds and chronic wounds. Acute wounds usually heal completely within 8-12 weeks with minimal scaring [296]. The primary causes of acute wounds include mechanical injuries and burns.

Chronic wounds fail to heal in the expected time frame and persist beyond 12 weeks, with the possibility to reoccur. A chronic wound does not heal properly because the orderly sequence of events is disrupted at one or more stages of the healing [297-299]. These types of wounds are produced as a result of specific diseases such as diabetes, tumors and severe physiological contaminations [300, 301]. Chronic wounds include decubitus wounds (pressure sores) and leg ulcers.

1.4.1. Principles of wound healing

Wound healing is a specific biological process related to the general phenomenon of growth and tissue regeneration. There are several reports describing the various biological and physiological stages of healing [300, 302, 303]. Wound healing process can be summarized into five independent and overlapping stages including hemostasis, inflammation, migration, proliferation and maturation (Figure 1.6).These events involve numerous cellular responses, with its respective impact on the healing process, which are described in Table 1.2.

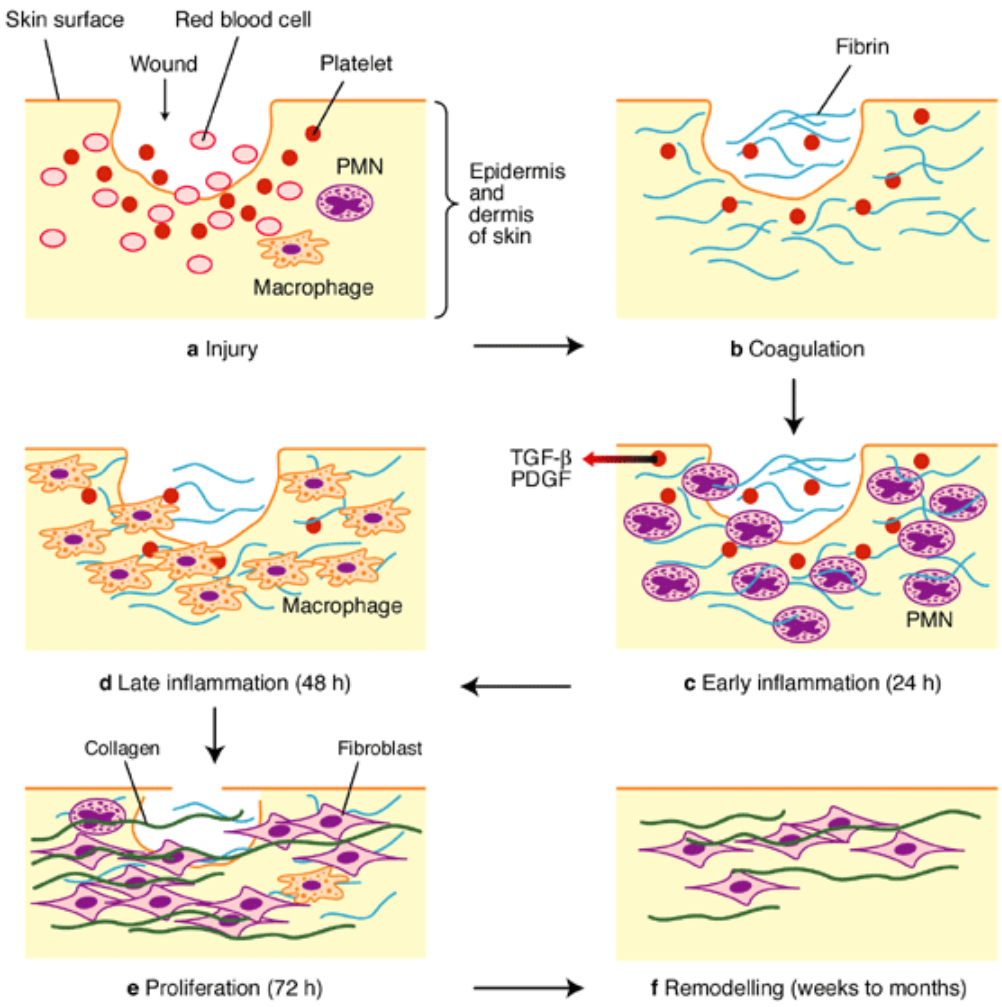

Figure 1.6. The phases of cutaneous wound healing (Reprinted from [304]).

Hemostasis and inflammation

This stage occurs soon after the damage of the skin, which is often accompanied by bleeding. This activates hemostasis through fibrinogen that leads to the coagulation of exudates (blood without cells and platelets) and, together with the formation of a fibrin network, produces a clot in the wound that stops the bleeding. Inflammation occurs almost simultaneously with hemostasis, from within a few minutes to 24 h and lasts for about 3 days, involving both cellular and vascular responses.

Migration

The migration phase involves the movement of epithelial cells and fibroblasts to the injured area to replace damaged and lost tissue. These cells regenerate from the margins, rapidly growing over the wound under the clot followed by epithelial thickening.

Proliferation

This phase occurs almost at the same time or just after the migration. This is characterized by the formation of granulation tissue and collagen is synthesized by fibroblasts giving strength and form to the skin.

Maturation

This phase is also named remodeling phase and involves the formation of cellular connective tissue and strengthening of the new epithelium which determines the nature of the final scar.

Table 1.2. Type of cells involved in the wound healing process

Cell type	Function in wound healing
Platelets	- Involved in thrombus formation - Rich source of inflammatory mediators including cytokines - Major initial stimulus for inflammation
Neutrophils	- First cells to infiltrate the wound - Phagocytosis and intracellular killing of invading bacteria
Monocytes (macrophages)	- Phagocytosis and killing of invading bacteria - Clear debris and necrotic tissue - Rich source of inflammatory mediators including cytokines - Stimulate fibroblasts division, collagen synthesis and angiogenesis
Lymphocytes	- Not clearly defined - May produce cytokines in certain types of wounds
Fibroblasts	- Produce various components of the ECM including collagen, fibronectin, hyaluronic acid, proteoglycans - Synthesized granulation tissue - Help to reorganize the “provisional” ECM

1.4.2. The proteolytic environment of chronic wounds

Wound fluid is a key component in all stages of wound healing, irrigating the wound continuously and keeping it moist [305]. Exudate supplies nutrients and leukocytes to the wound which helps to control bacteria and infection. In chronic wounds there is excessive amount of exudate that can cause maceration of healthy tissue around the wound [306]. In addition, exudate from chronic wounds differs from that of acute wounds with relatively higher levels of tissue destructive proteases namely metalloproteinases (MMPs) and polymorphonuclear elastase (PMN) [307]. Exudate obtained from chronic wounds has shown to contain human neutrophil elastase (HNE), Cathepsin G (CG), urokinase-type plasminogen activator (uPA) and gelatinase (MMP-9) [308, 309]. Herein, it will be described the role of human neutrophil elastase (HNE) in the next section.

1.4.3. Wound dressings

Early humankind employed many different materials from the natural surroundings to treat the wounds. These include natural fibers such as wool and linen, honey, eggs and animal fat [310, 311]. Continuous development result in the development of wound dressings with improved performance. Wound dressings can be classified covering different aspects [312, 313] as follows:

i) Passive dressings such as gauze and tulle that act to cover the wound. Gauze can stick to the wound and disrupt the wound bed when removed thus, are suitable for minor wounds. Tulle is as greasy gauze suitable for minimal to moderate exudates;

ii) Interactive dressings contain polymeric films and foams and hydrogels which are transparent and permeable to water and atmospheric oxygen. These are suitable for heavily exudating wounds (foams and hydrogels) and good barriers against permeation of bacteria to the wound environment;

iii) Bioactive dressings such as hydrocolloids, alginates, collagen and hydrofibers produced from a variety of biopolymers such as collagen, hyaluronic acid (HA), chitosan, alginate and elastin [314, 315]. These types of dressings have the ability to modify facing the physiological condition of the wound promoting the healing. The bioactive normally contain active ingredients such as antimicrobials and antibiotics [316] or, can target the reduction of high proteases levels on the wound [287, 317]. Depending on the wound type and its healing, one or more different types of dressings can be applied. The desirable properties of wound dressings, and their impact on wound healing, are described in Table 1.3.

Table 1.3. Properties of wound dressings and their impact on healing

Properties	Impact on wound healing
Debridement (wound cleansing)	- Enhances migration of leukocytes into the wound bed - Supports accumulation of enzymes
Provide and maintain moist	- Prevents desiccation and cell death - Promotes epidermal migration, angiogenesis and connective tissue synthesis - Supports autolysis by rehydration of desiccated tissue
Absorption (blood and excess of exudate)	- Excessive exudate blocks the proliferation and cellular activity and degrades connective tissue, factors that delay the healing - Causes maceration of healthy tissue surrounding the wound
Permeable (water, vapor, air)	- Permeability to water vapor controls the management of exudate - Low tissue oxygen levels stimulate angiogenesis - High tissue of oxygen stimulates ephitelialization and fibroblasts
Bacterial barrier	- Infection prolongs the inflammatory phase and delays collagen synthesis, inhibits epidermal migration and induces additional tissue damage
Provide thermal insulation	- Normal tissue temperature improves the blood flow to the wound bed and enhances epidermal migration
Low adherence	- Adherent dressings may be painful and difficult to remove causing further tissue damage

1.4.4. Mechanism-based wound dressings

The knowledge of the biochemical events associated with pathogenesis of the chronic wound result in the development of interactive wound dressings with specific activities including the regulation of HNE levels on the wound. Edwards et al. reported the inhibition of elastase by cotton fabric bounded to a synthetic elastase inhibitor [318]. This was assayed in commercial HNE and in a chronic wound exudate and, inhibition with cotton-inhibitor was similar to that obtained with free inhibitor. Incorporation of oleic acid albumin formulations into positively and

negatively charged cotton wound dressings also shown to inhibit HNE under aqueous conditions mimicking the chronic wound [319]. Modification of cotton dressings either by blending with alginate [320] or by phosphorylation [321] and sulfonation [322] also showed to effective on the control of HNE activity. Cotton/ alginate dressings are a suitable matrix for the release of an elastase inhibitor [320]. Phosphorylated cotton wound dressings were prepared to sequester elastase from wound exudate, through a cationic uptake binding mechanism involving salt bridge formation of the positively charged amino acids side chains of elastase with the phosphate counterions of the wound dressing fiber. These had shown to lower elastase activity by 40-80% more effectively than unmodified cotton dressings [321]. Other dressings such as collagen, oxidized regenerated cellulose (ORC) and blends of collagen/ORC have shown to bind and inactivate HNE. HNE binds to collagen by electrostatic interactions and, the negatively charged groups of ORC interact with the arginine side chains of HNE [323]. PROMOGRAN is a commercial available interactive wound dressing composed of collagen and ORC that physically modifies the wound microenvironment, and thereby promotes granulation tissue formation and stimulates wound repair [324]. Recognition sequences of elastase, Val-Pro-Val, were applied to cotton dressings with Gly used as a linker of the recognition sequence to the cotton cellulose. Solutions of elastase that were treated with Val-Pro-Val-Gly cellulose cotton gauze, demonstrated reduced elastase activity. This study demonstrates the use of elastase recognition sequences as sequestering agents of elastase when attached to cotton fibers and constitutes a model for the design of peptide-cellulose analogs in dressing fibers for chronic wounds [325]. Recently, silk fibroin/keratin films incorporating a small peptide HNE inhibitor, based on the reactive-site loop of Bowman-Birk inhibitor (BBI) protein, have shown to reduce elastase activity through the controlled release of inhibitor from the films [326].

1.5. Human neutrophil elastase (HNE)

Human neutrophil, or leukocyte, elastase (HNE, HLE) is a serine-protease of the chymotrypsin family stored in the azurophilic granules of polymorphonuclear neutrophils (PMNs). The serine proteases are characterized by the presence of a serine group in their active site [327] that is completed by histidine (His) and

aspartic acid (Asp) amino acids. These residues are widely separate in the primary sequence but are brought together at the active site of the enzyme in its tertiary structure. By convention, the catalytic triad for chymotrypsin-like serine proteases is numbered as Asp^{102}, Ser^{195}, His^{57} (Figure 1.7).

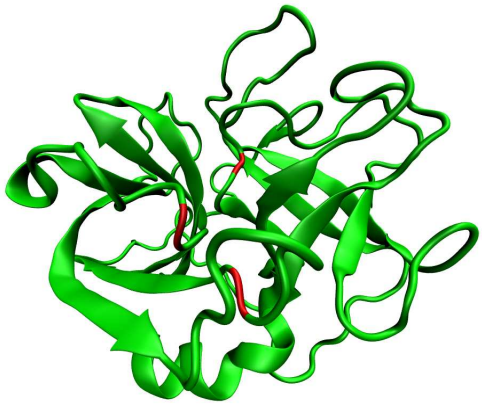

Figure 1.7. Ribbon representation of the three-dimensional structure of HNE (PDB code 1B0F). The side chains of the amino acids of the catalytic triad are shown in red.

The hydrolysis by serine proteases follows and acylation-deacylation mechanism (Figure 1.8). The first step of the catalytic reaction, after the formation of the enzyme-substrate or Michaelis complex, is the acylation step; that starts with the attack of the catalytic serine on the carbonyl group of the cleavable amide bond and the transfer of the hydroxyl hydrogen of the serine to the histidine (1). This leads to the release of the C-terminal end of the substrate and the formation of a covalent intermediate (i.e. the acyl enzyme) between the enzyme and the N-terminal part of the substrate (2). The second step of the reaction (termed deacylation) starts with the attack of a nucleophilic water on the substrate carbonyl and (3) ends with the release of the N-terminal part of the substrate, when the catalytic triad is regenerated (4). The nitrogen atoms of residues Gly193 and Ser195 stabilize the so-called oxyanion hole.

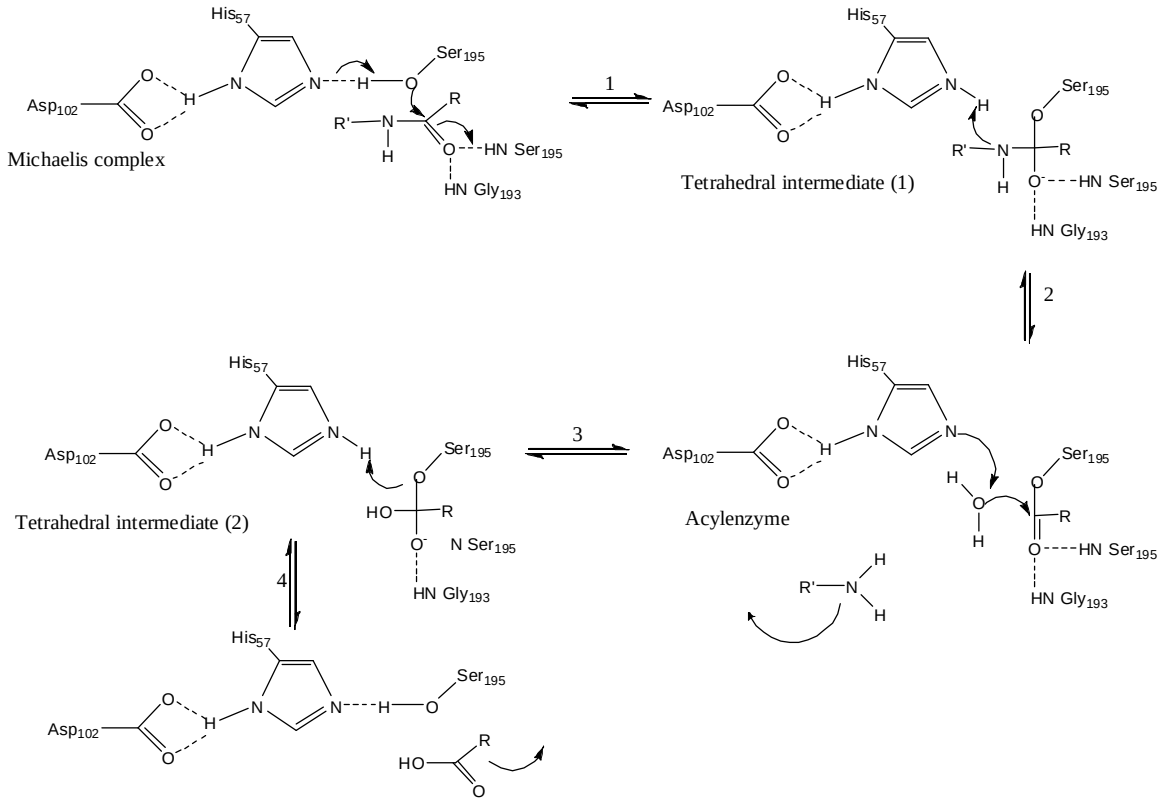

Figure 1.8. Reaction mechanism of serine proteases.

The nomenclature for describing the interaction of a substrate with a protease was introduced by Schechter and Berger in 1967 [328]. In this system, the binding site for a polypeptide substrate on a protease is visualized as a series of subsites, where each subsite interacts with one amino acid of the substrate. The substrate amino acid residues are called P (for peptide) and, the subsites in the protease are called S (for subsite). S subsites on the protease accommodate P residues in the substrate N-terminal side upstream of the scissile bond whereas, S' subsites accommodate P' residues on the substrate C-terminal side, downstream of the cleavage site.

X-ray analysis of the complex between HNE and natural and synthetic substrates [329-331] indicated that S_1-S_4 pockets are mostly made of hydrophobic amino acids [332, 333]. For this reason, substrates with small, hydrophobic side chains at P_1 are effectively cleaved by HNE with the preference for valine (Val) over alanine (Ala) or phenylalanine (Phe). Substrates with isoleucine (Ile) [334] and methionine (Met) can also be cleaved but, oxidation of Met decreases the affinity of HNE [335]. The activity of HNE increases with the length of synthetic substrates,

indicating that HNE has an extended substrate binding site [329, 336]. Consequently, HNE substrate specificity depends not only on the nature of the P_1 amino acid, but also on secondary interactions with S and S' subsites. The main characteristics of HNE are resumed in Table 1.3.

Table 1.3. Characteristics of human neutrophil elastase

Properties	HNE
Length	218 residues
Molecular mass (kDa)	29-33
Isoelectric point (pI)	≈10.5
Nº. glycosylation sites	2
Nº. disulfide bridges	4
Optimal pH	8.0-8.5
Substrate specificity	Small hydrophobic residues at P_1 (Val, Ala, Met, Ile, Leu, Ser)
Source	Neutrophil, monocyte, mastocyte, eosinophil
Endogenous inhibitors	α_2-Macroglobulin α_1-PI/MNEI/PI9 SLPI/Elafin/pre-elafin

1.5.1. Biological functions

HNE is expressed by neutrophils (PMNs), blood borne phagocytic cells, which act as a first line of defense against invading pathogens [337]. However, when the activity of neutrophil-derive proteases is excessive and/or prolonged, they can mediate tissue damage associated with chronic inflammatory diseases such as periodontal disease, rheumatoid arthritis, adult respiratory distress syndrome,

cystic fibrosis and chronic wounds [309, 338, 339]. HNE has broad substrate specificity capable of degrading the components of the extracellular matrix (ECM), remodeling damage tissues and can facilitate neutrophil migration into or through tissue [340]. HNE may also degrade critical soluble factors such as platelet-derived growth factor [341, 342] and cell surface receptor proteins [343-345]. HNE regulates inflammatory responses: induces degradation of cytokines, degrades chemokines, stimulates macrophages and inhibits lymphocyte migration [346, 347].

In an acute wound environment, the activity of HLE is regulated by endogenous inhibitors of the serpin (α_1-PI, MNEI, PI9), chelonianin (SLPI, elafin) families, and to a lesser extent by the polyvalent protease inhibitor α_2-macroglobulin. The serpins are high molecular weight inhibitors (40 to 50 kDa: 350-500 amino acids) that fold into a conserved, metastable structure and act as suicide substrate-like inhibitors using their reactive centre loop (RCL) [348, 349]. The exposed serpin reactive centre loop acts as a pseudosubstrate for the target protease forming a reversible, non-covalent Michaelis complex. Conformational changes results in the entrapment of the covalent inhibitory complex in which both molecules are inactivated. During infection and /or high levels of HNE the activity of these inhibitors is supplemented by the activity of secretory leukocyte protease inhibitor (SLPI, 11.7 kDa) and elafin (9.9 kDa) that are non-glycosylated proteins, produced by epithelial cells and cells of the immune system. In chronic wounds the continuous activation of inflammatory cells is followed by the release of large quantities of proteases which inactivate the inhibitor defense. Therefore, there has been considerable interest in the design of HNE inhibitors that may restore the normal levels of this enzyme in the above diseases. In addition to natural or engineered inhibitors proteins with high molecular masses, it was observed an increase in the research of both peptide-based and non-peptide small inhibitors compounds [350].

1.6. Bowman-Birk Inhibitor (BBI)

The Bowman-Birk inhibitors (BBI) are bi-headed serine proteinase inhibitors found in various plants of the Fabaceae family [351]. These were first isolated from soybean by Bowman [352] and then characterized by Birk [353]. These proteins

have a low molecular weight (6 – 9 kDa) and are characterized by the presence of seven disulphide bridges which allow the formation of a symmetrical structure comprising two independent heads located at opposite sides of the molecule (Figure 1.9). Each head is made of a tricyclic domain in which the functional reactive site loop is located. Loop I typically inhibits trypsin and loop I' chymotrypsin [354-357].

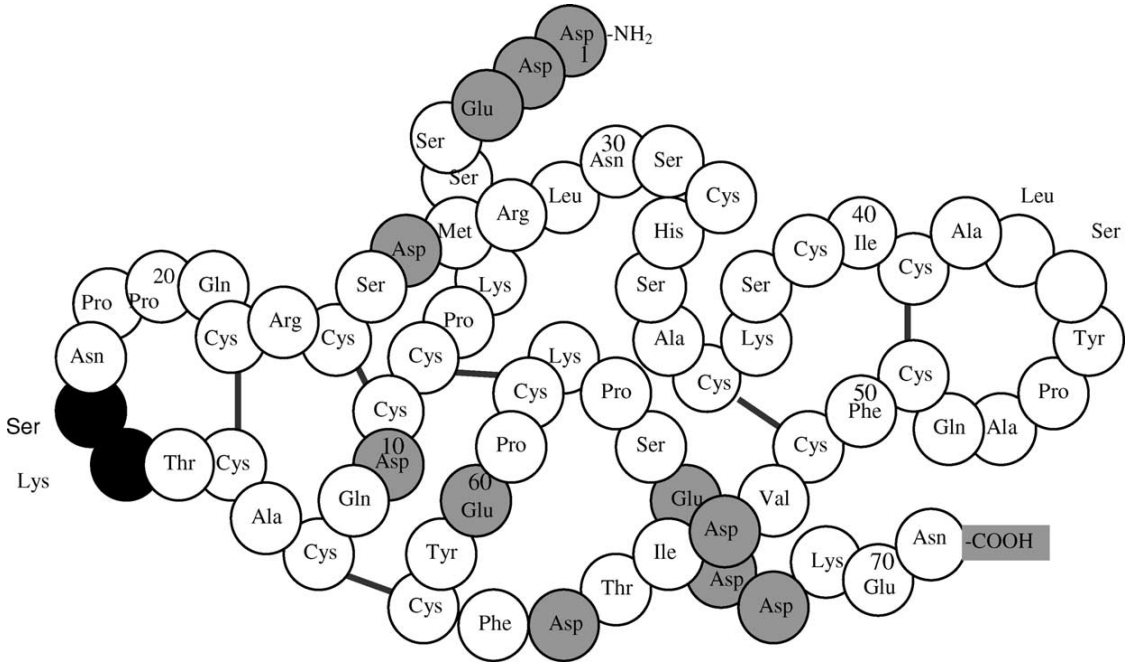

Figure 1.9. Complete covalent structure of the Bowman-Birk inhibitor protein (assumed from Birk [358]). Amino acids at the trypsin-inhibitory site are shown as solid black circles and, the amino acids at the chymotrypsin-inhibitory site are shown as white circles; available carboxylic acid moieties are marked in grey.

The interaction of BBI with serine proteases occurs via a well-defined disulfide linked short beta-sheet region which generates a non-covalent complex that renders the serine protease inactive [359]. The conformation of the reactive site loop is complementary to the active site of the protease inhibited and allows BBI to bind tightly to the protease [354]. Upon complex formation between BBI and protease, BBI is cleaved very slowly [360]. The inhibition kinetics of human neutrophil elastase (HNE) by BBI occurs in two steps: the first step involved a rapid interaction between BBI and HNE to form BBI-HNE complex with a inhibition constant (K_i) of 28 nM, and in the second step the BBI-HNE complex underwent a

slow conversion/rearrangement to a tighter-binding BBI-HNE complex with a K_i of 2.3 nM [361]. BBI-derived synthetic peptides have previously demonstrated to retain the inhibitory activity of the complete protein [359, 362, 363]. The structure of the peptides is based on the short disulfide bonded β-hairpin motif that forms the reactive site loop of the BBI protein. This loop adopts the same conformation as that of a bound peptide substrate [364, 365]. The primary contact region contains the scissile peptide bond P_1-P_1'. The specificity of the inhibition depends on the sequence of the reactive site, with P_1 residue dominating the specificity which typically reflects the substrate preference of the target enzyme [366, 367]. Figure 1.10 represents the typical amino acid sequence of the nine-residue loop disulfide-linked of BBI.

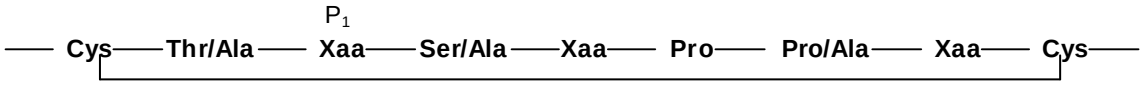

Figure 1.10. The amino acid sequence of the core disulfide-linked reactive site sequence form BBI. X_{aa} represents any amino acid.

In order to retain the canonical inhibition motif, there are some structural requirements for BBI-peptides. These include covalent cyclization given by the disulfide bond at P_3-P_6'. Removal of this bond resulted in loss of inhibition [368-370]. A *cis*-Pro (*cis*-proline) in the P_3' position which is absolutely conserved in all BBI proteins [371]. Finally, an extensive intramolecular hydrogen-bond network given by, the main-chain to main-chain hydrogen bond between P_2 and P_1', which is instrumental in projecting the P_1 side-chain outwards for the primary interaction with the enzyme [371]. BBI-peptides were further optimized for the inhibition of HNE using a combinatorial approach [362]. A peptide library was created with variations at P_4, P_1 and P_2' and, the consensus sequence had norleucine (Nle), alanine (Ala) and isoleucine (Ile), respectively, with a K_i of 65 nM [362]. BBI peptides are competitive inhibitors because they bind in the same manner as substrates. They are generally slowly hydrolyzed by the enzymes they inhibit [372]. The susceptibility to hydrolysis is sequence dependent and does not correlate with inhibitory potency [362, 370, 371, 373, 374]. Hydrolysis of the peptides results in the loss of inhibitory activity [368].

1.7. Final remarks and research objectives

This review has considered the different types of wounds and the effective parameters of healing process. Wounds can be classified in acute that heal in the expected time frame and chronic wounds, which fail to heal because the orderly sequence of events is disrupted at one or more stages of the healing process. Exudates from chronic wounds have shown to contain high levels of destructive proteolytic enzymes such as metalloproteases and human neutrophil elastase, which can delay the healing and cause maceration of healthy tissue around the wound. These enzymes are normally regulated by endogenous inhibitors that are inactivated by high levels of proteolytic enzymes. Therefore, there is a concern for the development of new inhibitors that can be applied to chronic wounds. Furthermore, wound dressings with this specific action have also been developed.
Fibrous proteins such as silk fibroin, keratin and elastin have the ability to self-assemble into various physical states. These have shown to undergo materials with improved mechanical strength, control of morphology and surface modifications options, allowing their application in controlled delivery systems and tissue engineering. Furthermore, wounds treated with these materials have shown to promote the healing by enhanced cellular proliferation, growth and differentiation and, reduced inflammation when applied to *in vivo* models.

The aim of this work, based on these exceptional characteristics, was the development of new protein materials to be used as wound dressings with the specific target of controlling high levels of elastase found on chronic wounds. Protein dressings (films and scaffolds) were developed by blend systems: silk fibroin/keratin and, for the first time, silk fibroin/elastin. The reduction of elastase levels was accomplished by the incorporation of new elastase inhibitors peptides into the materials. The physical, chemical and biofunctional properties of these materials were evaluated in the context of wound healing needs.

CHAPTER II

Materials and Methods

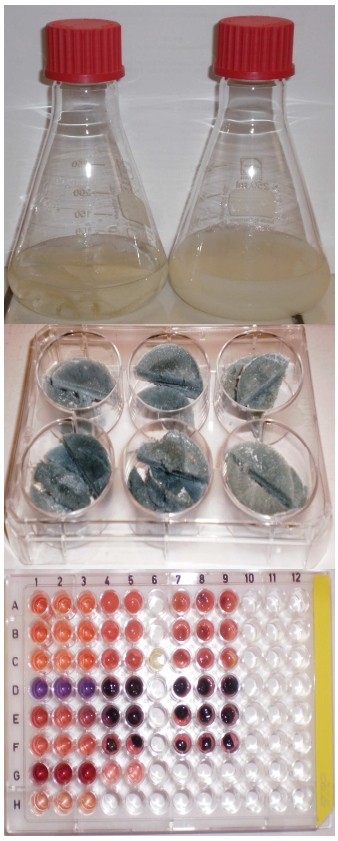

CHAPTER II

Materials and methods

2.1. Materials

Silk cocoons from *Bombyx mori* were donated from “Sezione Specializzata per la Bachicoltura” (Padova). Wool fabric was provided by Albano Antunes Morgado Lda (Portugal).

2.2. Reagents

Unless otherwise stated, all the chemical reagents used in the experimental results were purchased from Sigma-Aldrich (Spain). They presented analytical purity and were not submitted to further purification.
The inhibitor peptides used herein were synthesized by JPT Peptide Technologies GmbH (Germany). The NIH 3T3 cell line (mouse embryonic fibroblasts) was purchased from the European Collection of Cell Cultures (ECACC) and BJ5ta cell line (telomerase-immortalized human normal skin fibroblasts) was purchased from the European Collection of Cell Cultures (ECACC). Wound exudate was kindly supplied by Technical University of Graz (Austria).

2.3. Preparation of stock solutions

2.3.1 Silk fibroin

Silk fibroin (SF) was purified from its sericin content as previously described [15]. The cocoons were cut, cleaned from debris and larvae and autoclaved for 30 minutes at 120 ℃. SF was then thoroughly washed wi th distilled water and dried overnight at room temperature. SF solutions were prepared by dissolving degummed silk fibers in 9.6 M lithium bromide (LiBr) solution at 60 ℃ for 3 h. The resulting solution was filtered, and dialyzed against distilled water until complete removal of salts, using cellulose tubing (molecular-weight cut-off of 12000-14000 Da). The regenerated silk fibroin solution was either stored at 4 ℃ or freeze-dried.

2.3.2. Keratin

Lipids were removed from wool fabric using an organic solvent extraction procedure. Wool fabric was cut in small pieces and incubated with ethanol 100% (CH_3CH_2OH) 1:20 (w/v) for 2 h, with agitation, at room temperature. The supernatant was removed and a mixture of 1:2 (v/v) methanol/chloroform ($CH_3OH/CHCl_3$) was added to the fabric. This mixture was incubated 24 h, with agitation at room temperature. The delipided wool fabric was washed and dried for further applications. Two solvent systems were used for the extraction of keratin. They will be explained here and, the type of extraction used will be stated in further sections. **1.** Keratin (K) solutions were prepared by immersing delipided wool in a solution containing 8 M urea (NH_2CONH_2), 0.2 M sodium dodecyl sulfate (SDS, $CH_3(CH_2)_{11}OSO_3Na$) and 0.5 M sodium disulfite ($Na_2S_2O_5$). The mixture was heated to 100 ℃ for 30 min. **2.** Delipided wool was dissolved in a solution containing 0.1 M Tris-HCl buffer (Trizma/Hydrochloric acid, $NH_2C(CH_2OH)_3$/HCl), pH 9.0, 8 M urea and 0.1 M DL-dithiothreitol (DTT, $HSCH_2CH(OH)CH(OH)CH_2SH$) at 50 ℃ for 24 h in a shaker bath. The solutions were filtered and dialyzed against distilled water using cellulose tubing (molecular-weight cut-off of 12000-14000 Da). The regenerated keratin solutions were either stored at 4 ℃ or freeze-dried.

2.4. Preparation of blended systems

2.4.1. Films

Protein films were prepared by blends of silk fibroin and keratin (SF/K) by solvent cast evaporation. Keratin and silk fibroin solutions (10 ml of final volume) were blended in the ratios of 80/20, 60/40 and 40/60 of SF/K. The blends were cast in plastic Petri dishes with a circular area of about 40 cm^2 and dried at room temperature. The controls are 100SF and 100K.

Freeze-dried keratin and silk fibroin were dissolved in formic acid (HCOOH) to prepare 1% (w/v) solutions. The solutions were blended in the ratios of 75/25, 50/50 and 25/75 of SF/K. The blends were cast in plastic Petri dishes with a circular area of about 40 cm^2 and dried at room temperature. The controls are 100SF and 100K. The resulting films were 0.03 mm in average thickness.

In order to induce the transition of SF from random coil to β-sheet structure and consequently insolubility, the films were immersed in 90% (v/v) methanol solution for 30 minutes and then washed in distilled water and air dried. Unless otherwise stated, all films used were submitted to this treatment.

2.4.2. Scaffolds

Protein scaffolds were prepared by blending silk fibroin with soluble elastin (SF/EL) and subsequently lyophilized. Soluble elastin (EL) from bovine neck ligament was dissolved in distilled water to prepare EL solution. SF and EL were mixed to prepare blends of 100/0 SF/EL, 80/20 SF/EL and 50/50 SF/EL. The solutions were cast on 96-well plates and frozen at -20 ℃ for 2 days and freeze dried for 2 days to remove the solvent completely. To induce the transition of SF from random coil to β-sheet structure and consequently insolubility, sponges were immersed in 90% (v/v) methanol solution for 30 minutes and then washed in distilled water and air dried. Unless otherwise stated, all scaffolds used were submitted to this treatment.

2.4.2.1. Crosslinking reaction

SF/EL scaffolds were further crosslinked with Genipin (GE, $C_{11}H_{14}O_5$). Genipin is obtained from geniposide, via enzymatic hydrolysis with β-glucosidase. Geniposide is isolated from the fruits of *Genipa Americana* and *Gardenia jasminoides Ellis*, and constitutes for about 4-6% of dried fruit. Earlier studies indicated the formation of dimmers of genipin in the presence of glycine, which suggested that genipin could be used to covalent crosslink of proteins containing primary amines [375]. Since then it has been used to crosslink collagen [376], gelatin [377], chitosan [378] and silk fibroin [45, 294]. The major advantage of genipin is a lower cytotoxicity when compared to the widely used glutaraldehyde ($OHC(CH_2)_3CHO$) [379, 380]. The mechanism of interaction of genipin with proteins is similar to that observed for amino-group containing compounds (Figure 2.1). This reaction starts with an initial nucleophilic attack to the C3 carbon of genipin from a primary amine to form an intermediate aldehyde group. The opening of the dihydropyran ring is followed by the attack on the resulting

aldehyde group by the secondary amine formed in the first step of the reaction. A heterocyclic compound of genipin linked to both lysine and argine residues of SF and elastin is formed. An inherent phenomenon of genipin crosslinking is the formation of blue pigments obtained by the oxygen radical-induced polymerization of genipin, and dehydrogenation of the intermediate compounds, resulting from the ring-opening of genipin [381, 382].

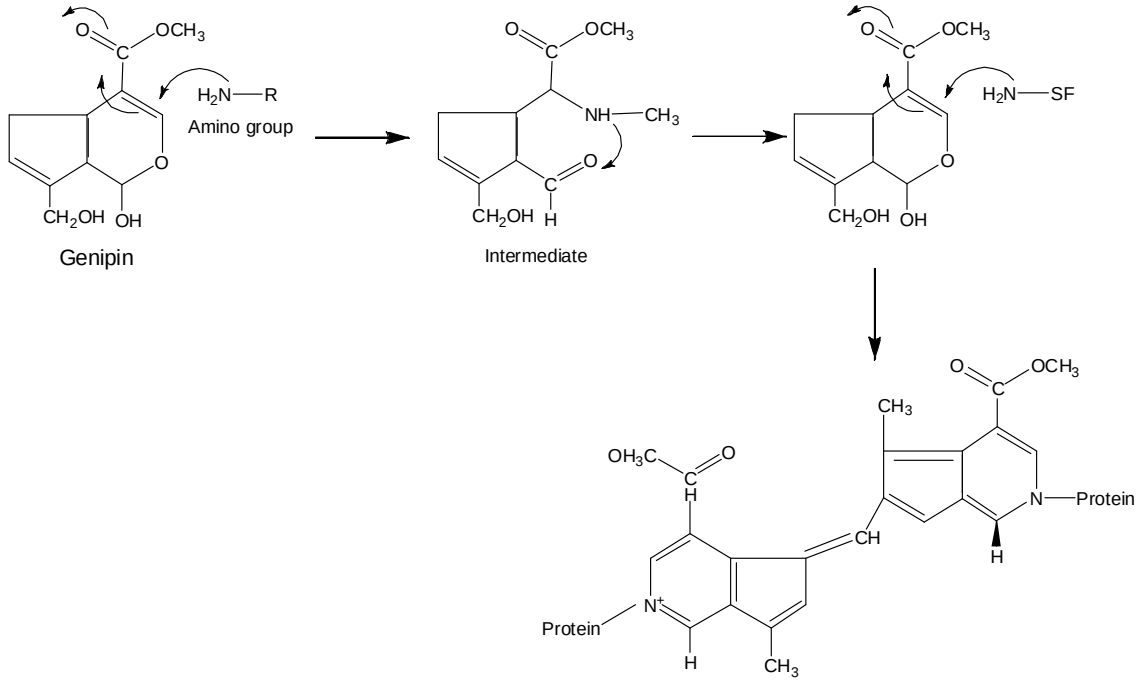

Figure 2.1. Crosslinking reaction of genipin with biopolymers containing free amine groups (NH_2).

2.4.2.2. Degree of crosslinking

The cross-linking degree was determined by the ninhydrin ($C_9H_6O_4$) assay [383, 384]. The reaction of ninhydrin with primary amino groups forms a purple dye named Ruhemann's purple (λ=570 nm, ε=22000) [383]. The reaction involves a nucleophilic-type displacement of an OH group of ninhydrin hydrate by a nonprotonated amino group. The products of the reaction are carbone dioxide and an aldehyde.

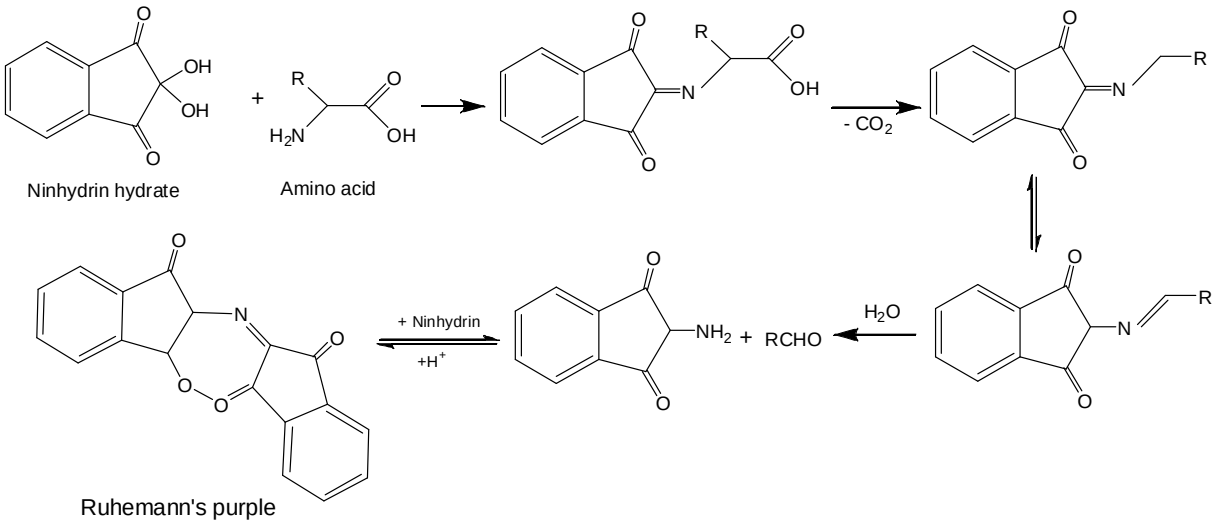

Figure 2.2. Mechanism of reaction of ninhydrin with compounds containing free amine groups (NH_2).

The concentration of free amine (NH_2) groups in the sample was determined from a standard curve of glycine (NH_2CH_2COOH) concentration vs absorbance. SF/EL scaffolds prepared without genipin were used as control materials. The degree of crosslinking was determined by equation 2.1.

$$Degree\,of\,crosslinking\,(\%) = \frac{[(NH_2)_{nc} - (NH_2)_c]}{(NH_2)_{nc}} \times 100$$

Equation 2.1. Degree of crosslinking where"nc" and "c" are respectively, the mole fraction of free NH_2 in non crosslinked and crosslinked samples.

2.5. Characterization techniques

2.5.1. Amino acid analysis

The amino acid composition of silk fibroin, keratin and elastin samples was determined after acid hydrolysis with 6 N HCl, at 105 ℃ for 24 h, under vacuum. Free amino acids analyzed by HPLC according to the AccQ-Tag Method (Waters). The eluate was detected at 254 nm. Samples were analyzed in duplicate (error: ± 2 %). The quantitative amino acid composition, expressed as mol % for each

amino acid, was determined by external standard calibration (Amino Acid Standard H, Pierce).

2.5.2 SDS-PAGE

SDS-PAGE was carried out using the Mini-PROTEAN 3 Cell system from Bio-RAD. The resolving gels (15 % acrylamide of about 0,75 mm thickness) were run at a constant voltage (170 V) and prepared according to the method described by Laemmli [385]. Proteins were visualized by Coomassie Brilliant blue G 250 staining using Phosphorylase b (97 kDa), Albumin (66 kDa), Ovalbumin (45 kDa), Carbonic Anhydrase (30 kDa), Trypsin inhibitor (20.1 kDa) and α-lactalbumin (14.4 kDa) for calibration.

2.5.3. Fourier transform infrared (FT-IR) spectroscopy

FT-IR spectra of SF/K films were measured with a Nicolet FT-IR Nexus spectrometer (Thermo Scientific), equipped with a ZnSe ATR cell (Smart Performer). FT-IR spectra of SF/EL scaffolds were measured with a Perkin-Elmer (Spectrum One FTIR) spectrometer with a ZnSe ATR cell. When stated, deconvolution of Amide I band was performed using Origin software (OriginLab Corporation, MA, USA).

2.5.4. Differential scanning calorimetry (DSC)

Thermal analysis was performed to both SF/K films and SF/EL scaffolds with a DSC-30 instrument (MettlerToledo), from room temperature to 120 ℃, at a heating rate of 10 ℃/min, and kept at 120 ℃ for 10 min, t o induce dehydration of samples. The temperature was lowered to room temperature and increased to 500 ℃ at a heating rate of 10 ℃/min. Sample weight was 2-3 mg . The open aluminum cell was swept with N_2 during the analysis.

2.5.5. Mechanical properties

The tensile properties of the SF/K films were determined using a tensile testing machine Instron dynamometer 5500. SF/K films strip with 1 cm width were measured using an Instron dynamometer 5500, with a 30 mm gauge length at a crossbar rate of 15 mm/min, corresponding to strain rate of $1.0\times10^{-2}.s^{-1}$.Tensile force was taken as the maximum force in the force deformation curve. Tensile modulus was estimated from the initial slope of the stress–strain curve. The values reported were the average of at least three specimens.

2.5.6. Atomic force microscopy (AFM*)*

Surface analysis of the SF/K films was performed in tapping mode using a Nanoscope III scanning probe microscope controller (Multimode Digital Instruments) with a silicon probe (RTESP14, Veeco). Root mean square (RMS) roughness data were collected from each sample according to manufacture instructions.

2.5.7. Scanning electron microscopy (SEM)

SEM analysis was performed on SF/EL scaffolds. Cross-sections were prepared by cutting the SF/EL samples with a razor blade in liquid nitrogen. Before analysis, the scaffolds were coated with gold and examined morphologically using a NOVA Nano SEM 200 FEI. The morphology was determined for SF/EL scaffolds with and without methanol treatment.

2.5.8. Mass spectrometry

Mass spectrometry analysis was performed to determine the hydrolysis rate of the inhibitor peptide by porcine pancreatic elastase (PPE). Mass spectra were obtained using a LxQ MS Detector, Thermo Electron Corporation. Samples were dissolved in methanol and ionized by Electrospray Ionization (ESI). The scan range was from *m*/*z* 100 to 2000 in positive-ion mode.

2.6. Swelling ratio

Swelling ratio was determined to both SF/K films and SF/EL scaffolds. Dried films and scaffolds (60 ℃ for 24 h), methanol treated, were immersed, respectively, in 100 mM Tris-HCl buffer, pH 8.0 and phosphate buffered saline (PBS) buffer (pH 3.0; 7.4 and 11) at 37 ℃ for 24 h. The excess of buffer was removed and the wet weight of the film was determined. The swelling ratio of the samples was calculated by equation 2.2.

$$Swelling\ ratio = \frac{W_S - W_d}{W_d}$$

Equation 2.2. Swelling ratio where W_S is the mass of the swollen material and W_d is the initial dry mass.

2.7. *In vitro* degradation

The biological degradation of SF/K films was determined using Trypsin from porcine pancreas and porcine pancreatic elastase (PPE) and, for SF/EL sponges, PPE and wound exudate were used. Dried (60 ℃ for 24 h) and methanol treated materials were incubated with respective enzyme solutions, for several days, at 37 ℃. Solutions were changed and collected daily. Control samples were incubated in the buffer solutions without enzyme and submitted to the same conditions. At designated time points, samples were washed thoroughly with distilled water, dried in a desiccator, and weighed to estimate the extent of degradation by equation 2.3.

$$Weight\ loss\ (\%) = \frac{m_0 - m_f}{m_0} \times 100$$

Equation 2.3. Weight loss where m_0 is the initial dry mass of the sample and, m_f is the final dry mass.

2.8. Cytotoxicity evaluation

2.8.1. Cell culture

The NIH 3T3 cell line (mouse embryonic fibroblasts) was maintained in Dulbecco's Modified Eagle's Medium (DMEM) supplemented with 10% (v/v) of fetal bovine serum (FBS) inactivated (20 min. at 56 ℃) and 1% (v/v) of Penicillin/Streptomycin (PS; 10,000 units/ml penicillin and 10,000 μg/ml streptomycin), all supplied by Gibco. The cells were maintained at 37 ℃ in a humi dified atmosphere of 5% CO_2. The medium was refreshed every 2 to 3 days. At pre-confluence, cells were harvested using trypsin (0.25% (w/v) trypsin, 0.1% (w/v) glucose and 0.05% (w/v) ethylenediaminetetraacetic acid – EDTA – in phosphate-buffered saline solution (PBS)).

The BJ5ta cell line (normal human skin fibroblasts) was maintained according to ATCC recommendations (4 parts Dulbecco's Modified Eagle's Medium (DMEM) containing 4 mM L-glutamine, 4.5 g/L glucose, 1.5 g/L sodium bicarbonate, and 1 part of Medium 199, supplemented with 10% (v/v) of fetal bovine serum (FBS), 1% (v/v) of Penicillin/Streptomycin solution and 10 μg/ml hygromycin B). The cells were maintained at 37 ℃ in a humidified atmosphere of 5% CO_2. Culture medium was refreshed every 2 to 3 days.

2.8.2. Cytotoxicity by indirect contact

SF/K films: Discs (ϕ=8mm) were punched out of the films with skin biopsy punches (Acu-Punch, USA) and sterilized by immersion in serial dilutions of ethanol (90%, 70% and 50% v/v) for 15 min, then hydrated and rinsed with PBS. The extracts were obtained by the incubation of the membranes in 2 ml of Dulbecco's Modified Eagle's Medium (DMEM) supplemented with 1% (v/v) PS in an orbital incubator at 37 ℃ for either 24 and 72 h at 180 rpm. At the end of these time points, the membranes were removed and the extracts were obtained. Before use, the extracts were supplemented with 10% (v/v) FBS and subsequently, serially diluted (100%, 50%, 25% and 10% (v/v)) in complete culture medium. A sample of the extract vehicle subjected to the same extraction conditions was used as a negative control, whereas a 1% (v/v) solution of Triton X-100 (Sigma) prepared in fresh

culture medium was used as a positive control. Cells seeded at a density of $5x10^3$ cells/200 µl/well on 96-well tissue culture polystyrene (TCPS) plates (Greiner Bio-one) were exposed to the serial dilutions of the extracts and incubated at 37 ℃ in a humidified atmosphere of 5% CO_2. At the end of each culture period (24 and 72 h) the cell viability was assessed using a resazurin based assay. Medium containing extract was refreshed ever 24 h of contact with the cells.

SF/EL scaffolds: Scaffolds (ϕ=3 mm and 6 mm thickness) were sterilized by immersion in ethanol 70% for 30 min, then hydrated and rinsed with PBS. The extracts were obtained by the incubation of the scaffolds in 1 ml of DMEM in a CO_2 incubator at 37 ℃ for 5 days. At the end, the materials were removed and the extracts were obtained. Before use, the extracts were filtered to remove degraded material and, subsequently, diluted (100%, 50% (v/v)) in complete culture medium. A sample of the extract vehicle subjected to the same extraction conditions was used as a negative control, whereas a 1% (v/v) solution of Triton X-100 (Sigma) prepared in fresh culture medium was used as a toxicity positive control.

Cells were seeded at a density of $20x10^3$ cells/100 µl/well on 96-well tissue culture polystyrene (TCPS) plates (TPP, Switzerland) the day before experiments and then exposed to extracts and incubated at 37 ℃ in a humidified atmosphere with 5% CO_2. At the each time point (24, 48 and 72 h) the cell viability was assessed using the Alamar Blue assay (alamarBlue® Cell Viability Reagent, Invitrogen).

2.8.3. Cytotoxicity by direct contact

SF/K films: Discs, prepared and sterilized as previously described (ϕ=14mm), were gently place in 24-well TCPS plates (Greiner Bio-one) and fixed with sterilized silicone rings (o-rings) with a 12 mm internal diameter (Epidor, Spain). The discs were let to dry overnight in a laminar flow hood. Prior to cell seeding, discs were equilibrated in PBS and subsequently in DMEM with 1% v/v PS (37 ℃ for 1 h). $2x10^4$ cells/ml/well were seeded and cultured for 24, 48 and 72 h. TCPS in the presence of the o-rings were used as control. Medium was refreshed daily. After each incubation periods, cell proliferation was determined quantitatively using the resazurin based assay and cell morphology was assessed using F-actin fluorescent labelling.

Peptides: Cells were seeded at a density of $10x10^3$ cells/100 µl/well on 96-well tissue culture polystyrene (TCPS) plates (TPP, Switzerland) the day before experiments and then exposed to different peptide concentrations added to fresh culture medium. At 24 and 48 h of exposure, cell viability was determined using the MTS assay (CellTiter 96® Non-Radioactive Cell Proliferation Assay, Promega, EUA).

2.9. Cell viability and proliferation assays

2.9.1. Resazurin assay

Resazurin is a blue, non fluorescent molecule that is reduced by several mitochondrial and cytoplasmic enzymes to a pink fluorescent product, called resorufin. 10% (v/v) of resazurin solution (0.1 mg/ml, in PBS) was added to each well. After 4 h of incubation at 37 ℃, 200 µl of the medium was transferred into a black walled 96-well plate (Greiner Bio-one) and fluorescence was measured in a microplate reader (Spectra Max Gemini XS – Molecular devices) at excitation and emission wavelengths of 530 nm and 590 nm, respectively.

2.9.2. Alamar blue assay

Resazurin, the active ingredient of alamarBlue® reagent, is a non-toxic, cell permeable compound that is blue in colour and reduced to resorufin, red colour compound, by viable cells. 10 µL of alamarBlue® reagent were added to each well containing 100 µL of culture medium. After 4 h of incubation at 37 ℃ the absorbance at 570 nm was measured, using 600 nm as a reference wavelength, in a microplate reader (Spectramax 340PC). The quantity of resorufin formed is directly proportional to the number of viable cells.

2.9.3. MTS assay

MTS assay (CellTiter 96® Non-Radioactive Cell Proliferation Assay, Promega, EUA). MTS tetrazolium compound (3-(4,5-dimethylthiazol-2-yl)-5-(3-carboxymethoxyphenyl)-2-(4-sulfophenyl)-2H-tetrazolium) is a coloured formazan

substrate which is converted by several mitochondrial and cytoplasmic enzymes in viable cells into a soluble, pink fluorescent product. 20 µL of MTS compound were added to each well containing 100 µL of culture medium. After 4 h of incubation at 37 ℃ the absorbance at 490 nm was measured in a microplate reader (Spectramax 340PC). The quantity of formazan formed is directly proportional to the number of viable cells

2.9.4. F-actin fluorescent labelling

After each incubation period, the samples were rinsed with PBS and fixed with 4% (w/v) *p*-formaldehyde in PBS for 10 min. After washing with PBS, cells were permeabilized with 0.1% (v/v) Triton X-100 (Sigma) in PBS for 10 min and then washed three times with PBS. Cell cytoskeletal filamentous actin (F-actin) was visualized by treating the cells with 5 U/mL Alexa Fluor® 488 phalloidin (Molecular Probes) for 20 min in the dark. Cells were then washed three times with PBS and cell nuclei were counterstained with 4,6-diamidino-2-phenylindole (DAPI) dye. Cells were examined using an inverted fluorescent microscope (Axiovert 200M, Zeiss, Germany).

2.11. *In vitro* release

The release of model compounds from SF/K films and SF/EL scaffolds was evaluated by the incorporation of FITC-BSA and Trypan-blue. Detailed information will be given in further sections. The resulting materials incorporating model compounds were incubated with enzymes and buffer solutions at 37 ℃ for several days. Solutions were changed every day. At determined time points, aliquots were taken and fluorescent and absorbance measurements were conducted. After each measurement, the samples were added back to the medium to restore the equilibrium conditions. FITC-BSA release was monitored by a multiplate reader (Synergy HT W/TRF from BioTek) in the fluorescence mode at emission wavelength of 490 nm. Trypan-blue release was determined by measuring the absorbance at 595 nm using a Heλios γ ThermoSpectronic spectrophotometer. The quantification of the release was established by a standard curve of both dyes.

2.11.1. Release kinetics

The release behaviour of compounds from polymeric systems can be determined by fitting the release data to the empirical relationship given by Ritger-Peppas equation [386].

$$\frac{M_t}{M_\infty} = kt^n$$

Equation 2.4. Ritger-Peppas equation.

M_t/M_∞ is the fractional drug release at time t; "t" is the release time; "k" is the kinetic constant that measures the drug release rate and, "n" is the diffusion exponent that depends on the release mechanism and on the geometry of the matrix. To determine "n" values, equation 2.4 is modified in equation 2.5 and, "n" is determined from the slope of the plot of log (%release) versus log t.

$$\log(\%released) = \log(M_t / M_\infty) = \log k + n \log t$$

Equation 2.5. Modified Ritger-Peppas equation.

2.12. Elastase activity determinations

The activity of porcine pancreatic elastase (PPE) was measured according to a method previously reported [387] using the synthetic substrate N-Succinyl-Ala-Ala-Ala-*p*-nitroanilide. The reaction was carried out for 5 min at 37 ℃ and the cleavage of the substrate was monitored spectrophotometrically at 410 nm. One unit is defined as the amount of enzyme that will hydrolyze 1.0 µmol of N-Succinyl-Ala-Ala-Ala-*p*-nitroanilide per minute at 25 ℃, pH 8.0.

The activity of human neutrophil elastase (HNE) was measured according to a method previously reported [388] using the synthetic substrate N-Methoxysuccinyl-Ala-Ala-Pro-Val-*p*-nitroanilide. The reaction was carried out for 1 min at 37 ℃ and the cleavage of the substrate was monitored spectrophotometrically at 410 nm. One unit will release 1.0 nmol of *p*-nitroanilide per second from N-

Methoxysuccinyl-Ala-Ala-Pro-Val-*p*-nitroanilide at 37 ℃, pH 6.5. Determination of half-life time and inhibition rates will be explained in further sections

2.12.1. Mechanisms and kinetics of inhibition

The mechanism of enzyme catalysis can be explained by the Michaelis-Menten equation.

$$V = V_{\max} \times \frac{[S]}{[S] + K_m}$$

Equation 2.6. Michaelis-Menten equation.

V is the enzyme reaction velocity; V_{max} is the maximum enzyme reaction velocity which is attained when all the subsites of the enzyme are occupied by the substrate; [S] is the substrate concentration and K_m is the Michaelis-Menten constant that represents the substrate concentration when half of the binding sites are occupied. The enzyme reaction velocity can be reduced by four mechanisms of inhibition:

1. Competitive Inhibition

A competitive inhibitor is a molecule that resembles the substrate and occupies the catalytic site because of its similarity in structure, but is completely unreactive. By occupying the active site, the inhibitor prevents normal substrates from binding and being catalyzed. Unlike other mechanisms, inhibition can be reversed by increasing substrate concentration. Competitive inhibitors cause an apparent increase of K_m (i.e., the inhibitor interferes with substrate binding), but does not affect V_{max} (inhibitor cannot bind to the complex enzyme-substrate).

$$V = V_{\max} \times \frac{[S]}{[S] + K_m \left(1 + \frac{[I]}{K_i}\right)}$$

Equation 2.7. Modified Michaelis-Menten equation for competitive inhibition.

[I] is the inhibitor concentration and K_i (inhibition constant) is the dissociation constant of the enzyme-inhibitor complex.

2. Noncompetitive Inhibition

A noncompetitive inhibitor is one that binds reversibly to the enzyme, but not at the active site itself, so that the substrate can still bind at the active site, but there is no catalysis. Non-competitive inhibitors have identical affinities for enzyme and complex enzyme-substrate ($K_i = K_i'$). A noncompetitive inhibitor decreases V_{max} without affecting the apparent K_m.

$$V = \frac{V_{\max}}{1 + \frac{[I]}{K_i}} \times \frac{[S]}{[S] + K_m}$$

Equation 2.8. Modified Michaelis-Menten equation for noncompetitive inhibition.

3. Mixed Inhibition

Mixed inhibitors are capable of binding to both free enzyme and enzyme-substrate complex with different affinities ($K_i \neq K_i'$). Thus, mixed-type inhibitors interfere with substrate binding (increase K_m) and with catalysis in the enzyme-substrate complex (decrease V_{max}).

$$V = \frac{V_{\max}[S]}{K_m\left(1 + \frac{[I]}{K_i}\right) + [S]\left(1 + \frac{[I]}{K_i'}\right)}$$

Equation 2.9. Modified Michaelis-Menten equation for mixed inhibition.

4. Uncompetitive Inhibition

Uncompetitive inhibition is a special case of mixed inhibition and occurs when the inhibitor only binds to the enzyme-substrate complex. Both V_{max} and K_m decrease (maximum velocity decreases as a result of removing activated complex while binding efficiency increases as a result of Le Chatelier's principle).

$$V = \frac{V_{\max}[S]}{K_m + [S]\left(1 + \frac{[I]}{K_i}\right)}$$

Equation 2.10. Modified Michaelis-Menten equation for uncompetitive inhibition.

The **half maximal inhibitory concentration (IC_{50})** is a measure of the effectiveness of a compound in inhibiting biological or biochemical function i.e. is defined as the concentration of inhibitor necessary to cause the decrease of 50% in enzyme activity. For competitive binding studies, the IC50 can be determined using the Cheng-Prusoff equation [389].

$$IC_{50} = K_i \times \left(1 + \frac{[S]}{K_m}\right)$$

Equation 2.11. Determination of IC_{50}.

CHAPTER III

Biodegradable materials based on silk fibroin and keratin

CHAPTER III

Biodegradable materials based on silk fibroin and keratin

Abstract

Wool and silk were dissolved and used for the preparation of blended films. Two systems are proposed: 1) blend films of silk fibroin and keratin aqueous solutions; 2) silk fibroin and keratin dissolved in formic acid. The resulting silk fibroin/keratin (SF/K) films were characterized and, the non-linear trend of the different parameters obtained from FTIR analysis and DSC curves of both SF/Keratin systems indicate that when proteins are mixed do not follow additives rules but are able to establish intermolecular interactions.

Degradable polymeric biomaterials are preferred candidates for medical applications. It was investigated the degradation behavior of both SF/keratin systems by *in vitro* enzymatic incubation with Trypsin. The SF/Keratin films cast from water underwent a slower biological degradation than the films cast from formic acid. The weight loss obtained is a function of the amount of keratin in the blend. This study encourages the further investigation of the type of matrices presented here to be applied whether in scaffolds for tissue engineering or as controlled release drug delivery vehicles.

This chapter is based on the following publication: **Andreia Vasconcelos**, Giuliano Freddi & Artur Cavaco-Paulo, Biodegradable Materials Based on Silk Fibroin and Keratin, *Biomacromolecules* 2008, *9,* 1299–1305

3.1. Introduction

Keratin is the major structural fibrous protein providing outer covering such as hair, wool, feathers, nail and horns of mammals, reptile and birds [131]. At the molecular level, the most distinctive feature is the high concentration in cysteine residue (7-20 number% of the total amino acid residues) [390]. These cysteine residues are oxidized to give inter and intra-molecular disulfide bonds, which decide about mechanical, thermal and chemical properties of wool fibers. Wool keratins are a family of proteins that can be roughly classified into two groups: the intermediate filament proteins (IFPs) and the matrix proteins. The most abundant are the fibrous, low-sulphur keratins that are part of the IFPs. They have a α-helical structure and have an average molar mass in the range of 40-60 kDa. The matrix proteins have a high content in either cysteine or glycine and tyrosine residues. The ones with high cysteine content are referred to the high-sulphur proteins (HSPs) and have a molecular weight in the range of 11-26 kDa. Those high in glycine and tyrosine residues are referred to high-glycine/tyrosine proteins (HGTPs) and have a molecular weight between 6-9 kDa. The matrix proteins are thought to surround the IFPs and interact with them through inter-molecular disulfide bonds [141]. The keratin macromolecule in wool fiber takes the following conformations: helical (α-keratin), rectal (β-keratin) and undefined. The α-helix conformation is characteristic for wool fiber in its native state, it is, the fiber that is not stretched along its axis. During stretching, the α-helix declines and β-keratin appears. It is an unstable conformation and when the stretching force disappears the conformation of keratin reverts to α-helical [145-147].

Extraction of keratins from wool has been conducted in various ways [151-157] but all of them involve the presence of reducing or denaturant agents to break disulfide bonds. Regenerated keratin from wool is then dissolved in proper solvents before processing into other applications. Although regenerated keratin has been used for many applications [161-164], this material presents poor mechanical strength so that the use of crosslinking agents and blending with structural fibrous polymers is often necessary to improve its processing and final mechanical properties. Regenerated keratin blended with silk fibroin has already

been reported [188] and formic acid represents an ideal medium for this polymer blend because while wool is partially soluble in formic acid, regenerated keratin and silk fibroin are readily soluble [64, 391].

Silk from silkworms and orb-weaving spiders represent a unique family of structural proteins that are biocompatible, degradable, mechanically superior, offer a wide range of properties such as environmental stability, controlled proteolytic biodegradability, morphologic flexibility and can be chemically modified to suit a wide range of biomedical applications [6, 37, 39, 61, 85, 93, 102, 111, 115]. The silk fibers from silkworm *Bombyx mori* consist of two proteins: a light chain (≅ 25 kDa) and a heavy chain (≅ 390 kDa) which are present in a 1:1 ratio and linked by a single disulphide bond [12]. These proteins are coated with a family of hydrophilic proteins called sericins (20-310 kDa) [2, 12-14] which correspond to 25-30 % of silk cocoons mass that is removed during the degumming process.

The amino acid composition of silk fibroin from *B. mori* consists primarily of glycine, alanine and serine amino acids in the molar ratio of 3:2:1 which forms typical -(-ala-gly-)$_n$- repeating motifs [2]. In the fiber, fibroin chains are aligned along the fiber axis held together by a close network of interchain hydrogen bonds with adjacent -(-ala-gly-)$_n$- sequences forming the well known β-sheets crystals [12, 392]

Both keratin and fibroin are excellent biopolymers with outstanding properties that make them extremely valuable in the biomedical field. Keratin films prepared from reduced keratin are biodegradable *in vivo* and *in vitro* [183] supporting cell adhesion and proliferation [183, 189]. Silk fibroin films which are easily prepared by casting aqueous silk proteins solutions at room temperature are highly attractive for their discrete permeability to oxygen and water vapor [88, 89]. Silk fibroin has also been used for the preparation of polymer-hydroxyapatite composites for bone regeneration [393], wireropes for the substitution of the anterior cruciate ligament [394], novel silk-based sutures and protective gauzes for the treatment of skin burns with improved blood compatibility [395], for supporting cell adhesion and growth, as scaffolds for skin and bone regeneration [34, 60, 396, 397].

In the present work, blend films of silk fibroin from *B. mori* and regenerated keratin from merino wool were prepared by water and formic acid casting and characterized in the solid state by FT-IR spectroscopy, DSC thermal analysis, and

tensile measurements. The corresponding solutions were characterized by amino acid analysis and SDS-PAGE electrophoresis.

3.2. Materials and methods

Herein it will be given a detailed description of some of the methods presented in the previous chapter. All other techniques were performed as described in Chapter II.

3.2.1. Preparation of stock solutions

Silk was purified from its sericin content as previously described in section 2.3, Chapter II. SF, 1 % (w/v) (SF1) was prepared by dissolving 1 g of degummed silk fibers into 10 ml of saturated aqueous LiBr at 60 °C for 3 h. The solution was then diluted by adding 90 ml of deionised water, filtered, and dialyzed against distilled water until complete removal of salt, using cellulose tubing (molecular-weight cut-off of 12000-14000 Da). A similar solution was prepared in the same manner that was then freeze-dried (SF2).

Keratin 1 % (w/v) (K1) solution was prepared by immersing 1 g of delipided wool in 10 ml of a solution containing 8 M Urea, 0.2 M SDS and 0.5 M $Na_2S_2O_5$. The mixture was heated to 100 ℃ for 30 min. The solution was then diluted with 90 ml of distilled water, filtered and dialyzed against distilled water using cellulose tubing (molecular-weight cut-off of 12000-14000 Da). Delipided wool (1 g) was dissolved in 25 ml of a solution containing 0.1 M Tris-HCl, pH 9.0, 8 M Urea and 0.1 M DTT at 50 ℃ for 24 h in a shaker bath. The solution was filtered and dialyzed against distilled water using cellulose tubing (molecular-weight cut-off of 12000-14000 Da). After dialysis the solution was freeze-dried (K2).

3.2.2. Preparation of blended films

Keratin (K1) and silk fibroin (SF1) solutions (10 ml of final volume) were blended in the ratios of 80/20, 60/40 and 40/60 of SF1/K1. The blends were cast in plastic Petri dishes with a circular area of about 40 cm^2 and dried at room temperature. The controls are 100 % SF1 and 100 % K1.

Freeze-dried keratin (K2) and silk fibroin (SF2) were dissolved in formic acid to prepare 1% (w/v) solutions. The solutions were blended in the ratios of 75/25, 50/50 and 25/75 of SF2/K2. The blends were cast in plastic Petri dishes with a circular area of about 40 cm^2 and dried at room temperature. The controls are 100 % SF2 and 100 % K2. The resulting films were 0.03 mm in average thickness.

3.2.3. *In vitro* degradation

Protein matrices were incubated at 37 ℃ in 6 ml of a solution containing 0.5 mg/ml of Trypsin from Porcine Pancreas prepared in phosphate-buffered saline (PBS) or in PBS as a control. Before incubation with Trypsin, SF1/K1 films were treated with 90 % (v/v) of methanol during 1 h at room temperature. The SF2/K2 films were directly used for the degradation studies. Solutions were changed and collected daily. At designated time points, samples were washed thoroughly with distilled water, dried in a desiccator, and weighed to estimate the extent of degradation determined by equation 2.3., Chapter II.

3.3. Results and discussion

3.3.1. Amino acid and SDS-PAGE analysis

The protein solutions of wool keratin and silk fibroin were characterized by amino acid analysis and SDS-PAGE electrophoresis. Amino acid analysis on Table 3.1 indicated that the cysteine residues occupied 8 – 9 mol% of the total amino acid residues of the reduced keratin as already described before [162, 398]. The amino acid composition of SF is characterized by a high content of Gly, Ala, and Ser, residues which corresponds to about 85 mol% of total mass; Tyr accounts for 5.3 mol%; acidic and basic amino acids are a total of about 3.0 and 1.1 mol%, respectively. This characteristic amino acidic pattern results from the contribution of two polypeptides, i.e. the heavy and light chains. The heavy chain represents about 90% of the total weight of silk fibroin and predominates with its characteristic $-(Gly-Ala)_n-$ rich sequences [12] over the more heterogeneous primary structure of the light chain [13].

Table 3.1. Amino acid composition of silk fibroin and keratin

Amino acid	Silk fibroin (mol %)	Keratin (mol %)
Cyst	-	0,46
Asp	1.67	5,94
Ser	11.48	10,77
Glu	1.37	10,96
Gly	43.68	11,02
His	0.20	1,00
Arg	0.62	5,55
Thr	0.96	5,12
Ala	29.34	4,52
Pro	0.67	7,06
Cys	0.10	9,09
Tyr	5.30	6,26
Val	2.23	5,29
Met	0.10	0,37
Lys	0.33	1,17
Ile	0.66	3,06
Leu	0.58	8,46
Phe	0.72	3,88

The electrophoretic pattern of wool keratin (Figure 3.1) shows the main two groups of keratin associated proteins, the intermediate filament proteins (IFPs) and the matrix proteins. It can be observed (Figure 3.1a) two high molecular weight bands (60-45 kDa) attributed to the low-sulphur IFPs that are mainly α-helical, and several low molecular weight bands attributed to the high-sulphur (HSPs) (20 - 10 kDa) and high-glycine/tyrosine (HGTPs) (6-9 kDa) proteins of the matrix [141]. Regenerated aqueous SF solution (Figure 3.1b) shows a broad dull band from 200-30 kDa and a very weak band at approximately 25 kDa [52]. The former band might result from the degradation products of the heavy chains (350 kDa) of raw

silk protein formed by degumming and dissolution in a solvent system, and the latter band at 25 kDa corresponds to the light chain of raw silk protein [399].

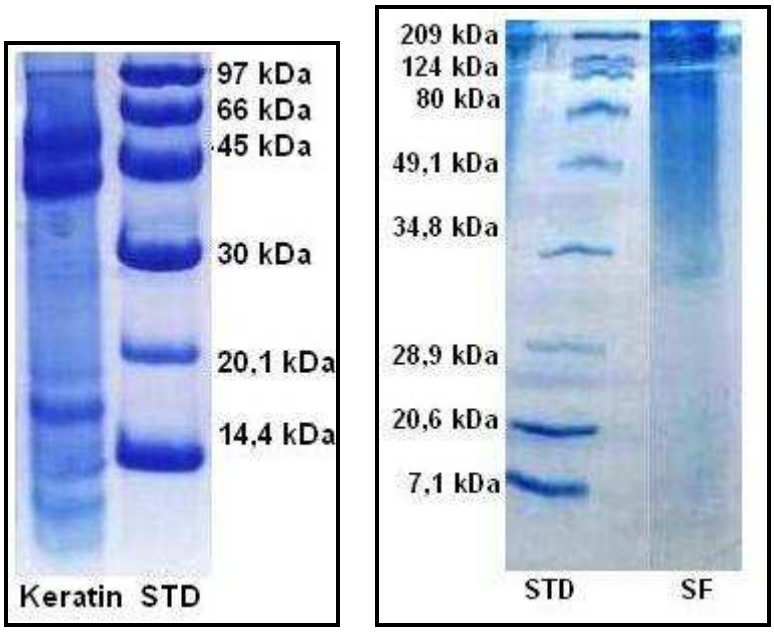

a) b)

Figure 3.1. SDS-PAGE of a) wool keratin and b) silk fibroin solutions.

Keratin was extracted from wool by sulphitolysis [158]. During this process cysteine disulphide bonds are cleaved by sulphite to give cysteine thiol (reduced keratin) and Bunte salts residues [131, 158, 159]. This method gives a keratin extraction yield about 30 % of the total protein content of the original wool [160]. Keratin extracted by the system using DTT as the reducing agent gives a protein extraction yield of approximately 80 % [157]. However, the solution obtained by this method became partially insoluble after dialysis. This is due to the fact that the high-sulphur proteins responsible for the reoxidation of the SH groups into disulphide bridges are insoluble. The SDS-PAGE gel shows that the HSPs (20-10 kDa) remains on the insoluble fraction of the solution. In the protein solution obtained by sulphitolysis this fact is not observed because these type of proteins are not extracted by this method (data not shown). In terms of processing this fact is an advantage because the solution is ready for film preparation but the films obtained have low mechanical strength when compared with the films obtained by formic acid casting (Table 3.2).

3.3.2. Mechanical properties

The load/elongation curves of pure SF1 films (data not shown) do not present any yield point. The load increases almost linearly until a plateau, then the film brakes or continues elongating (failure is not sharp).These SF1 films are prevalently amorphous. The tensile behaviour can be due to the presence of amorphous domains which display a plastic behaviour. Addition of keratin (K1) to SF1 makes films weaker. The average values of stress are about half of those of pure SF1 films when 40% of K1 is present. Elasticity increases slightly at small keratin content (Table 3.2). SF films cast from formic acid (SF2) display average stress values similar to water cast films, but failure is much sharper. This can be attributed to the more crystalline character of these films. The SF2/K2 films obtained with formic acid display better tensile properties than those obtained in water. At 50 % of K2 the tensile behaviour is typical of brittle films, the failure is sharp. At lower K2 content (25 %) failure can be sharp or plastic. Important to note that the stress values are quite high, similar to those of pure SF2 films (Table 3.3).

Table 3.2. Mechanical properties of SF1/K1 blends

K1 (%)	Stress (MPa)	Elongation (mm)	Modulus (MPa)
0	23,690 ± 7,311	0,518 ± 0,0416	3411 ± 479
20	11,265 ± 5,167	0,679 ± 0,1948	1597 ± 588
40	9,153 ± 3,250	0,407 ± 0,1135	1409 ± 203

Table 3.3. Mechanical properties of SF2/K2 blends

K2 (%)	Stress (MPa)	Elongation (mm)	Modulus (MPa)
0	23,568 ± 7,669	0,427 ± 0,051	2893 ± 387
25	29,755 ± 6,544	0,570 ± 0,130	2724 ± 207
50	17,730 ± 4,660	0,363 ± 0,111	2005 ± 210

3.3.3. FT-IR analysis

Infrared absorption spectra of blended films of silk fibroin (SF1 and SF2) and keratin (K1 and K2) show characteristic absorption bands assigned to the peptide bonds (-CONH-) that originate bands known as amide I, amide II and amide III. The amide I is useful for the analysis of the secondary structure of the proteins and is mainly related with the C=O stretching and it occurs in the range of 1700-1600 cm^{-1}. The amide II which falls in 1540-1520 cm^{-1} range is related with the N-H bending and C-H stretching vibration. The amide III occurs in the range of 1220-1300 cm^{-1} and it results from phase combination of C-N stretching and C=O bending vibration [399]. In addition, the positions of these bands indicate the conformations of the protein materials: 1650 cm^{-1} (random coil) and 1630 cm^{-1} (β-sheet) for amide I; 1540 cm^{-1} (random coil) and 1520 cm^{-1} (β-sheet) for amide II; 1230 cm^{-1} (random coil) and 1270 cm^{-1} (β-sheet) for amide III [400-402].

The keratin (K1) spectra (Figure 3.2) shows a peak at 1641 cm^{-1} with a shoulder at about 1620 cm^{-1} for amide I, 1533 cm^{-1} amide II and 1225 cm^{-1} for amide III. The peaks at 1203 cm^{-1} and 1024 cm^{-1} are related, respectively, to the asymmetric and symmetric S-O stretching vibrations of the Bunte salts residues [403] that are no longer observed in the spectra of K2 (Figure 3.3). The absorption value of the amide I band of pure K1 film indicates that the secondary structure of K1 mainly consist of α-helix and random coil conformation The IR spectra of SF showed a peak at 1639 cm^{-1} for amide I, 1518 cm^{-1} with a strong shoulder at about 1535 cm^{-1} for amide II and 1236 cm^{-1} for Amide III. This FT-IR pattern is characteristic of SF films with prevalently amorphous structure (random coil/Silk I conformation). The half-peak width of amide I of K1 is larger than that of SF1 which might reflect a more heterogeneous molecular conformation. Wool treatment with formic acid increases the amount of β-sheet and disordered keratin structures [404, 405] as it can be seen by the appearance of band peaks at 1697-1670 cm^{-1} range in keratin dissolved in formic acid (K2, Figure 3.3) [406, 407]. Amide I appear at 1643 cm^{-1} with a strong shoulder at around 1620 cm^{-1}, amide II is showed at 1539 cm^{-1} with a shoulder at about 1529 cm^{-1} and amide III at 1238 cm^{-1}. The higher wavenumber of amide I can be explained by the protein extraction procedure suggesting again the presence of α-helix structure. Nevertheless, the decrease in the peak area of

the amide I band in K2 spectra in respect to the same band in K1 spectra indicates that formic acid destabilized the α-helix conformation and stabilizes the supramolecular β-sheet structure of keratin. This occurs because formic acid has a higher polarity than water and forms strong interactions with the polar side chains groups of keratin. As a consequence, the molecular chains became closer and this organization can promote crystallization in β-sheet structure [408]. The FT-IR pattern of SF2 dissolved in formic acid is different from the one in water and characteristic of SF film with prevalently β-sheet conformation, with β-sheet crystallites embedded in an amorphous matrix. Half-peak width of amide I and II of K2 are larger than those of SF2 suggesting a more heterogeneous molecular conformation as it was observed for aqueous solutions.

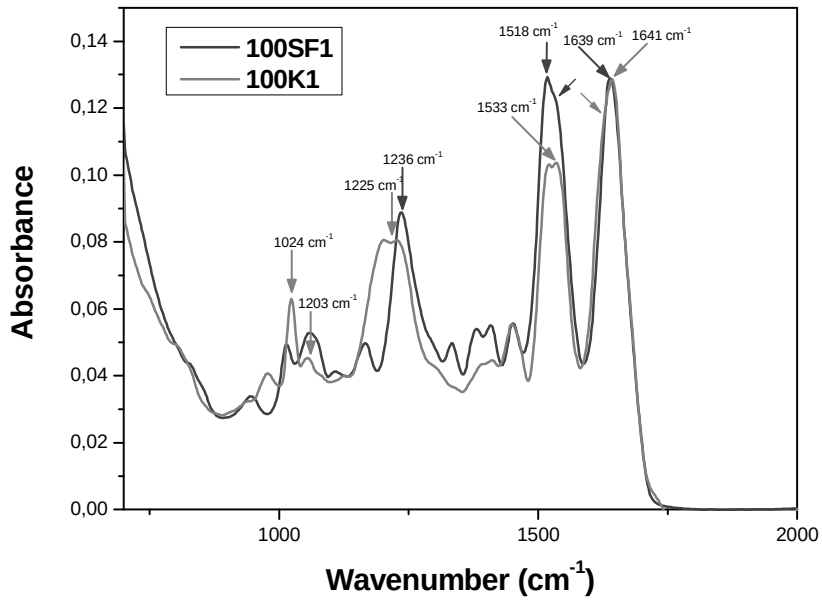

Figure 3.2. FTIR spectra of pure films of silk fibroin (SF1) and keratin (K1) aqueous solutions.

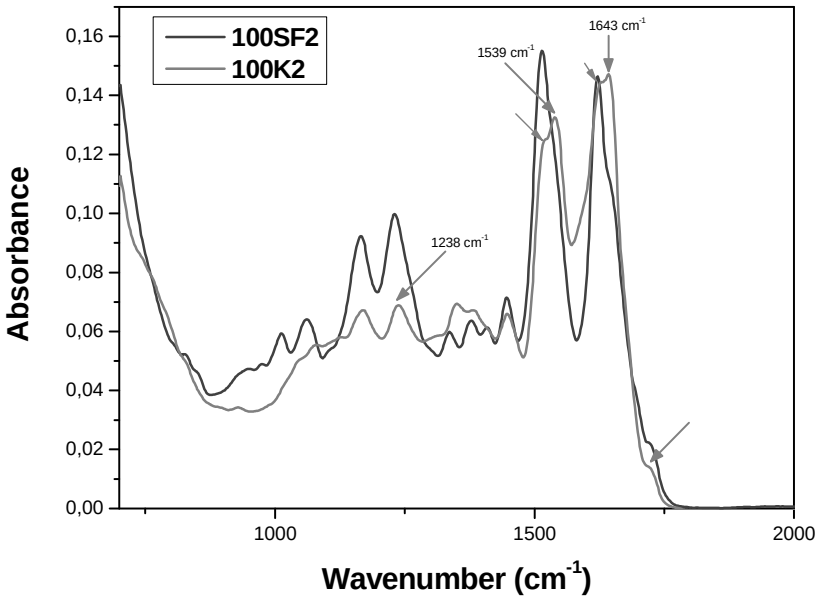

Figure 3.3. FTIR spectra of pure films of silk fibroin (SF2) and keratin (K2) dissolved in formic acid.

It can be observed (Figure 3.4 and Figure 3.5) that the position, shape and intensity of amide bands show a transition from SF-like to K-like spectral pattern, for both SF/K systems, with the increase of keratin present in the film. The plot of the intensity ratio between the amide II (Figure 3.6) bands fit a second order polynomial curve, suggesting that SF and keratin do not follow additive rules when mixed. This might be indicating of intermolecular interactions, more likely hydrogen bonding, between SF and keratin.

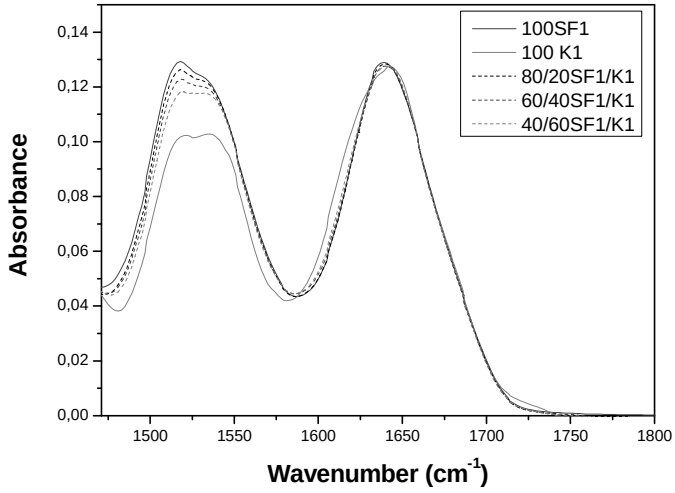

Figure 3.4. FTIR spectra of blended films with silk fibroin (SF1) and keratin (K1) aqueous solutions.

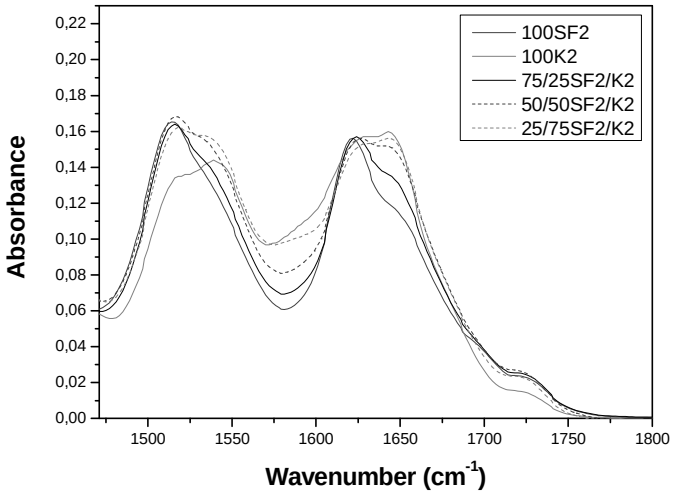

Figure 3.5. FTIR spectra of blended films with silk fibroin (SF2) and keratin (K2) dissolved in formic acid.

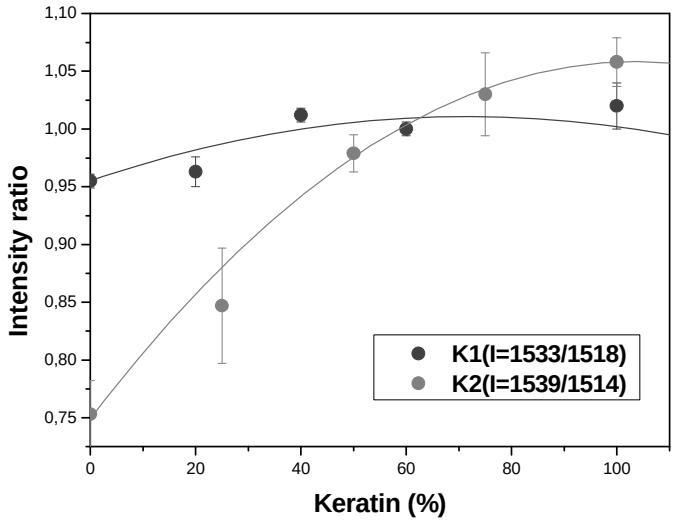

Figure 3.6. Behaviour of intensity ratio of the amide II bands typical of SF1 (1518 cm^{-1}) and K1 (1533 cm^{-1}) in water and, SF2 (1514 cm^{-1}) and K2 (1539 cm^{-1}) in formic acid.

The amide I band was deconvoluted to determine the fraction of the β-sheets formed during crystallization. In this approach, the amide I band is transformed to yield a fitted self-deconvoluted set of bands from which the secondary structure is determined. The assignment of the amide I region bands was determined by reference to the literature [250, 409-412]. The results from Table 3.4 indicated higher β-sheet content for the crystallization induced by methanol treatment. The increase in crystallization seems to occur due to the random coil/Silk I structure as

it can be seen from its decrease from AU→FA→AM. Nevertheless, it can not be excluded a formation of a β-type structure intermediate before the final transition from random coil to β-sheet.

Table 3.4. Results from the curve fitting of the amide I range of the FT-IR spectrum of SF films

	Untreated (AU)	Formic acid (FA)	Methanol(AM)
β-sheet (Silk II)	29,30%	40,14%	58,15%
Random coil/Silk I	43,36%	37,58%	19,63%
Turns and bends	27,33%	22,27%	22,21%

3.3.4. DSC analysis

The DSC curve of SF1 (Figure 3.7) exhibits an endothermic shift at 178 ℃ that corresponds to the glass transition temperature (Tg) of SF, an exothermic peak at 226 ℃ (broad and weak) related to crystallization via conformational transition to β-sheet structure of amorphous SF chains, and an intense bimodal endotherm at 274 ℃ (main peak) and 296 ℃ assigned to the melti ng/decomposition of SF chains. The exothermic peak at 226 ℃ can be dimini shed by treatment with polar solvents [413] that was afterwards observed (Figure 3.8). The thermal behaviour is typical of a prevalently amorphous SF film with non-oriented SF chains. Weakness of the crystallization peak at 226 ℃ and presence of a high temperature peak of thermal degradation at 296 ℃ suggest the presence of aggregated SF domains embedded in a prevalently amorphous matrix, as suggested by FTIR results.

The DSC curve of keratin (K1) (Figure 3.7) shows and endothermic peak at 224 ℃ related to the melting of α-helices of the IFPs and an endotherm peaking at 277 ℃ that corresponds to the melting/degradation of keratin proteins which comprise the high sulphur (highly cross-linked) keratins of the intermacrofibrillar matrix. The glass transition temperature of SF1, Tg, shifts to higher temperature following addition of keratin. At higher keratin content (> 60%), Tg is no longer detectable. The melting peak of keratin α-helix at 224 ℃ remains almost unchanged; the

value of ΔH (peak intensity) sharply decreases by addition of SF1. When 80% of SF1 is present in the blend the melting peak of keratin is hardly detectable. The melting/decomposition endotherm of SF1 at 274 °C shows a marked low temperature broadening (the peak shifts downwards of about 10 °C, from 274 °C to about 264 °C). It is still detectable in the 60% keratin blend as a low temperature shoulder of the main keratin degradation endotherm. When silk fibroin (SF2) and keratin (K2) were dissolved in formic acid (Figure 3.8) the DSC pattern of both components changed. The glass transition temperature and the exothermic peak of β-sheet crystallization are no more detectable because formic acid is able to induce a partial crystallization to β-sheet structures of SF chains during drying. The melting/decomposition endotherm of partially crystallized/non-oriented SF chains occurs at 278 °C with a high temperature shoulder.

The DSC curve of keratin dissolved in formic acid (K2) is characterized by three main endothermic events at 204 °C (weak and broad), 244 °C and the most intense at 295 °C. The transition at low temperature (204 °C) is hardly attributable and could be related to small molecular weight keratin fractions with low thermal stability. The thermal transitions peaking at 244 °C and 295 °C can be attributed to melting and melting/decomposition of keratin fractions with intermediate and high thermal stability, which is probably related to the different extent of cross-linking of the various keratin fractions. The characteristic α-helix melting peak of keratin is lost upon formic acid casting as already observed elsewhere [408]. This suggests that the α-crystallites formed by keratin/formic acid systems are thermally less stable. Furthermore, the peak area decrease (Figure 3.8) is a support of the lesser α-helix content in the K2 films. In the blends, the melting/decomposition endotherm of SF2 at 278 °C shifts to lower temperature with the increase of keratin present in the film. The energy associated with melting/decomposition of pure SF, pure keratin, and SF2/K2 blends was calculated by integrating the endothermic peaks in the range 200-350 °C (Figure 3.9). Values were expressed as ΔH (J/g). The energy associated with thermal degradation of SF2 is higher than that required by K2 (influence of the different chemical and physical structure). The plot of ΔH vs. the composition of the blend does not follow a linear trend. The best fit is given by a second order polynomial curve.

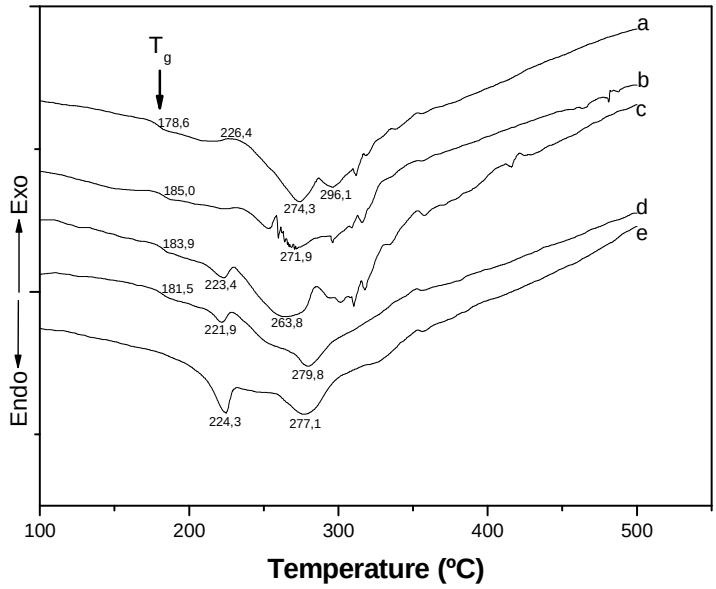

Figure 3.7. DSC curves of blended films with silk fibroin and keratin (SF1/K1) aqueous solutions. (a)100SF, b) 80/20SF1/K1, c) 60/40SF1/K1, d) 40/60SF1/K1 and e) 100K1)

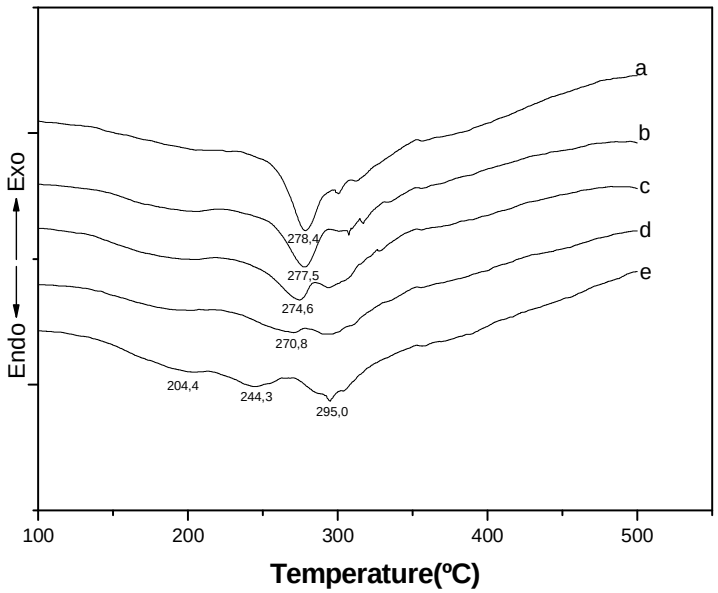

Figure 3.8. DSC curves of blended films with silk fibroin and keratin (SF2/K2) dissolved in formic acid. (a) 100SF, b) 75/25SF2/K2, c) 50/50SF2/K2, d) 25/75SF2/K2 and e) 100K2)

The non-linear trend of the different parameters obtained from the DSC curves of both SF/Keratin systems indicate that, when the proteins are mixed, the thermal behaviour of one component is more or less strongly influenced by the other. This

confirm the assumption raised by FT-IR results that SF and Keratin are able to establish intermolecular interactions, more likely based on hydrogen bonding

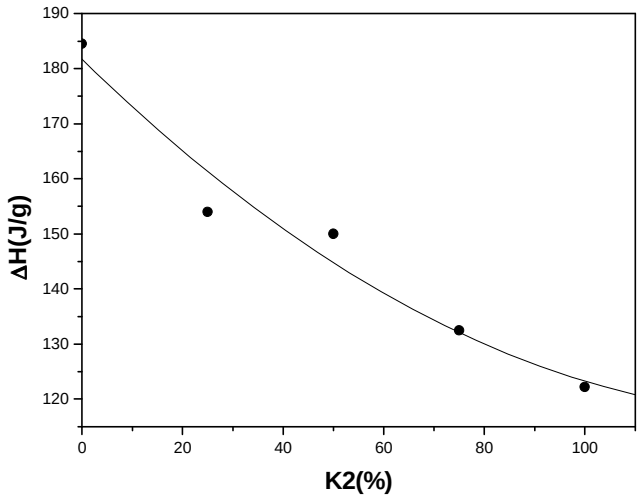

Figure 3.9. Enthalpy variation (ΔH) of decomposition peak of SF2 and K2 (temperature range: 200-350ºC)

3.3.5. *In vitro* degradation

In vitro degradation was observed for protein films of both SF/K systems incubated in Trypsin. In the water system (Figure 3.10) it can be observed that pure SF1 films presented very low degradation that remains constant over the time exposure to Trypsin. In the blends it can be seen that the weight loss obtained is a function of the amount of keratin (K1) present in the blend. When the minimum amount of K1 is present (20%), it was obtained a degradation of 23% in a slower manner over the time. With the increase of keratin to 40%, the degradation took place rapidly during the first 14 days remaining constant after that without exceeding 70% of degradation. At higher keratin amounts, only debris was obtained after 1 day of incubation. In the formic acid SF2/K2 system (Figure 3.11) a similar behaviour is observed. Nevertheless, pure SF films presented higher weight loss values because crystallization to β-sheet, induced by formic acid results in decreased β-sheet contents as showed in Table 3.4. As described in the literature β-sheet rich regions are degraded in a slower rate. In this way, in the Silk II

conformation the molecular chains are entangled leading to a more closed structure, which leads to slower degradation rates.

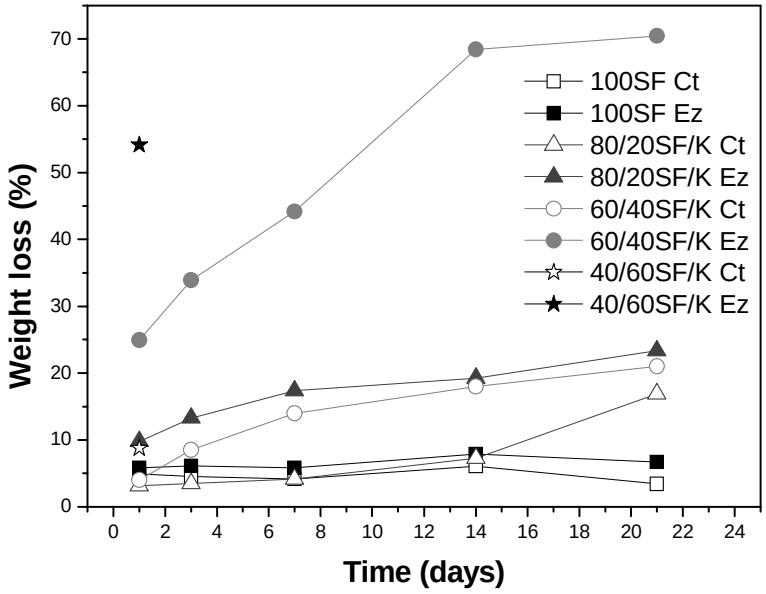

Figure 3.10. Weight loss of SF1/K1 films (water system) incubated in buffer (Ct) and Trypsin solution (Ez) as a function of time.

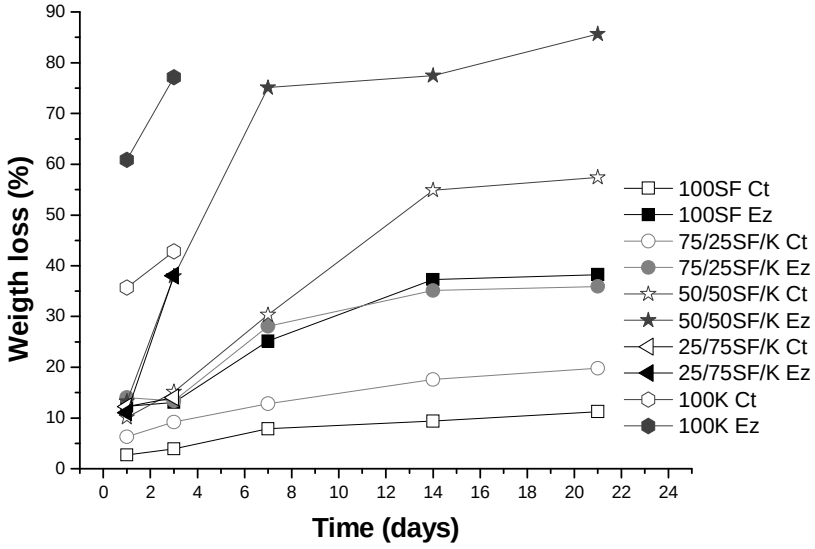

Figure 3.11. Weight loss of SF2/K2 films (formic acid system) incubated in buffer (Ct) and Trypsin solution (Ez) as a function of time.

3.4. Conclusions

In the present study an extensive characterization of wool and silk proteins in the film form was presented. Films were made by blending silk fibroin (SF1) and keratin (K1) aqueous solutions; silk fibroin (SF2) and keratin (K2) dissolved in formic acid. The presence of K1 on the blends makes films weaker with a slight increase in elasticity whereas films obtained from formic acid (SF2/K2) presented better strength results. The FT-IR spectra of pure K1 indicates that its structure mainly consists of α-helix and random coil conformations. The IR spectrum of pure SF1 is characteristic of films with prevalently amorphous structure (random coil conformation). Pure keratin film cast from formic acid (K2) show an increase in the amount of β-sheet and disordered keratin structures. The FT-IR pattern of SF2 is characteristic of films with prevalently β-sheet conformation with β-sheet crystallites embedded in an amorphous matrix. In the blends, the position, shape and intensity of amide bands showed a transition from SF-like to K1-like or SF-like to K2-like spectral pattern. The thermal behaviour of the blends confirmed the FT-IR results. DSC curve of pure SF is typical of amorphous SF and the curve of pure K1 show the characteristic melting peak of α-helixes. These patterns were no longer observed in the films cast from formic acid due to the ability of formic acid to induce crystallization of SF and to increase the amount of β-sheet structures on keratin. The non-linear trend of the different parameters obtained from FTIR analysis and DSC curves of both systems indicated that wool keratin and silk fibroin are able to establish intermolecular interactions. The properties of the films depend on the nature and strength of these interactions. The SF/K films cast from water underwent a slower biological degradation than the films cast from formic acid. The knowledge of the degradation rates will allow the design of matrices for the release of active compounds. The results presented showed that the protein matrices developed are suitable to further biomedical and biotechnological applications.

CHAPTER IV

Protein matrices for improved wound healing: elastase inhibition by a synthetic peptide model

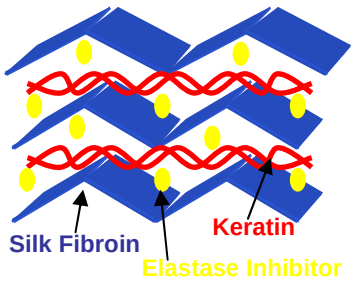

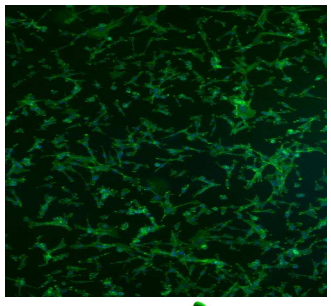

CHAPTER IV

Protein matrices for improved wound healing: Elastase inhibition by a synthetic peptide model

Abstract

The unique properties of silk fibroin were combined with keratin to develop new wound dressing materials. Silk fibroin/Keratin (SF/K) films were prepared to reduce high levels of elastase found on chronic wounds. This improved biological function was achieved by the incorporation of a small peptide synthesized based on the reactive-site loop of the Bowman-Birk Inhibitor (BBI) protein. *In vitro* degradation and release were evaluated using porcine pancreatic elastase (PPE) solution as a model of wound exudate. It was found that biological degradation and release rate are highly dependent on film composition. Furthermore, the level of PPE activity can be tuned by changing the film composition showing therefore, an innovative way of controlling the elastase-antielastase imbalance found on chronic wounds.

This chapter is based on the following publication: **Andreia Vasconcelos**, Ana Paula Pêgo, Meriem Lamghari, Lara Henriques & Artur Cavaco-Paulo, Protein matrices for improved wound healing: Elastase inhibition by a synthetic peptide model, *Biomacromolecules* 2010, 11(9), 2213–2220

4.1. Introduction

Wound healing is a specific biological process related to the general phenomenon of growth and tissue regeneration. Wound healing progresses through a series of interdependent and overlapping stages in which a variety of cellular and matrix components act together to reestablish the integrity of damaged tissue and the replacement of lost tissue [300, 302, 303]. The interruption of the orderly sequence of events during the healing process results in chronic wounds [297-299].

Skin ulcers are the most common types of chronic wounds and are the focus of this study. These wounds can be created by many factors including vascular insufficiency, prolonged inflammation, pressure necrosis, physical agents, infection and cancer [300, 301]. Chronic wounds stop the healing process in the inflammatory phase, remaining nonhealed for several months or even years.

Excessive amounts of exudates are present in these types of wounds. Although wound exudate is a key component in all stages of the wound healing, irrigating the wound continuously and keeping it moist [305], the excessive production of exudates can cause maceration of healthy skin tissue around the wound, inhibiting the healing [414]. In addition, exudate from chronic wounds differs from acute wounds fluid, containing higher levels of tissue destructive protease enzymes namely, matrix metalloproteinases (MMPs) and polymorphonuclear (PMN) elastase [307]. The excessive action of elastase leads to reduce amounts of growth factors [309] and endogenous proteinase inhibitors, causing the cleavage of collagen, elastin and fibronectin, and consequently the destruction of extracellular matrix [340]. As a result, there has been considerable interest in the design of inhibitors that restore the elastase – antielastase imbalance.

Bowman-Birk inhibitors (BBIs) are small plant proteins of typically 60 to 90 residues stabilized by seven disulfide bridges. They have a symmetrical structure of two tricyclic domains each containing and independent binding loop [354, 355, 357, 358]. The inhibition of serine proteases is often mediated by these binding regions. The reactive site loop is fixed in a “canonical” conformation which is complementary to the proteinase active site [415, 416]. Small peptides mimicking the reactive-site loop of BBIs protein have shown to retain much of the inhibitory activity of the complete protein [359].

This study focus on the development of wound dressings with the ability to control elastase activity. Silk fibroin and keratin blends were used to incorporate a synthetic BBI peptide. The peptide sequence was removed from a combinatorial library of synthetic BBI-based peptides [359, 362, 363]. The excellent properties of silk fibroin such as high mechanical strength, low degradability and biocompatibility were combined with keratin protein in order to modulate the physical and bifunctional properties of the final material to fulfill the wound healing needs.

4.2. Materials and methods

Herein it will be given a detailed description of some of the methods presented in the previous chapter. All other techniques were performed as described in Chapter II.

4.2.1. Materials

The Porcine Pancreatic Elastase (PPE) was purchase from Sigma, Spain. The peptide 5(6)-Carboxyfluorescein-YCQPPWSATCF-OH was synthesized by JPT Peptide Technologies GmbH (Germany). The NIH 3T3 cell line (mouse embryonic fibroblasts) was purchased from the European Collection of Cell Cultures (ECACC). All other reagents were analytical grade and purchased from Sigma, Spain.

4.2.2. Preparation of aqueous silk fibroin and keratin solutions

Silk was purified from its sericin content as previously described in section 2.3, Chapter II Silk fibroin (SF) solution 1% (w/v) was prepared by dissolving 1 g of degummed silk fibers into 10 mL of saturated aqueous LiBr at 60 ℃ for 3 h. The solution was then diluted by adding 90 mL of deionised water. Keratin (K) solution 1% (w/v) was prepared by immersing 1 g of delipided wool fabric in 10 mL of a solution containing 8 M Urea 0.2 M SDS and 0.5 M $Na_2S_2O_5$. The mixture was heated to 60 ℃ for 12 h. Both solutions were filte red, and dialyzed against distilled

water using, cellulose tubing (molecular-weight cut-off of 12000-14000 Da), until complete removal of salts.

4.2.3. Preparation of blended silk fibroin/keratin films

Keratin (K) and silk fibroin (SF) solutions (10 mL of final volume) were blended in the ratios of 80/20, 60/40 and 40/60 of SF/K. The blends were cast in plastic Petri dishes with a circular area of 40 cm^2 and dried at room temperature. The controls are 100% SF and 100% K. The resulting films were 0.03 mm in average thickness. In order to induce the transition of SF from random coil to β-sheet structure and consequently insolubility, all the films were immersed in 90% (v/v) methanol solution for 30 minutes and then washed in distilled water and air dried. All films used were submitted to this treatment.

4.2.4. *In vitro* degradation

SF/K films were incubated, for 14 days, at 37 ℃ in a solution containing 0.1 U/mL of porcine pancreatic elastase (PPE) in 100 mM Tris-HCl buffer, pH 8.0. The control samples were incubated in the same buffer without PPE and submitted to the same conditions. Solutions were changed every 12 h. At designated time points, samples were washed thoroughly with distilled water, dried in a desiccator, and weighed to estimate the extent of degradation according to equation 2.3., Chapter II.

4.2.5. Swelling ratio of SF/K films

Dry SF/K films (60 ℃ for 24 h) were immersed in 10 0 mM Tris-HCl buffer, pH 8.0 at 37 ℃ for 24 h. The excess of buffer was removed and the wet weight of the film was determined. The swelling ratio of the film was calculated by equation 2.2., Chapter II.

4.2.6. Protein adsorption to protein films

SF/K films were incubated with 0.1 U/mL of porcine pancreatic elastase (PPE) solution at 37 ℃ for 24 h. Adsorption of the proteins to the SF/K films was determined by measuring the reduction of elastase activity in the supernatant.

4.2.7. Cytotoxicity evaluation

SF/K films were tested for cytotoxicity according to the ISO standards (10993-5, 2009). Both, tests by direct contact and tests on extract were performed to analyse the cytotoxicity of the developed materials as previously describe in Chapter II. Data are presented as average (standard deviation (SD). For multiple comparisons, homogeneity of variances was assessed by Barlett's test and after confirmation of the nonsignificant difference of variances, one-way ANOVA, followed by post hoc Bonferroni test was performed. Differences were considered statistically significant when $p < 0.05$. All calculations were performed using SPSS software for Windows (version 16.0, SPSS).

4.2.8. *In vitro* release

The release of model compounds from SF/K films was evaluated by the incorporation of FITC-BSA in the films. FITC-BSA (2 mg/mL) was mixed with protein solutions before film casting. The resulting films incorporating FITC-BSA were incubated with 100 mM Tris-HCl buffer, pH 8.0 and 0.1 U/mL of PPE solution at 37 ℃. Solutions were changed every day. At determined time points, aliquots were taken and the FITC-BSA release was monitored by a multiplate reader (Synergy HT W/TRF from BioTek) in the fluorescence mode at emission wavelength of 490 nm. After each measurement, the samples were added back to the medium to restore the equilibrium conditions. The quantification of the release was established by a standard fluorescence curve. The release studies were performed in triplicate and for a period of 7 days.

4.2.9. Elastase activity determinations

The activity of porcine pancreatic elastase was measured according to a method previously reported [387] with some modifications. Briefly, 30 µL of enzyme was mixed with 900 µL of reaction buffer 100 mM Tris-HCl, pH 8.0. The reaction was started by the addition of 70 µL of 4.4 mM of N-Succinyl-Ala-Ala-Ala-*p*-nitroanilide, a synthetic substrate for PPE. The reaction was carried out for 5 min at 37 ℃ and the cleavage of the substrate was monitored spectrophotometrically at 410 nm. One unit is defined as the amount of enzyme that will hydrolyze 1.0 µmol of Suc-$(Ala)_3$-*p*NA per minute at 25 ℃, pH 8.0.

To examine the inhibitory activity of 5(6)-Carboxyfluorescein-YCQPPWSATCF-OH, different peptide concentrations were added to a fixed amount of PPE solution. The incubation was carried out a 37 ℃ and, at determined time points, aliquots were taken to monitor the decrease in elastase activity determined as previously described. The peptide, 20 µM, was mixed with the proteins solutions before film casting. The films were incubated with PPE solution at 37 ℃. In this case, a fixed ratio of elastase solution per weight of film (0.2 mL/mg film) was kept. The inhibitory activity was determined as described above.

4.3. Results and discussion

In this work, films designed to be wound dressing materials, based on silk fibroin and keratin proteins with delivery properties were developed. Our previous work [15] indicated that SF and keratin are able to establish intermolecular interactions like hydrogen bonding. This fact was proven by the nonlinear trend of the different parameters such as intensity ratio of amide II bands and, enthalpy variation (ΔH) of the decomposition peak obtained respectively, from FTIR and DSC analysis. In addition, in the presence of protease enzyme, the films underwent a slow biological degradation, that is a function of the amount of keratin present in the blend. The combination of our results with the excellent biocompatibility both *in vitro* and *in vivo* [108, 417], the promotion of cellular adhesion and proliferation [123, 190, 396] and slow biodegradation already demonstrated, were the main factors to study the ability of SF/K films to act as wound dressings.

4.3.1. Characterization of protein blend films

Films were prepared by casting the regenerated solutions of silk fibroin and keratin on Petri dishes. After overnight solvent evaporation, uniform and transparent films were obtained. Blend films with concentrations of: 100%, 80%, 60%, 40%, 20% and 0% of SF were prepared. However, it was observed that with the increase of keratin in the blend it was not possible to obtain a film with mechanical integrity. Therefore, the maximum concentration of keratin that can be used in the blend is 60%.

Degradability of a given material is a very important parameter. It is directly linked to the drug release. The fast polymer degradation is not desirable because a high drug concentration will be released, which can be disadvantageous. *In vitro* degradation of SF/K films was determined by incubating protein films for several days in the presence of elastase enzyme which is one of the major components of the chronic wounds exudate. PPE was used as a model. It can be observed (Figure 4.1) that pure SF films present a low degradation rate that remains constant over the time exposure to elastase. This weight loss can be related with the degradation of the small hydrolytically peptide sequences present on the films even after crystallization [48]. In the blends, it can be observed that the weight loss obtained is a function of keratin content present in the film. At low keratin amounts (20%) the degradation is relatively slower. On the other hand, at maximum keratin concentration (60%), the degradation took place rapidly and after 7 days we obtained debris. Consequently, the weight loss, for this sample, after 14 days of incubation, was not measured because of the high error associated with the measurement. It is important to notice that the weight loss obtained for the blends is almost the same of the keratin content on the blend. Therefore, the debris obtained for 40/60 SF/K film is probably the fibroin that is not degraded but is not in sufficient amount to maintain the mechanical structure of the film. From our results the maximum keratin amount that promotes a constant degradation is 40%. The films kept in buffer solution showed little or no degradation in 14 days.

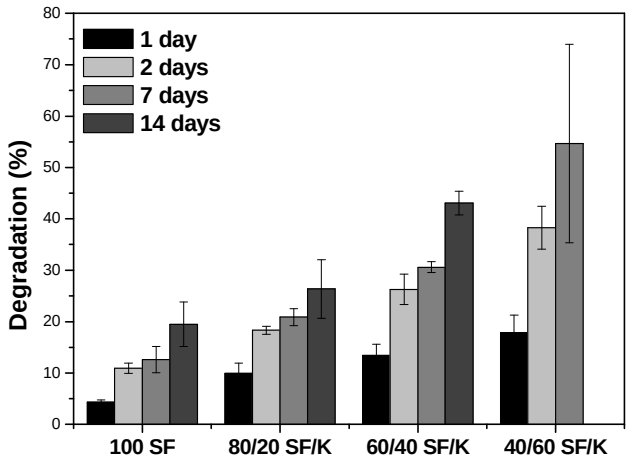

Figure 4.1. *In vitro* degradation of protein films incubated with 0.1 U/mL of elastase solution at 37 ℃ for several days.

On the wound dressing research, swelling is other important parameter in materials characterization. If the material has the ability to swell, it will give moisture to the wound contributing for a better healing [303]. Swelling ratio was found to increase with the increase of keratin present in the blend (Figure 4.2). It results from diffusion, and involves the transport of ions or fluid into the biomaterial. The driving forces of film formation by casting and solvent evaporation are attributed to hydrophobic interactions and partial electrostatic interactions [48]. The increase in keratin amount decreases these types of interactions due to the high content in polar residues such as cysteine. This will promote a more open structure thereby increasing the film swelling.

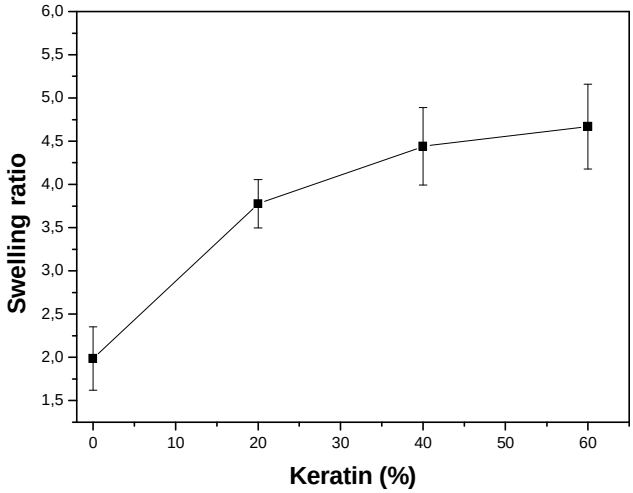

Figure 4.2. Swelling ratio calculated after 24 h of incubation in 100 mM Tris-HCl buffer, pH 8.0 at 37 ℃.

Silk fibroin/keratin films morphology was assessed by atomic force microscopy (AFM). With this analysis we intend to determine the effect of surface topography on the degradation as well on cell adhesion. On Figure 4.3 the roughness height images are shown. The pure SF film presented the higher roughness value and, its surface is characterized by well defined globular structures (Figure 4.3a) as already observed by others authors[40]. The formation of these structures is a consequence of the methanol treatment.

In the blends, the addition of keratin enables the formation of the globular structures making the surface of the film smoother. It can also be observed a decrease in the roughness value with the increase of keratin in the blend (Data not shown). Addition of keratin alters surface topography of the films and, as a consequence this might cause lost of film strength as already confirmed by *in vitro* degradation results [396].

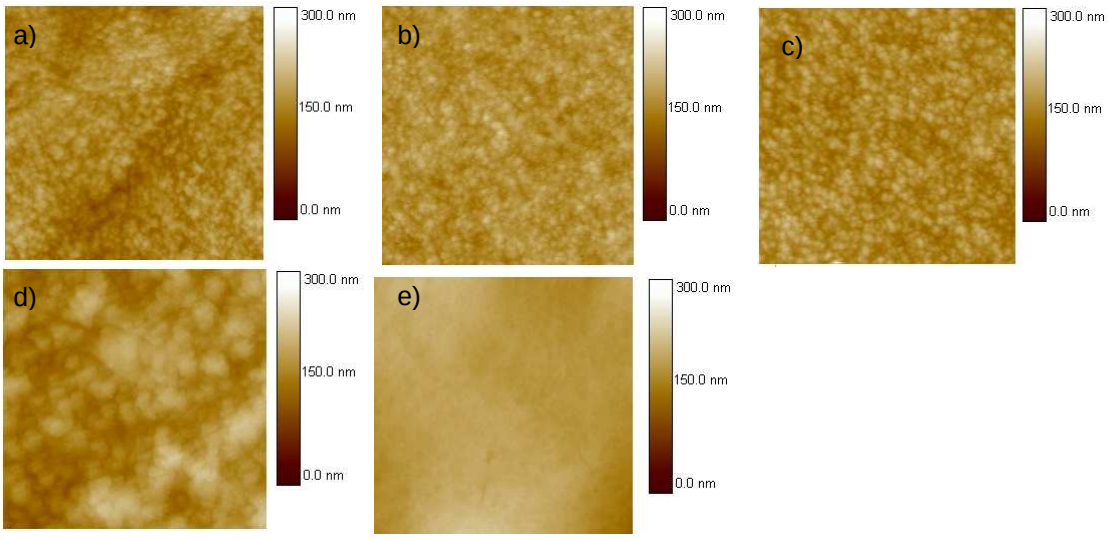

Figure 4.3. AFM height images of pure and blend silk fibroin/keratin films. (a) 100 SF; b) 80 SF; c) 60 SF; d) 40 SF; e) 100 K). The area measured was 10×10 μm.

Biocompatibility is an essential parameter to be evaluated for a biomaterial to be used in wound dressing. This was assessed for our materials through the use of mouse embryonic fibroblasts cultures. Two parameters were determined, cytotoxicity and cell adhesion. The results of the indirect contact study following fibroblast incubation with material extracts at different dilutions showed no cytotoxicity effect of the protein film extracts regardless of the extraction time.

Figure 4.4 represents the viability results for cells in contact with undiluted extract (extraction time 72 h). In all cases, the metabolic activity of cells in contact with the extracts was statistically equal or higher than the one obtained with negative control (complete medium).

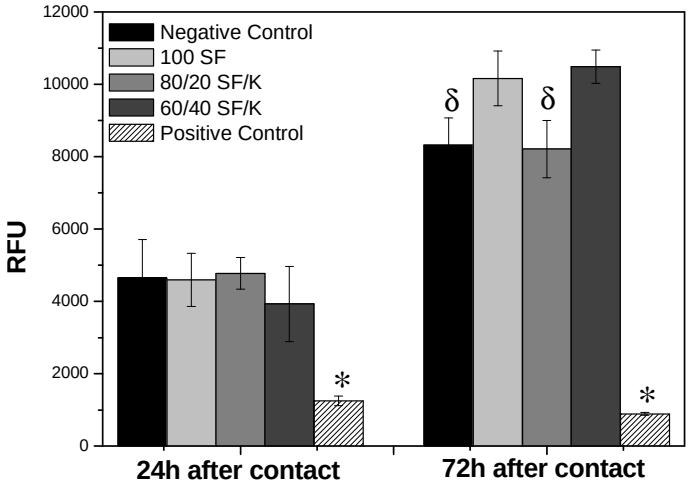

Figure 4.4. NIH 3T3 cell viability at 24 and 72 h of culture post contact with extracts of the different materials tested (72 h extraction time). The results obtained with the four materials were compared among each other and with the controls: * = significantly different from all the other tested conditions; δ = significantly different from 100 SF, 80/20 SF/K and 60/40 SF/K.

Direct contact study performed by seeding the cells on the membranes showed a time dependent increase of cell metabolic activity (Figure 4.5) that may suggest an increase of cell proliferation. This was confirmed by cell microscopic observation where cell number increased as a function of time. However, at the different time points studied, no significant differences were observed among the materials and the control suggesting that the structures observed in AFM analysis on the film surface did not affect cellular adhesion. Microscopic observations showed similar cell number, distribution and morphology on all materials, regardless of the time of contact. At 48 h (Figure 4.6), cells exhibited an elongated morphology with fusiform fibroblastic appearance already at confluence, as on the control (TCPS). F-actin staining revealed a well-defined cytoskeleton and numerous filopodia as well as cell-cell contacts. The same result was observed by Shudong et al. using mouse fibroblast cell lines [418]. These results are in agreement with the literature indicating that the processing steps involving the use of solvent systems will not

cause detrimental effects on the resulting material [36, 39, 43, 419]. Despite the fact that no cytotoxic effect was observed, it should be consider for posterior work, test the materials using cells form human source and use in vivo assays conditions such as wound animal models. In this way, parameters like inflammatory reactions and wound closing and healing will be determined.

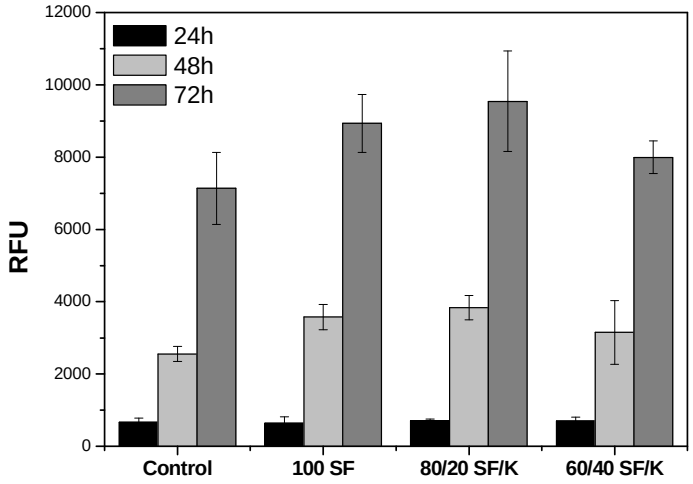

Figure 4.5. NIH 3T3 cell proliferation on discs of 100 SF, 80/20 SF/K and 60/40 SF/K.

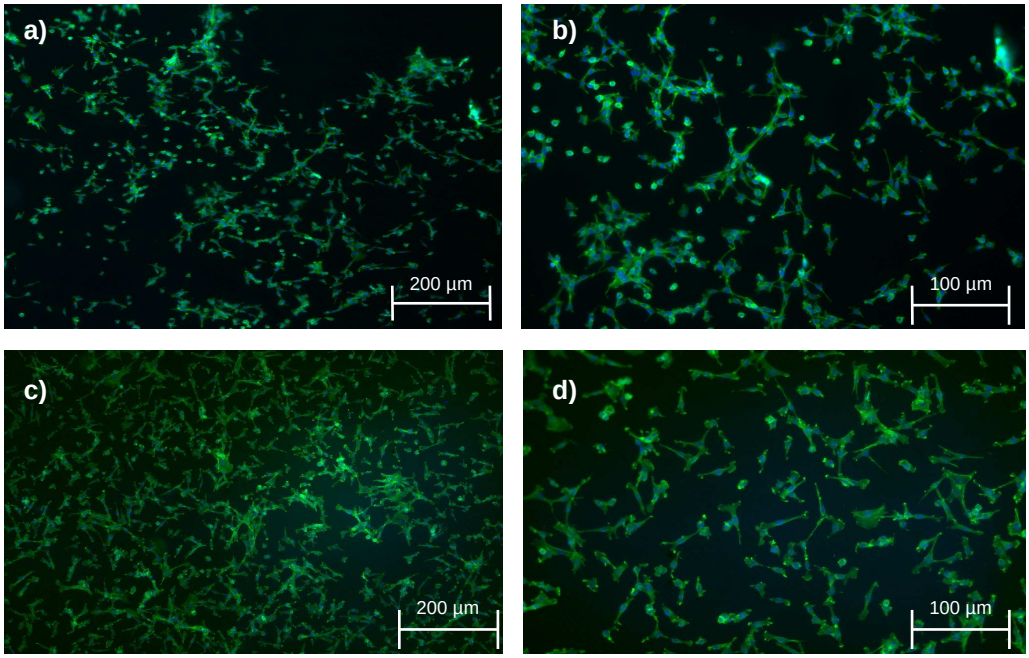

Figure 4.6. Fluorescent labelling of F-actin (green) and DNA (blue) of NIH 3T3 cells cultured for 48 h on TCPS(a and b) and discs prepared from 80/20 SF/K film (c and d).

4.3.2. *In vitro* release

The release profile of FITC-BSA from SF/K films is presented in Figure 4.7. Considering the loaded amount as 100% and normalizing the amount of FITC-BSA released in PPE solution, the profile is obtained. The release can be divided into two phases: an initial burst phase in the first 6 h and, a continuous release over the remaining time. The initial burst release might be related to the compound molecules that are on the surface of the film. Nevertheless, for pure SF film, the release is controlled and slow. In the blends, the release is fast and is dependent on the keratin amount. Methanol treatment leads to higher crystallinity making the film rigid and compact. Although this treatment leads to physical crosslinking of the films, incorporation of keratin, of hydrolytic nature, had a pronounced effect on the FITC-BSA release. This may be due to keratin dissolution causing more void volume for the release of the compound. The methanol treatment does not provide adequate stability for sustained release over days for films with high keratin content. The previous results obtained from mechanical tests [15] indicate that increase in keratin content leads to the decrease of the mechanical strength of the films. This will allow the formation of cracks in the film from where the compound can rapidly diffuse out.

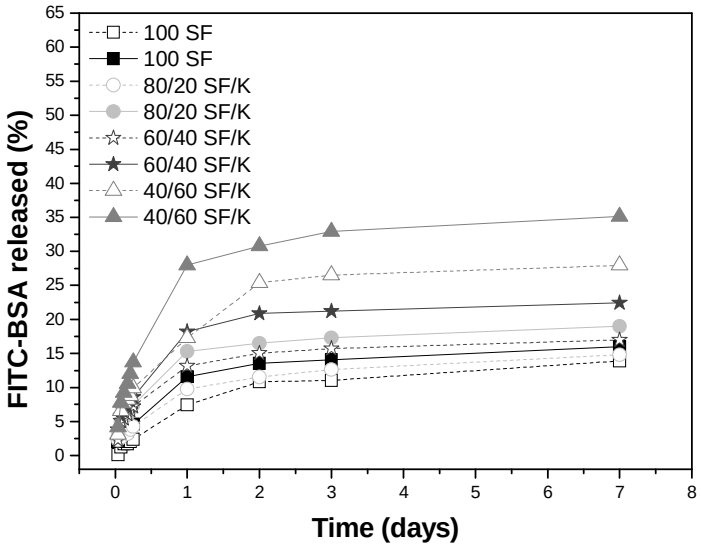

Figure 4.7. *In vitro* release profile of the peptide from SF/K films incubated with 0.1 U/mL of PPE solution.

To evaluate if the release from SF/K films is controlled by diffusion or dominated by film degradation, experimental data was fitted into the Ritger-Peppas equation as described in chapter II, equations 2.4 and 2.5. For a thin film, a Fickian diffusion of first-order is observed when n has the limiting value of 0.5; when n = 1, case II transport (polymer relaxation/degradation) occurs leading to zero-order release. When n lies between 0.5 and 1 anomalous transport is observed, coupling of Fickian diffusion and polymer degradation [420]. It can be concluded from the data obtained in Table 4.1 that for samples 100 SF and 80/20 SF/K the release is dominated by Fickian diffusion of first-order. The n value obtained for the blend 80/20 SF/K is closer to 0.5 indicating that addition of 20% of keratin decreases the rigidity of the compact structure of pure SF film improving the release properties. There is an increase in film swelling and consequently the diffusion of FITC-BSA.
For the blend 60/40 SF/K, the release is non-Fickian nature, "n" lies between 0.5 and 1 indicating that the release is due to the combination of diffusion and film degradation. The sample 40/60 SF/K show the highest "n" value (n>1) indicating that for this sample the release is totally dominated by film degradation. The sample 40/60 SF/K presents higher swelling ratio, degradation rate and, as a consequence, higher release rate. Furthermore, correlation coefficient "R^2" is above the permissible range, i.e. (R^2 = 0.95) indicating the validity of the results.

Table 4.1. Model compound release kinetic data obtained from fitting experimental release data to Ritger-Peppas equation where "n" is the diffusion exponent and R2 is the correlation coefficient

Sample	n	R^2
100 SF	0.411	0.996
80/20 SF/K	0.507	0.997
60/40 SF/K	0.551	0.997
40/60 SF/K	1.03	0.993

4.3.3. Inhibitory activity

The major goal of this work is the development of wound dressings with specific biological functionality - the inhibition of high levels of elastase. For this purpose, it was important to determine the inhibitory activity of the synthetic peptide selected. Several studies have been made to control elastase activity and promote chronic wound healing. A cotton-bound serine protease inhibitor has shown to decrease elastase activity on a chronic wound fluid [318]. The release of epidermal growth factor (EGF) from electrospun silk mats had also shown the promotion of wound healing [128]. Even so, there are few or no studies on the release of synthetic peptides from protein films to promote the inhibition of high levels of elastase found on chronic wounds exudate. Thus, this work presents an original system to control high levels of elastase found on chronic wounds. To determine the inhibitory activity of the peptide, increasing peptide amounts were incubated with elastase solution at 37 ℃. At determined time points, aliquots were taken to determine the residual activity. From the results obtained on Table 4.2 it can be seen that for high peptide concentrations PPE activity rapidly decreases, suggesting its ability to act as an elastase inhibitor. For lower peptide concentrations the decrease in half-life time of PPE is not so pronounced. It can be concluded that the decrease in PPE activity is dependent of peptide concentration.

Table 4.2. Hal-life time of PPE activity after 24 h of incubation with different peptide (5(6)-Carboxyfluorescein-YCQPPWSATCF-OH) concentrations at room temperature

Sample	$t_{1/2}$ (h)
PPE	28.3 ± 3.7
PPE + 20 μM	15.3 ± 2.1
PPE + 40 μM	11.6 ± 2.3
PPE + 60 μM	5.3 ± 1.2
PPE + 80 μM	3.8 ± 1.1

In order to understand the inhibition mechanism of this peptide, assays were performed to determine the inhibition constant. When the residual activity was plotted against substrate concentration it was observed that the elastase activity curve in the presence of peptide inhibitor converge, over the time, to the curve of elastase activity without peptide. This result might indicate that the peptide is being hydrolyzed by elastase which was confirmed by mass spectrometry analysis (Data not shown). Hydrolytic stability of BBI peptides as the one selected for this study is very important. Generally hydrolysis rates are low and are affected by the peptide sequence [363, 374]. The hydrolysis of our peptide occurred after 6 h of incubation with PPE. Nevertheless, its was observed a high decrease in elastase activity in the presence of peptide (Table 4.2) suggesting that its function was not affected by hydrolysis. Simulations performed based on the decrease in the mass value (from m/z = 1659.83 to m/z = 1512.75) indicated that hydrolysis might occur in one amino acid residue of the C-terminal. Probably this will not change the conformational structure of the peptide which allows it to retain the inhibitory activity. However, this fact has to be further investigated by other techniques such as NMR analysis. To determine if the peptide retains its inhibitory activity after incorporation onto SF/K films, films with 20 µM of peptide were incubated with PPE solution for 24 h. At determined time points the PPE activity was measured and the results are presented in Table 4.3 as half-life time of PPE. It can be seen that for 100 SF and 80/20 SF/K films, incorporation of the peptide increases the half-life time of PPE (22.7 ± 4.2 and 17.5 ± 3.3 h respectively) when compared with the peptide alone (15.3 ± 2.1 h). This result indicates the ability of the SF/K films to act as elastase inhibitors wound dressings. For the blends 60/40 and 40/60 SF/K the half-life time of PPE decrease in comparison to the peptide in solution (Table 4.3). The release of the peptide from SF/K films was also monitored for 24 h by fluorescence measurements (Data not shown). With the data obtained it was not possible to determine the release mechanism. Nevertheless, the release kinetics obtained with FITC-BSA allows concluding that in the first 24 h the decrease in PPE activity is mainly due to the swelling ratio. The high swelling ratio obtained for 60/40 and 40/60 SF/K blends means that PPE solution is rapidly in contact with inhibitor peptide into the film causing the fast decrease in PPE activity. If the measurements were prolonged for more time, the

release of peptide and consequently the decrease in PPE activity will be more influenced by degradation rate.

Table 4.3. Hal-life time of PPE after 24 h of incubation with SF/K films with 20 μM of peptide incorporated

Sample	Activity Loss (%)
PPE	28.3 ± 3.7
PPE + 20 μM	15.3 ± 2.1
100 SF	22.7 ± 4.2
80/20 SF/K	17.5 ± 3.3
60/40 SF/K	14.1 ± 2.1
40/60 SF/K	8.1 ± 1.1

In a heterogeneous system like this is important to determine the protein, PPE, adsorption to the SF/K films. In particular, it is important to distinguish the decrease of PPE activity due to the peptide action from the decrease in activity due to adsorption to the films. In order to evaluate this difference, films with and without peptide were incubated with PPE solution and the decrease in PPE activity was monitored.

It can be seen from Figure 4.8 that when PPE was incubated with SF/K films without peptide, the decrease in activity is much lower in comparison with films with peptide. This result validates the action of the peptide when it is incorporated into the SF/K films. Furthermore, it can be seen that protein (PPE) adsorption is also a function of the keratin amount.

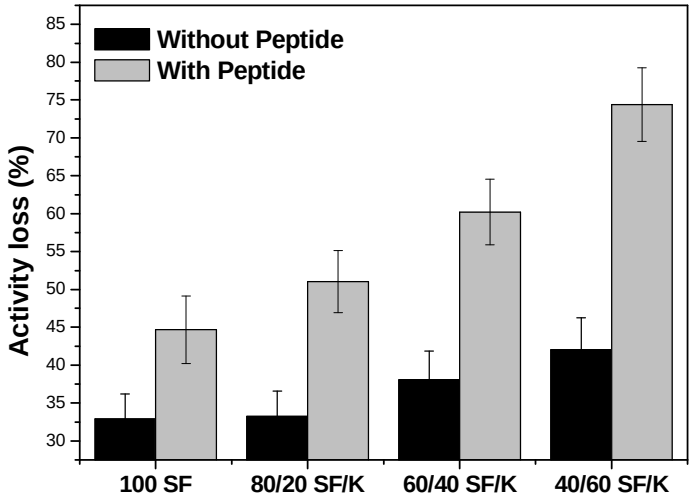

Figure 4.8. PPE activity loss after 24 h of incubation with SF/K films with and without peptide incorporated.

4.4. Conclusions

This study evidenced that blending silk fibroin and wool keratin results into a protein matrix suitable for sustained delivery of elastase inhibiting agents. The release pattern is affected by the degradation rate of the films and the knowledge of this allows the design of matrices with controlled release ability.

In vitro degradation was evaluated under PPE solution and, it was found that biological degradation is a function of keratin amount present in the film. The SF/K films were also tested for *in vitro* release using PPE solution as release medium. The results presented indicated that the release mechanism of molecules from the films is dominated by film degradation and diffusion. In this work the dehydrating step of methanol treatment was used to control the structure and stability of the self-assembly SF/K films. Pure fibroin films (100SF) present a rigid and compact structure, addition of keratin leads to a decrease in β-sheet content causing a more open structure which will affect swelling, degradation and release rates. Furthermore, our study indicated that the protein films developed are not cytotoxic and are able to support the adhesion of fibroblasts cells, making them suitable for biomedical applications such as wound dressings.

CHAPTER V

Novel silk fibroin/elastin scaffolds for wound dressings

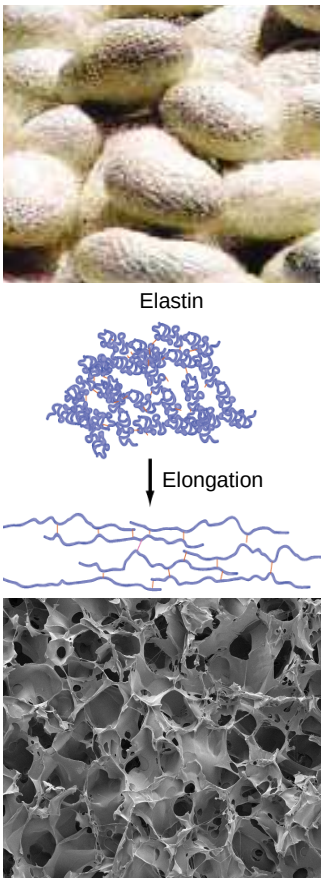

CHAPTER V

Novel silk fibroin/elastin scaffolds crosslinked with genipin for wound dressings

Abstract

Silk fibroin (SF) and elastin (EL) scaffolds were successfully produced for the first time by means of lyophilization technique. The self-assembly properties of SF, together with the excellent chemical and mechanical stability and, biocompatibility, were combined with elastin protein to produce scaffolds with the ability to mimic the extracellular matrix (ECM). Porous scaffolds were obtained and were further crosslinked with genipin (GE), through the formation of amide bonds. Genipin crosslinking induces the conformational transition from random coil to β-sheet of SF chains yielding scaffolds with smaller pore size, reduced swelling ratios, degradation and release rates. The evaluation of such biochemical properties using a human chronic wound exudate and the cytocompatibility demonstrated with human skin fibroblasts make these SF/EL scaffolds suitable for wound dressing applications.

This chapter is based on the following publication: **Andreia Vasconcelos**, Andreia C. Gomes & Artur Cavaco-Paulo, Novel silk fibroin/elastin scaffolds crosslinked with genipin for wound dressings, *Submitted*

5.1. Introduction

Skin wounds are the disruption of normal skin physiology. From the moment the wound is created, the healing mechanism is initiated to re-establish skin continuity. The healing process is complex and involves an integrate response of different cell types and growth factors [297-299, 421, 422]. Promotion of healing is often accompanied by the use of biocompatible wound dressings; these should promote a moist environment in the wound and serve as a shield against external factors like dust and bacteria; enhance water and vapor permeation and promote ephitelization by releasing biological agents to the wounds. Due to its unique properties of high mechanical strength and excellent biocompatibility, silk fibroin has been explored for the development of wound dressings. The degradation rates of electrospun silk materials applied to wound dressing have been evaluated [127] and the incorporation of growth factors into electrospun silk mats have shown to accelerate wound healing [128]. Moreover, silk films have been shown to heal full thickness skin wounds in rats faster than traditional porcine-based wound dressings [122]. Blending silk fibroin with other components has shown to improve the properties of the resulting material. This allows the modulation of biodegradation and release rates, important parameters in the biomaterials field. Recently, we developed silk fibroin/keratin films incorporating a synthetic inhibitor of elastase, to control the high levels of this enzyme produced in a chronic wound environment [326]. Silk fibroin/alginate sponges demonstrate higher healing effect than both components acting alone [123]. In this work, scaffolds based on silk fibroin and soluble elastin were developed and tested.

Elastin is an insoluble extracellular matrix protein that provides elasticity and resilience to the arteries, lungs and skin [203-205]. Due to it's highly crosslinked nature, elastin is highly insoluble and difficult to process into new biomaterials. As a consequence, soluble forms of elastin including tropoelastin [243], α-elastin [251, 253] and elastin-like polypeptides [233, 255, 261] are frequently used to develop elastin-based biomaterials. Nevertheless, a crosslinking step is required to obtain an insoluble material. There are several crosslinking methods for elastin including chemical [243, 251, 263], enzymatic [423], physical [253, 424-426] and

γ-irradiation [258]. Among them, chemical crosslinking agents are widely used. Aldehydes and epoxy compounds have been commonly used in biomaterial constructs due to their efficient formation of crosslinks with amino acid side chains, low antigenicity and sufficient mechanical strength. Despite these advantages, they exhibit high cytotoxicity [263, 427, 428]. Genipin (Ge) is a natural covalent crosslink agent isolated from the fruits of *Gardenia jasminoides Ellis* [375] that offers comparable crosslinking efficacy. It has been reported that genipin binds with biological tissues [381, 429] and biopolymers [380, 430] leading to matrices with good mechanical properties, reduced swelling extent and significantly reduced cytotoxicity when compared to synthetic crosslinking agents like glutaraldehyde and epoxy compounds [379, 380].

To our knowledge, elastin has been crosslinked with collagen [278, 279], fibrin [269, 270] and gelatin [279, 280] for the development of biomaterials, but never with silk fibroin. In this work, we developed silk fibroin/elastin (SF/EL) scaffolds crosslinked with genipin. The resulting materials were characterized by their physical-chemical properties and the effect of crosslinking on those properties was evaluated. Moreover, the wound dressing functionality of these materials was tested with a real chronic wound exudate.

5.2. Materials and methods

Herein it will be given a detailed description of some of the methods presented in the previous chapter. All other techniques were performed as described in Chapter II.

5.2.1. Materials

Elastin soluble from bovine neck ligament was purchased from Sigma (Spain). Genipin is a product of Wako Chemicals (Germany). The BJ5ta cell line (telomerase-immortalized human normal skin fibroblasts) was purchased from ATCC through LGC Standards. All other reagents, including those used in cell culture, were analytical grade and purchased from Sigma, Spain.

5.2.2. Preparation of Silk fibroin solution

Silk was purified from its sericin content as previously described in section 2.3, Chapter II. Silk fibroin (SF) solution (2% (w/v)) was prepared by dissolving fibroin in 9.6 M LiBr solution at 60 ℃ for 3 h. The resulting solution was filtered, and dialyzed against distilled water until complete removal of salts, using cellulose tubing (Sigma, Spain) (molecular-weight cut-off of 12000-14000 Da).

5.2.3. Silk fibroin/Elastin blends preparation; Crosslinking reaction; Scaffold formation

Elastin (EL) solution was prepared by dissolving the elastin powder in distilled water. SF (2%) and EL (1%) were mixed to prepare blends of 100/0 SF/EL, 80/20 SF/EL and 50/50 SF/EL. Genipin (GE) powder, 0.1% and 0.5% (w/v) was added to blend solutions under constant stirring at room temperature until complete dissolution of GE powder. The crosslinking reaction was carried out for 3, 6 and 24 h at 37 ℃. The resulting solutions were cast on 96-well plates and frozen at -20 ℃ for 2 days and freeze dried for 2 days to remove the solvent completely. SF/EL scaffolds without genipin were used as controls and were prepared by the same process described above. The control samples were identified as 100SF, 80SF and 50SF which correspond to 0, 20 and 50% of elastin and, crosslinked sponges were identified as 100SFyGE, 80SFyGE and 50SFyGE where y is the genipin concentration used. In order to induce the transition of SF from random coil to β-sheet structure and consequently insolubility, scaffolds were immersed in 90% (v/v) methanol solution for 30 minutes and then washed in distilled water and air dried.

5.2.4. Degree of crosslinking

The crosslinking degree was determined by the ninhydrin assay [45, 383, 384]. Samples (6.0 ± 0.7 mg) were heated with a ninhydrin solution (2% (w/v)) at 100 ℃ for 20 min. The optical absorbance of the resulting solution was recorded at a wavelength of 570 nm using a Heλios γ ThermoSpectronic spectrophotometer. The amount of free amino groups in the test sample after heating with ninhydrin is

proportional to the optical absorbance of the solution. The concentration of free NH_2 groups in the sample was determined from a standard curve of Glycine concentration vs. absorbance. SF/EL scaffolds prepared without genipin were used as control materials. Triplicate samples were evaluated. The degree of crosslinking was determined by the equation 2.1., Chapter II.

5.2.5. Swelling ratio

SF/EL scaffolds, treated with methanol and completely dry (60 ℃ for 24 h) were immersed in PBS buffer (pH 3.0; 7,4 and 11) at 37 °C for 24 h. The excess of buffer was removed and the wet weight of the scaffolds was determined. The swelling ratio of the film was calculated accordingly to equation 2.2., Chapter II.

5.2.6. *In vitro* degradation

Porcine pancreatic elastase (PPE): SF/El scaffolds previously treated with methanol, with and without crosslinking were incubated for 21 days at 37 ℃ in a solution containing 0.1 mg/mL of PPE in 100 mM Tris-HCl buffer, pH 8.0. The control samples were incubated in PBS buffer solution (pH 7.4) without enzyme and submitted to the same conditions. The solutions were replaced every 24 h.
Wound exudate: Wound exudate was collected from pressure wounds using a vacuum assisted closure system. Wound fluid was diluted 10-fold in PBS solution and centrifuged to remove cells and tissue material. SF/EL scaffolds were incubated with exudate in the same conditions described above in a fixed ratio of exudate per mg of scaffold of 6 mg/mL. At designed time points, samples were washed thoroughly with distilled water, dried in a desiccator and weighted to estimate the extent of degradation by equation 2.3., Chapter II.

5.2.7. *In vitro* release

The release of model compounds from SF/EL scaffolds was examined by the incorporation of Trypan-Blue (100 µg/mL) and FITC-BSA (2 mg/mL). For control samples, dyes were dissolved in the protein solution and stirred for 5 min at room temperatures. The resulting solutions were casted in 96-well plates to prepare the

SF/EL scaffolds. In the case of crosslinked ones, dyes were dissolved in the protein solution before crosslinking reaction. Before release studies, control and crosslinked scaffolds were treated with methanol. SF/EL scaffolds were incubated at 37 ℃ in PBS buffer and in a solution containing 0.1 mg/ml of PPE. Solutions were changed every 24 h, at determined time points aliquots were taken and, Trypan-blue release was determined by measuring the absorbance at 595 nm using a Heλios γ ThermoSpectronic spectrophotometer. FITC-BSA release was monitored by a multiplate reader (Synergy HT W/TRF from BioTek) in the fluorescence mode at emission wavelength of 490 nm. After each measurement, the samples were added back to the medium to restore the equilibrium conditions. The quantification of the release was established by a standard curve of both dyes. Release studies were performed in triplicate samples and for a period of 21 days.

5.2.8. Cytotoxicity evaluation

SF/EL scaffolds were tested for cytotoxicity according to the ISO standards (10993-5, 2009). Tests on extract were performed to analyse the cytotoxicity of the developed materials as previously describe in Chapter II. Data are presented as average ± S.D. Two-way Anova with Bonferroni post-tests was performed, with statistically significant differences when $p < 0.001$. All calculations were performed using GraphPad software (version 5.03) [431].

5.3. Results and discussion

5.3.1. Biochemical and biophysical properties of SF/EL scaffolds

Amino acid composition of the proteins used in this work was determined by HPLC analysis and the result is present on Table 5.1. The SF molecule is mainly composed of glycine (43.68%), alanine (29.34%) and serine (11.48%) amino acids which forms the typical -(-ala-gly-)$_n$- repeating motifs responsible for the formation of the β-sheet crystals [12]. Elastin is mainly composed of glycine (32.15%), alanine (24.12%), proline (11.85%) and valine (11.36%). *In vivo*, elastin results

from the directed crosslinking of its precursor, tropoelastin whose hydrophobic region is mainly composed of the mentioned amino acid residues [207-209].

Table 5.1. Amino acid composition of silk fibroin and soluble elastin

Amino acid	Silk fibroin (mol %)	Elastin (mol %)
Cyst	-	-
Asp	1.67	0.54
Ser	11.48	1.17
Glu	1.37	1.72
Gly	43.68	32.15
His	0.20	0,36
Arg	0.62	0,74
Thr	0.96	1.07
Ala	29.34	24.12
Pro	0.67	11.85
Cys	0.10	0.37
Tyr	5.30	1.49
Val	2.23	11.36
Met	0.10	0.31
Lys	0.33	0.33
Ile	0.66	2.24
Leu	0.58	6.03
Phe	0.72	4.16

The formation of covalent bonds on blended systems may produce stable and ordered materials with benefic effect on their properties. To achieve such effect, genipin was used to crosslink SF/EL scaffolds. Different crosslinking conditions were tested and the results are summarized on Table 5.2. After 3 h of reaction it was observed a color change in the solutions from light yellow to light blue indicating the reaction between both SF and elastin with genipin. It is described that genipin react with amino acids or proteins to form dark-blue pigments associated with the oxygen-radical polymerization of genipin [429, 430, 432]. After

6 h of reaction, the solutions became dark-blue and, from the results in Table 5.2, the maximum crosslinking degree was reached for the different scaffolds.

The exact mechanism behind the interaction of genipin with both SF and elastin is yet to be fully described. The generally accepted mechanism is similar to that observed for amino-group containing compounds [430, 433] where the ester groups of genipin interact with the amino groups of SF and elastin leading to the formation of secondary amide linkages. Moreover, the amino groups initiate nucleophilic attacks which results in the opening of the genipin dihydropyran ring. An inherent phenomenon of genipin crosslinking is self-polymerization which occurs by radical reaction of two amino-attached open rings [381, 382]. Some authors [432] reported that genipin preferentially reacts with the amino acids lysine and arginine. SF and elastin contain respectively, 0.95% and 1.07% of these amino acids (Table 5.1) which is a very low fraction. The crosslinking sites are thus low in number which results in lower crosslinking degrees when compared with other genipin crosslinked blend systems [44]. The highest crosslinking degree obtained for sponges containing elastin (Table 5.2) might be related with the slightly higher fraction of lysine and arginine amino acids.

Table 5.2. Degree of crosslinking obtained for SF/EL scaffolds for the different reaction conditions

Cross-linking treatment	Degree of cross-linking (%)		
	100SF	80/20 SF/EL	50/50 SF/EL
3h; 0.1% GE	15.2 ± 1.1	18.4 ± 1.5	22.6 ± 2.1
6h; 0.1% GE	22.1 ± 1.3	29.3 ± 1.1	31.7 ± 1.8
24h; 0.1% GE	23.5 ± 2.1	30.2 ± 1.5	29.8 ± 2.5
3h; 0.5% GE	20.3 ± 1.9	24.2 ± 1.1	27.3 ± 2.1
6h; 0.5% GE	28.6 ± 1.4	48.3 ± 2.2	52.2 ± 1.6
24h; 0.5% GE	29.4 ± 1.6	46.7 ± 1.3	50.6 ± 2.2

The genipin crosslinking of SF/EL scaffolds might induce conformational changes due to the structural rearrangement of chains to form covalent bonds. FT-IR spectra of SF and elastin, with and without crosslinking, in the range of 600-

2000 cm^{-1} are represented on Figure 5.1 and 5.2. SF protein exists in three conformations namely random coil, Silk I (α-form) and Silk II (β-sheet conformation).

The 100SF spectrum in Figure 5.1 showed bands at 1640 cm^{-1} for amide I (C=O stretching), 1517 cm^{-1} with a shoulder at 1532 cm^{-1} for amide II (N-H deformation) and 1238 cm^{-1} for amide III (C-N stretching, C=O bending vibration) indicating a random coil/Silk I conformation [45, 51, 78, 434]. SF molecules can structurally rearrange due to changes in the hydrogen bonding by methanol treatment acquiring a β-sheet conformation. Genipin crosslinking is also able to induce β-sheet conformation of SF molecules. Comparing the SF spectra obtained after genipin crosslinking (Figure 5.1) it is clearly the transition of random coil to β-sheet conformation confirmed by the shifting to lower wavenumbers of amide I (1620 cm^{-1}) and amide II (1514 cm^{-1}) bands [45, 51, 78, 434]. The shoulder observed at 1532 cm^{-1} for amide II assigned to random coil, progressively disappears with the increase in genipin concentration. Moreover, characteristic band of genipin at 1105 cm^{-1} (-COH) that appeared in the spectra of 100SF0.1GE and 100SF0.5GE confirms once again the reaction between genipin and SF. The FT-IR results evidenced that genipin crosslinking of SF is followed by protein conformational changes already shown by other authors [44, 45].

Figure 5.2 shows the spectrum for elastin protein that was acquired in powder form by diffuse reflectance. Due to the higher background obtained with this technique, the wavenumbers obtained are relatively higher. 100EL spectrum shows characteristic protein bands at 1689 cm^{-1} (amide I), 1550 cm^{-1} (amide II) and 1238 cm^{-1} (amide III), assigned to random coil conformation [26, 435, 436]. It can be seen that genipin induces in elastin structural changes into a more β-sheet conformation. This was confirmed by the shifting to lower wavenumbers of the bands mentioned above. In addition, the appearance of a new peak at 1109 cm^{-1}, characteristic of genipin, confirms the crosslinking reaction. The results obtained after methanol treatment of the scaffolds (Data not shown) show no additional changes, for both proteins, when compared with genipin crosslinked spectra.

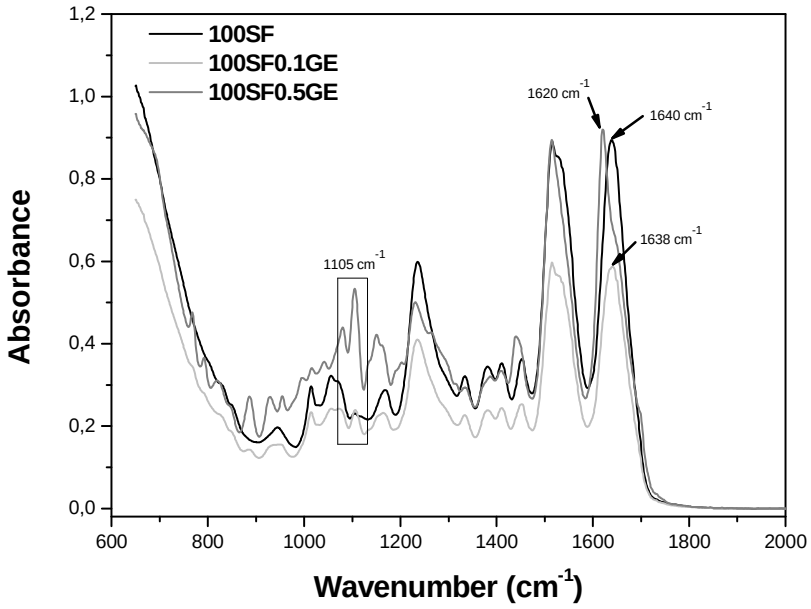

Figure 5.1. FT-IR absorbance spectra of pure silk fibroin (100SF) and crosslinked with genipin (100SF0.1GE and 100SF0.5GE).

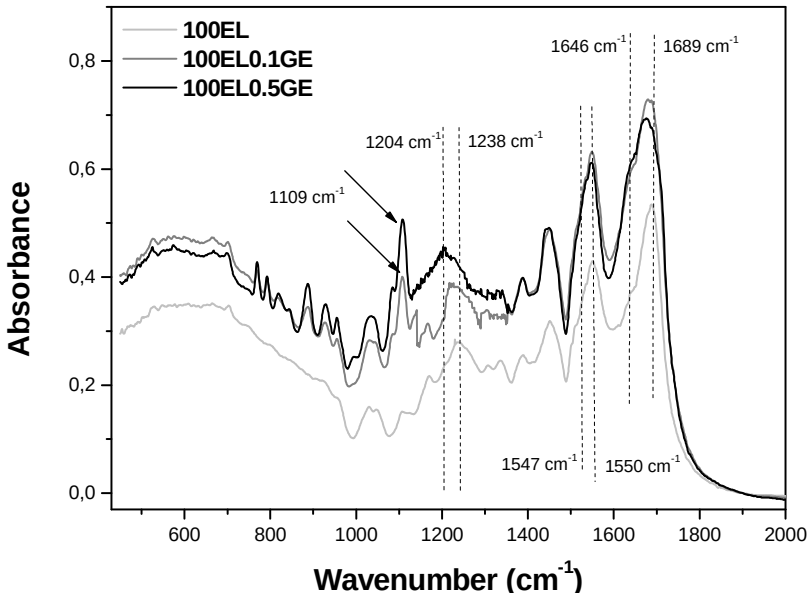

Figure 5.2. FT-IR absorbance spectra of pure elastin (100EL) and crosslinked with genipin (100EL0.1GE and 100EL0.5GE).

Deconvolution was limited to the amide I range (1590-1720 cm^{-1}) because protein conformation can be identified in this range [44, 437, 438].The results are shown in Table 5.3, indicated that pure SF scaffolds, without methanol treatment, are mainly in the conformation of random coil (46.06%) but presents also other

conformations like β-sheet and some intermediate forms like turns and bends [437, 438]. The addition of genipin promoted conformational changes into SF, especially with the sample with higher genipin concentration (100SF0.5GE). It can be observed an increase in the β-sheet content from 30.57% (100SF) to 57.96% (100SF0.5GE) indicating the crystallization of the SF chains. Moreover, the deconvolution results obtained after methanol treatment are similar to the results obtained for 100SF0.5GE sample indicating that methanol treatment will not cause additional conformational changes in the scaffolds. These results support the hypothesis that SF molecules can be structurally rearranged after addition of genipin as already demonstrated by others [44]. Deconvolution analysis was also performed on elastin (Data not shown). As already showed [439], the secondary structure of elastin is mainly characterized by a β-sheet conformation with the presence of undefined conformations. Our results correlate previous ones and, it can also be observed that after genipin crosslinking, there is an increase of undefined conformations for elastin.

Table 5.3. Deconvolution results obtained from the amide I region in the FT-IR spectra of SF scaffolds

	100SF	100SF0.1GE	100SF0.5GE	Methanol
β-sheet (Silk II)	30.57%	29.43%	57.96%	58.15%
Random coil/Silk I	46.06%	48.02%	18.87%	19.63%
Turns and bends	23.34%	22.56%	23.17%	22.21%

FT-IR spectra of blend systems show slightly changes of the wavenumbers and on the areas of the bands due to mixing effects of SF with elastin. The areas under the peaks for pure and blend systems were calculated by integration and, the ratio A_{N-H} (area of N-H bending) to $A_{C=O}$ (area of C=O stretching) is presented in Table 5.4. It can be observed that addition of elastin decrease the ratio of $A_{N-H}/A_{C=O}$. Moreover, the area of C-O-C, attributed to genipin, increases along with the ratio $A_{N-H}/A_{C=O}$ due to carboxyl group from genipin. This fact is an evidence of the crosslinking reaction. The higher decrease in the ratio $A_{N-H}/A_{C=O}$ obtained for the blend systems is the combined effect of addition of elastin and crosslinking.

Table 5.4. Peak areas of A_{C-O-C} (1150-940 cm^{-1}), A_{N-H} (1580-1470 cm^{-1}) to $A_{C=O}$ (1790-1580 cm^{-1}) as a function of scaffold composition and crosslinking conditions

Sample	A_{C-O-C}	$A_{N-H}/A_{C=O}$ (%)
100SF	-	99.6
80SF	-	89.4
50SF	-	70.0
100EL	-	58.1
100SF0.1GE	6.8	98.4
80SF0.1GE	8.4	87.0
50SF0.1GE	9.4	70.3
100EL0.1GE	11.3	57.4
100SF0.5GE	13.9	77.1
80SF0.5GE	14.1	74.0
50SF0.5GE	15.1	69.3
100EL0.5GE	15.4	55.5

The interaction between SF and elastin, crosslinked with genipin, was further investigated using thermal analysis (DSC). DSC scans for SF and elastin are shown in Figures 5.3 and 5.4 respectively. The DSC curve for 100SF shows an endothermic shift at 184 ℃ that corresponds to the glass transition temperature (T_g) of SF. This value is in the range of others previously reported for SF with a random coil conformation [15, 93]. The exothermic peak at 226 ℃ is related to the crystallization of amorphous SF chains cause by the transition to β-sheet structure [26, 27, 78]. The DSC curve of SF is also characterized by an intense endothermic peak at 284 ℃ (Td) related to the decomposition of SF chains. The thermal behavior of 100SF is typical of an amorphous SF with random coil conformation as previously shown by FT-IR results. Addition of genipin induces a small decrease in the T_g and an increase in the decomposition temperature. The increase in the thermal stability, given by the increase in T_d, of 100SF scaffolds containing genipin is due to the increase in the extent of covalent crosslinks. This fact is the confirmation of the crosslinking reaction between genipin and SF. Furthermore, the exothermic peak at 226 ℃ shifts to lower tempe rature (100SF0.1GE) and

disappears for the sample 100SF0.5GE. This result shows once again the change in the SF conformation from random coil to β-sheet after genipin crosslinking and, how this change is affected by the concentration of crosslinking agent.

The DSC curve of elastin (Figure 5.4) shows an endothermic shift at 197 ℃ assigned to the glass transition temperature of soluble elastin peptides [226]. The thermogram is further characterized by a weak and broad endothermic peak at 265 ℃, related to the decomposition of small aggregated structures and, a more intense endothermic peak at 320 ℃ related to component decomposition at high temperature. Addition of genipin caused the decrease in the T_g and, although it was not observed an increase in the decomposition temperature (320 ℃), the weak peak at 265 ℃ progressively disappears with the addition of genipin. This fact indicates that the small aggregates disappeared due to the crosslinking reaction between genipin and elastin. In the blend system (Data not shown) it is observed an increase in the decomposition temperature suggesting once again the crosslinking effect. Nevertheless, the increase in T_d is not dependent on blend composition because blends with higher crosslinking degree will not have higher thermal stability.

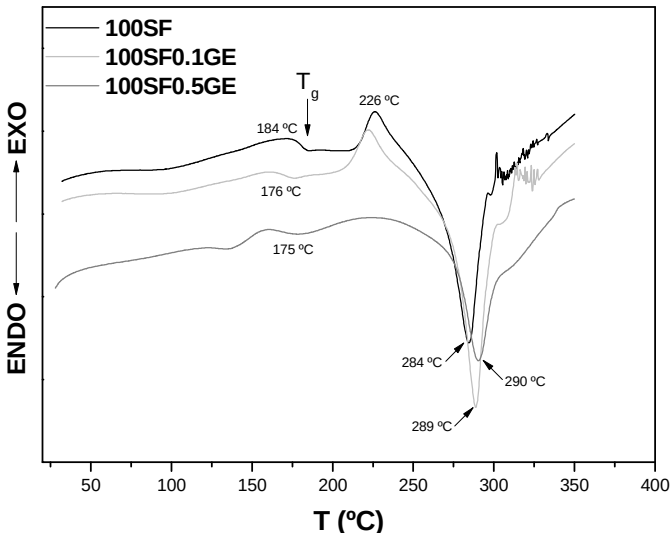

Figure 5.3. DSC scans of pure silk fibroin (100SF) and crosslinked with genipin (100SF0.1GE and 100SF0.5GE).

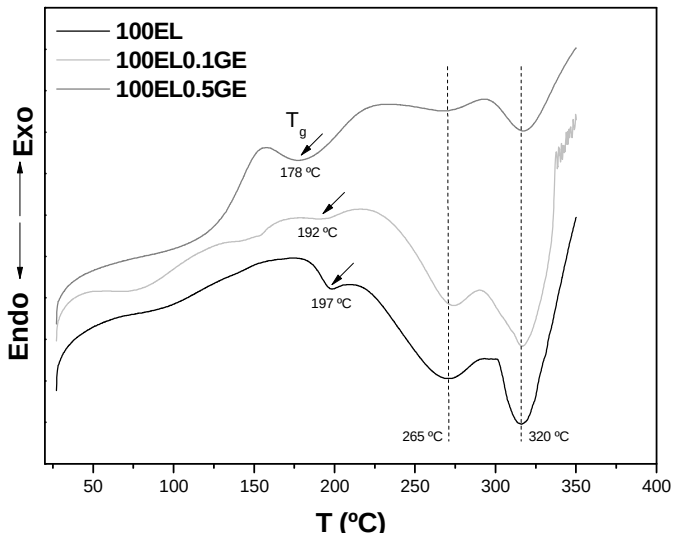

Figure 5.4. DSC scans of pure elastin (100EL) and crosslinked with genipin (100EL0.1GE and 100EL0.5GE).

The 3D morphology of the SF/EL scaffolds was analyzed by SEM. The images presented are related to control and crosslinked samples without methanol treatment. 100SF scaffold (Figure 5.5a)) shows a disordered pore-like structure with a rough surface. The pores are interconnected by a number of even smaller pores. Addition of elastin creates a more open and loose structure with thinner walls (Figure 5.5b) and 5c)). In the case of 50SF (Figure 5.5c)) it can be observed a fibrilar structure. The presence of large pores in the scaffolds facilitates cellular infiltration and growth within the 3D structure [252, 253]. However, such loose network will have detrimental effects on mechanical, swelling and release properties. To overcome this, genipin crosslinking was performed and the results clearly evidenced that genipin changes the scaffold morphology. 100SF0.5GE sample (Figure 5.5d)) shows a more ordered pore structure interconnected between sheets, characteristic of a β-sheet conformation [27, 56]. In addition, the SEM images obtained after methanol treatment (Data not shown) showed the same morphology observed with genipin crosslinking. This result indicated the interaction between genipin and SF with conformational changes that are patent on the scaffold morphology. This was further confirmed by FT-IR and DSC results. In the blended system, it can be seen that the loose network obtained upon addition of elastin becomes more closed and compact due to genipin crosslinking.

The fibrils observed in 50SF sample disappeared after crosslinking originating thicker walls (Figure 5.5f)).

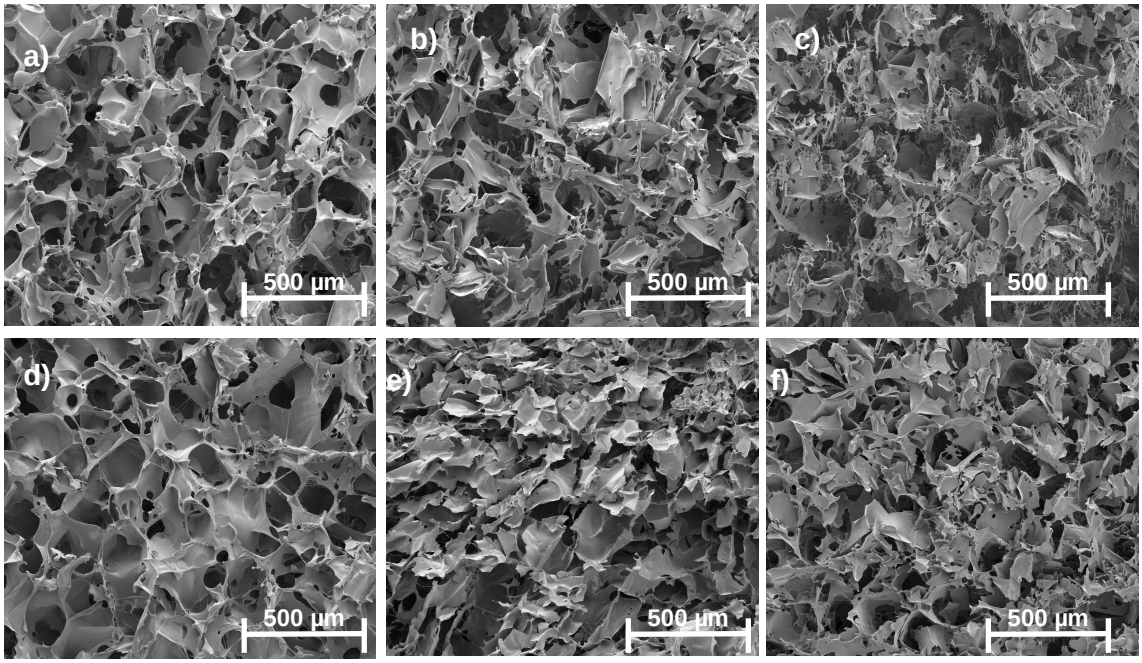

Figure 5.5. SEM images of SF/EL scaffolds without genipin (100SF a), 80SF b) and 50SF c)) and after genipin crosslinking (100SF0.5GE d), 80SF0.5GE e) and 50SF0.5GE f)).

Water-binding of scaffolds is an important parameter of biomaterials properties. To study the swelling ratio in response to external pH conditions, SF/EL scaffolds were immersed in PBS buffer solutions at pH 3, 7.4 and 11 for 24 h at 37 ℃. The swelling ratio of SF/EL samples was lower in acidic conditions and became progressively higher at neutral and alkaline media. The lowest swelling ratio obtained at pH 3 might be attributed to the formation of hydrogen bonds between SF and elastin due to the presence of carboxylic acid groups (-COOH) and hydroxyl groups (-OH). Increasing the pH, the carboxylic acid groups became ionized ($-COO^-$) and consequently, higher swelling ratios are observed due to a higher swelling force induced by the electrostatic repulsion between the ionized acid groups. The swelling ratio was found to be dependent on scaffold composition 50SF, with and without genipin, showed maximum swelling ratios (Figure 5.6). SEM analysis (Figure 5.5) indicates that 50SF samples presented larger pores with a loose network, still observed after crosslinking, which results in a higher

hydrodynamic free volume to accommodate more of the solvent molecules thus, increasing scaffold swelling [49, 440]. Crosslinking with genipin also affects the swelling ratio of the scaffolds, increasing genipin concentration leads to a decrease in the swelling ratios. Generally, the swelling behavior of the scaffolds can be controlled by its composition and crosslinking degree. In the SF/EL scaffolds, genipin crosslinking created stable structures that hinders the mobility and relaxation of the macromolecular chains, lowering the swelling ratio due to water restrict mobility [441]. This effect is more pronounced in 80SF and 50SF samples that attained higher crosslinking degrees when compared with 100SF (Table 5.2). The decrease in the swelling ratio can also be correlated with the scaffold compact structures formed after crosslinking (Figure 5.5d) e) f)).

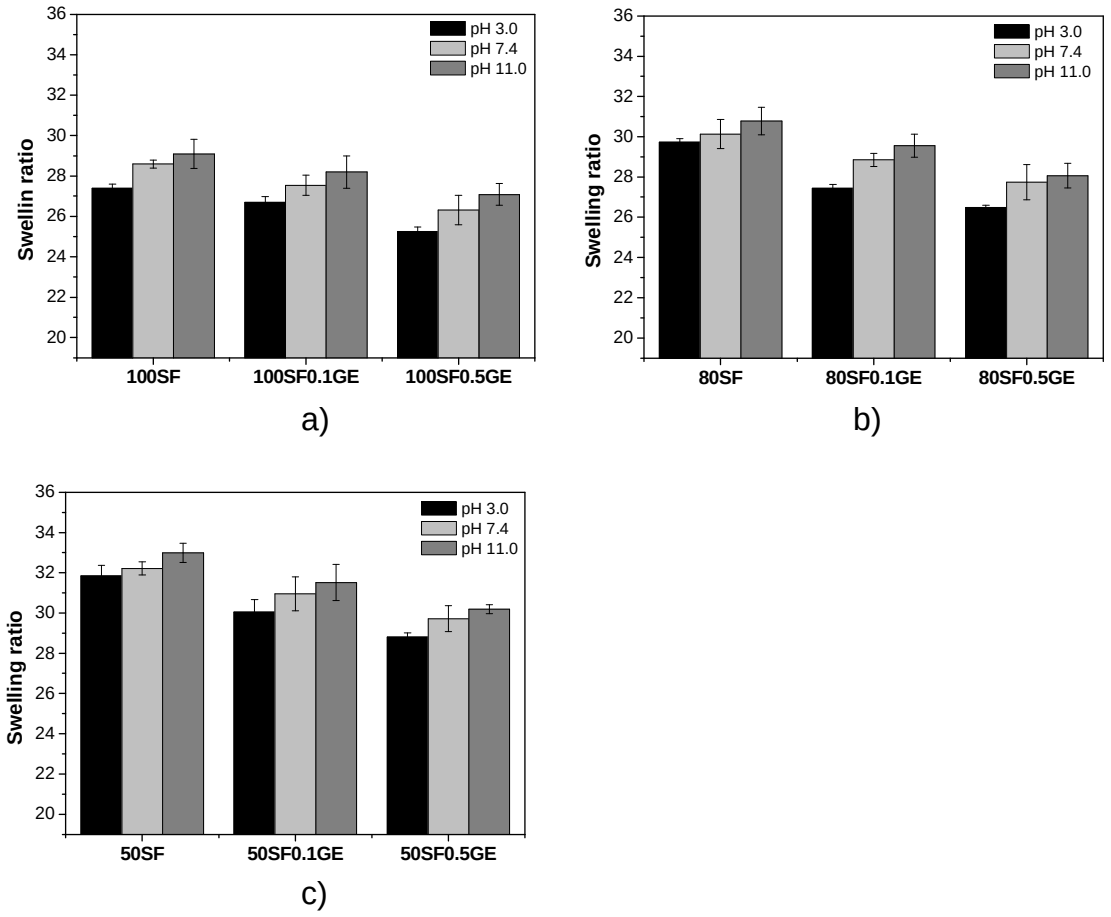

Figure 5.6. The pH-dependent swelling ration of 100SF a) 80SF b) and 50SF c) scaffolds after 24 h of immersion at 37 ℃.

5.3.2. *In vitro* and *ex vivo* biological degradation

Degradation rate of matrices plays an essential role on the determination of the release of entrapped bioactive agents. The *in vitro* degradation of SF/EL scaffolds was investigated by incubation in a physiological pH solution (PBS, pH 7.4) and a protease rich medium (PPE and human exudate from chronic wounds) at 37 ℃ for several days. At determined time points, samples were removed, washed with distilled water, dried and weighted to determine the extent of degradation.

The results are presented in Figure 5.7. Scaffolds incubated with PBS solution showed almost no degradation within 21 days. From the results in Figure 5.7 it can be seen that the degradation is dependent on scaffold composition. Higher weight loss was obtained for scaffolds containing higher amounts of elastin. After 21 days of incubation, the weight loss obtained for 100SF, 80SF and 50SF in PPE solution around 26, 36 and 49% respectively. The low weight loss obtained for 100SF is related to the crystallinity of fibroin due to the presence of β-sheet structures. Therefore, the observed weight loss is probably due to the degradation of small hydrolytically peptide sequences that remain after sponge crystallization [48]. Nevertheless, this effect is minimized after genipin crosslinking that increases the β-sheet content creating a closed and compact scaffold network (Figure 5.5d)). This will diminish the diffusion of solution within the scaffold increasing the resistance to protease degradation. The higher weight loss obtained with scaffolds containing elastin is because elastin is a substrate for elastase. In the human body, elastin, one of the major components of connective tissues, is degraded by human leukocyte elastase (HLE) [442-444]. In this way, SF/EL scaffolds might be used as elastase-specific wound dressings for chronic wounds. Moreover, elastin-based dressings have already demonstrated to promote a better wound healing either by an improvement of fibroblasts adhesion and proliferation [252, 253] or by the reduction of wound contraction [284, 445]. The loose network observed for scaffolds containing elastin (Figure 5.5c)) is also responsible for the higher weight loss obtained due to the increase in the surface area. As observed before, the genipin crosslinking decreases the weight loss observed. The creation of a more compact structure between SF and elastin hinders the scaffold degradation. These results show that genipin crosslinking was effective on the control of degradation.

The results obtained with wound exudate show the same degradation pattern but with higher values. The exudate solution used for incubation was less concentrated than PPE solution (2.4 µg/mL of total protein content). Nevertheless, the wound exudate is a mixture of several proteases, including HLE, that act synergistically increasing the hydrolysis.

Plotting the percentage of weight loss versus time, the degradation rates (%weight loss/day) can be calculated from the linear slope. The results on Table 5.5 show the degradation rates obtained for PPE and exudate in the first 7 days, during which the degradation is linear. It can be seen that scaffold degradation is faster for higher amounts of elastin and in the presence of wound exudate. The genipin crosslinking of the scaffolds induces a slower degradation.

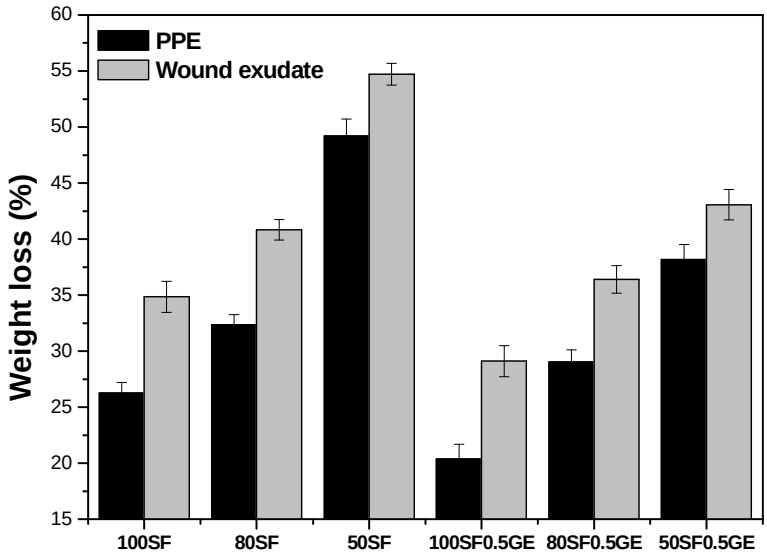

Figure 5.7. *In vitro* degradation of SF/EL scaffolds incubated with 0.1 mg/ml of PPE and wound exudate (2.4 µg/mL of total protein content) at 37 ℃ for 21 days.

Table 5.5. Degradation rates of SF/EL scaffolds calculated from the linear slope of the weight loss (%) versus time (days)

Sample	Degradation rate (%weight loss/day)			
	PPE	R^2	Exudate	R^2
100SF	1.8 ± 0.3	0.941	2.4 ± 0.5	0.943
80SF	2.1 ± 0.3	0.958	2.7 ± 0.6	0.924
50SF	3.6 ± 0.3	0.981	4.0 ± 0.4	0.971
100SF0.1GE	1.6 ± 0.3	0.907	2.1 ± 0.3	0.926
80SF0.1GE	2.1 ± 0.2	0.974	2.6 ± 0.5	0.921
50SF0.1GE	2.9 ± 0.2	0.984	3.7 ± 0.5	0.954
100SF0.5GE	1.4 ± 0.1	0.996	2.0 ± 0.5	0.907
80SF0.5GE	1.5 ± 0.1	0.998	2.4 ± 0.4	0.915
50SF0.5GE	2.6 ± 0.4	0.945	3.2 ± 0.6	0.905

5.3.3. *In vitro* release

The effect of scaffold composition and genipin crosslinking on the release of model compounds was investigated. The release behaviour of Trypan blue and FITC-BSA from SF/EL scaffolds in PPE solution is shown on Figure 5.8. The release of these compounds was monitored in PBS solution (Data not shown) and the release observed was low. Trypan blue has a small molecular weight (961 Da) while FITC-BSA has a molecular weight of 66 kDa, therefore, the release behaviour was also evaluated as a function of compound size.

In Figure 5.8 the release profile shown can be divided into three parts: an initial burst release in the initial 24 h, due to the release of the compound bound to the surface of the scaffold; a continuous phase release from 24 to 72 h and a stagnant phase release for the remaining period of time. This release profile is observed for both molecules but with higher released amounts attained for trypan blue. Due to its small molecular weight and hydrophilic nature, the diffusion through the scaffold and dissolution into the release medium is higher giving higher release. In contrast, the release of FITC-BSA is lower primarily because of its higher molecular weight but also to the relative hydrophobicity of FITC that hinders the

dissolution into PPE solution and, consequently, the release. Furthermore, for both molecules, it was observed that higher release was obtained for scaffolds containing higher amounts of elastin. The release of a compound from a matrix is governed by several factors such as nature and size of the compound, degree and density of crosslinking and pore size among others. From the SEM results discussed previously, it was concluded that higher elastin content leads to scaffolds with higher pore size which in turn cause the release of higher amounts of compounds. The effect of genipin crosslinking on the release profile was also evaluated. It can be observed from Figure 5.8 that crosslinking makes the release slower. This is attributed to the fact that genipin crosslinking enhances the decrease of pore size. In this way, the diffusion of the compounds through the sponge pores is more difficult and lower release is attained.

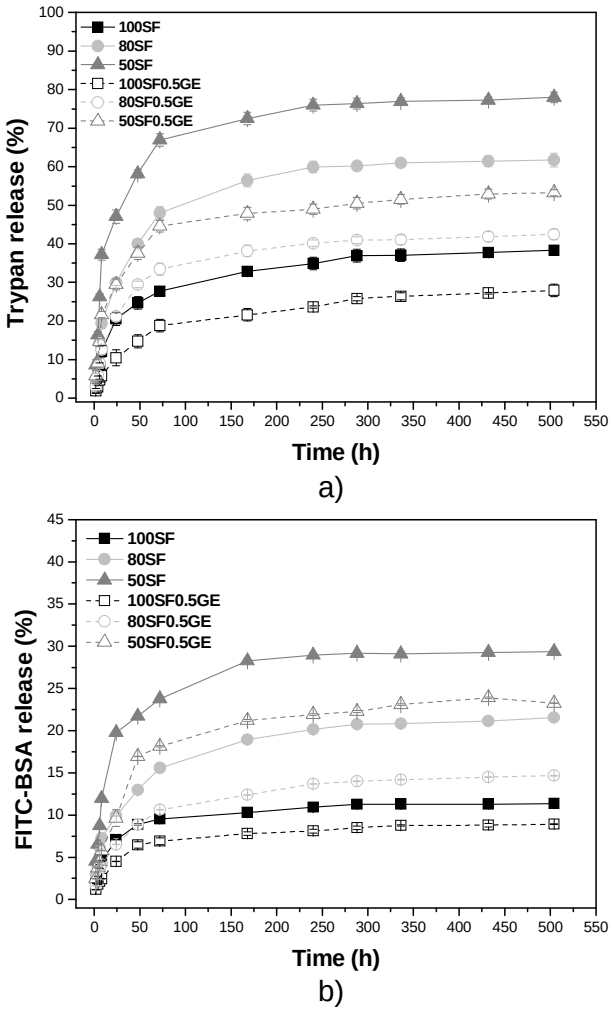

Figure 5.8. Cumulative release of trypan-blue a) and FITC-BSA b) from SF/EL scaffolds incubated with 0.1 mg/ml of PPE at 37 ℃ for 21 days.

To determine the release mechanism present in the SF/EL scaffolds, the experimental data was fitted to the semi-empirical power law model [446, 447] given by the Ritger-Peppas equation (equation 2.4., Chapter II). This equation is further modified to determine the diffusional exponent, n (equation 2.5., Chapter II) that depends on the release mechanism and on the geometry of the matrix [386, 446]. There are three different mechanisms that can be concluded from the n value. Therefore, the release, from a cylindrical geometry like the scaffolds developed, is purely Fickian diffusion when n = 0.45; for 0.45 < n > 0.89 anomalous (non-Fickian) transport is present and, for n = 0.89 the release is dominated by Case II transport (matrix relaxation or swelling-controlled mechanism). From the results presented on Table 5.6, for control samples without crosslinking, it can be concluded that the release of both compounds is dominated by anomalous transport because n values are above 0.45. In the blends, it can be seen that the increasing elastin content, the diffusional exponent, n, and release rate, k, values became progressively higher. As previously discussed, addition of elastin increases the swelling ratio and degradation rate. Thus, the higher n and k values obtained for the blends indicated that the influence of swelling and/or erosion in the release mechanism is higher for these samples. On the other hand, the n value for 100SF closest to 0.45 suggests that diffusion may play the major role on the mechanism. Moreover, the lowest k values obtained for the release of FITC-BSA confirm the considerations made earlier about the steric hindrance of the molecule size and nature on the release rate. Addition of genipin gradually changes the mechanism from anomalous transport to Fickian diffusion which is given by the n values closest to 0.45. Furthermore, the crosslinking effect on the scaffold morphology (compact and closed structure with smaller pores) also influences the release rate that becomes slower with higher amounts of genipin (lower k values). The release results clearly support the fact that the release from SF/EL scaffolds is affected by compound size and sponge composition and that genipin crosslinking can be used to modulate the release mechanism and rate of the compounds.

Table 5.6. Model compound release kinetic data obtained from fitting the experimental release data to Equation 5, Chapter II

Sample	Trypan Blue			FITC-BSA		
	n	k	R^2	n	k	R^2
100SF	0.481	0.383	0.960	0.474	0.255	0.945
80SF	0.523	0.683	0.956	0.503	0.416	0.958
50SF	0.553	1.03	0.947	0.500	0.618	0.938
100SF0.1GE	0.467	0.344	0.954	0.466	0.125	0.975
80SF0.1GE	0.517	0.636	0.958	0.478	0.187	0.984
50SF0.1GE	0.531	0.920	0.948	0.498	0.397	0.965
100SF0.5GE	0.451	0.137	0.990	0.433	-0.010	0.982
80SF0.5GE	0.474	0.491	0.952	0.452	0.148	0.973
50SF0.5GE	0.485	0.771	0.941	0.463	0.317	0.976

5.3.4. Cytocompatibility of SF/EL scaffolds *in vitro*

Biocompatibility of SF/EL scaffolds, with and without genipin crosslinking, was assessed in human skin fibroblasts *in vitro* cultures. The results of the indirect contact study after fibroblast incubation with material extracts showed no cytotoxicity caused by medium conditioned by the scaffolds regardless of the incubation time. Figure 5.9 represents the viability results for cells in contact with undiluted conditioned medium. In all cases, the metabolic activity of cells in contact with the extracts was statistically similar or higher than the one obtained with negative control (complete culture medium). This result constitutes a preliminary study of the biocompatibility of SF/EL scaffolds. Further evaluation of the cytotoxicity by direct contact is necessary.

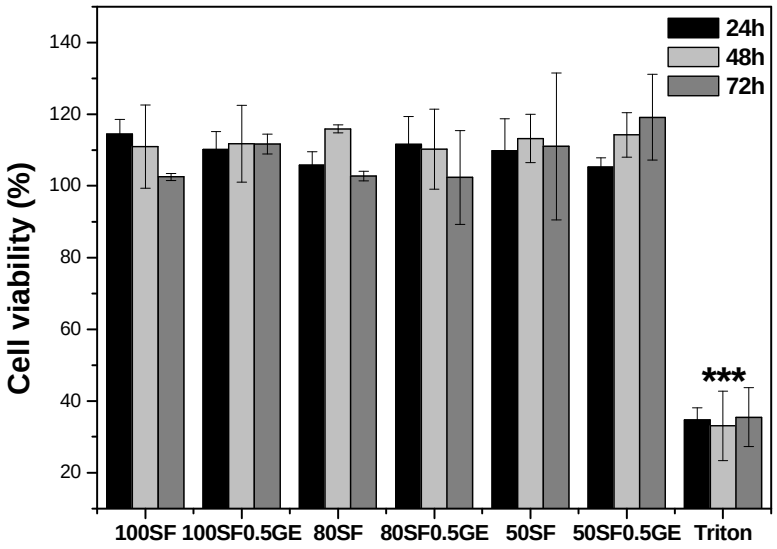

Figure 5.9. Viability of human normal skin fibroblasts after 24 h, 48 h and 72 h of contact with conditioned medium (culture medium where scaffolds were incubated). Only the positive control (treatment with Triton detergent) revealed diminished cell viability. (***= significantly different from all the other tested conditions, $p<0.001$).

5.4. Conclusion

Novel SF/EL scaffolds crosslinked with genipin were successfully prepared. The genipin crosslinking results in the conformational transition of SF chains from random coil to β-sheet conformation. The SF/EL scaffolds presented different pore sizes and distinct morphologies which are related with the elastin ratio and genipin crosslinking. The biochemical and biophysical properties of the scaffolds such as higher thermal stability, pH-swelling dependence and reduced biological degradation and drug release rates were obtained after genipin crosslinking with a concentration of 0.5%. A very important and new approach of this study was the use of a human wound exudate. Scaffolds degradation was evaluated using wound exudate and, genipin crosslinking promotes the decrease in the degradation rate. SF/EL scaffolds showed no cytotoxicity for human skin fibroblasts. The results presented are important in the design and application of tailor-made biomaterials for wound dressings.

CHAPTER VI

Tailoring elastase inhibition with synthetic peptides

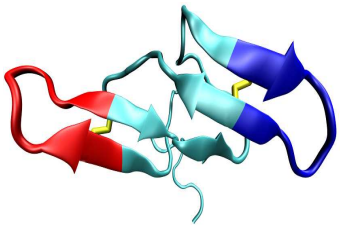

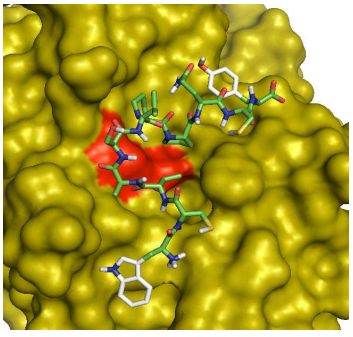

CHAPTER VI

Tailoring elastase inhibition with synthetic peptides

Abstract

Chronic wounds are the result of excessive amounts of tissue destructive proteases such as human neutrophil elastase (HNE). The high levels of this enzyme found on those types of wounds inactivates the endogenous inhibitor barrier thus, the search for new HNE inhibitors is required.

This work presents two new HNE inhibitor peptides, which were synthesized based on the reactive-site loop of the Bowman-Birk inhibitor (BBI) protein. The results obtained indicated that these new peptides are competitive inhibitors for HNE and, the inhibitory activity can be modulated by modifications introduced at the N- and C-terminal of the peptides. Furthermore, these peptides were also able to inhibit HNE from a human wound exudate while showing no cytotoxicity against human skin fibroblasts *in vitro*, greatly supporting their potential application in chronic wound treatment.

This chapter is based on the following publication: **Andreia Vasconcelos**, Nuno G. Azoia, Ana C. Carvalho, Andreia C. Gomes & Artur Cavaco-Paulo, Tailoring elastase inhibition with synthetic peptides, *Submitted*

6.1. Introduction

Elastases belong to the family of serine proteases that hydrolytically degrade connective tissues components such as elastin, proteoglycan, fibronectin and collagen types I, II, III and IV [448] Human neutrophil elastase (HNE) (EC 3.4.21.37) is a serine protease of the chymotrypsin family that is stored in the primary (azurophil) granules of polymorphonuclear neutrophils (PMNs) and is released by inflammatory stimuli. Under normal conditions the activity of HNE is regulated by endogenous inhibitors of the serpin (α_1-PI, MNEI, PI9), chelonianin (SLPI, elafin) families, and to a lesser extent by the polyvalent protease inhibitor α_2-macroglobulin. The serpins are high molecular weight inhibitors (40 to 50 kDa: 350 to 500 amino acids) that fold into a conserved, metastable structure and act as suicide substrate-like inhibitors using their reactive centre loop [348, 349]

The continuous activation of inflammatory cells is followed by the release of large quantities of HNE which inactivate the inhibitor defense. Excessive and uncontrolled HNE activity has been implicated in mediating tissue damage associated with chronic wounds and other major chronic inflammatory diseases including rheumatoid arthritis, chronic obstructive pulmonary disease, cystic fibrosis and adult respiratory distress syndrome [309, 338, 339].

In the area of wound healing, the presence of high levels of HNE is associated with the degradation of important growth factors [309] and major proteins of the extracellular matrix like fibronectin [449] which are vital for the normal wound healing process. Due to its involvement in such pathological processes, there has been considerable interest in the design of HNE inhibitors that may restore the normal levels of this enzyme in the above diseases. Apart from natural or engineered inhibitor proteins of high molecular mass, there has been an increasing interest in studying both peptide-based and non-peptide small inhibitor compounds [350]. In many natural inhibitor proteins, the portion responsible for the inhibitory activity is an extended or canonical loop which is complementary to the proteinase active site [354].

The Bowman-Birk inhibitors (BBI) are bi-headed serine proteinase inhibitors found in plants of the Fabaceae family [358]. These proteins have a low molecular weight (6-9 kDa) and are characterized by the presence of seven disulphide

bridges which allow the formation of a symmetrical structure comprising two independent heads located at opposite sides of the molecule (see Figure 6.1). Each head is made of a tricyclic domain in which the functional reactive site loop is located. Loop I typically inhibits trypsin and loop I inhibits chymotrypsin [354-357]. The interaction of BBI with serine proteases occurs via a well-defined disulfide linked short beta-sheet region which generates a non-covalent complex that renders the serine protease inactive [359]. The conformation of the reactive site loop is complementary to the active site of the protease inhibited and allows BBI to tightly bind to the protease [354]. BBI-derived synthetic peptides have previously been demonstrated to retain the inhibitory activity of the complete protein [359].

The present work is based on the ability in retaining the inhibitory activity of short peptide sequences that reproduce the reactive site-loop of BBI protein [359, 362, 363]. The synthetic peptide sequences were tested as inhibitors of HNE and PPE to determine the specificity of the peptides. Furthermore, the inhibitory activity of these peptides was also tested using chronic wound exudate, in order to evaluate their ability to be used as a part of a wound management strategy.

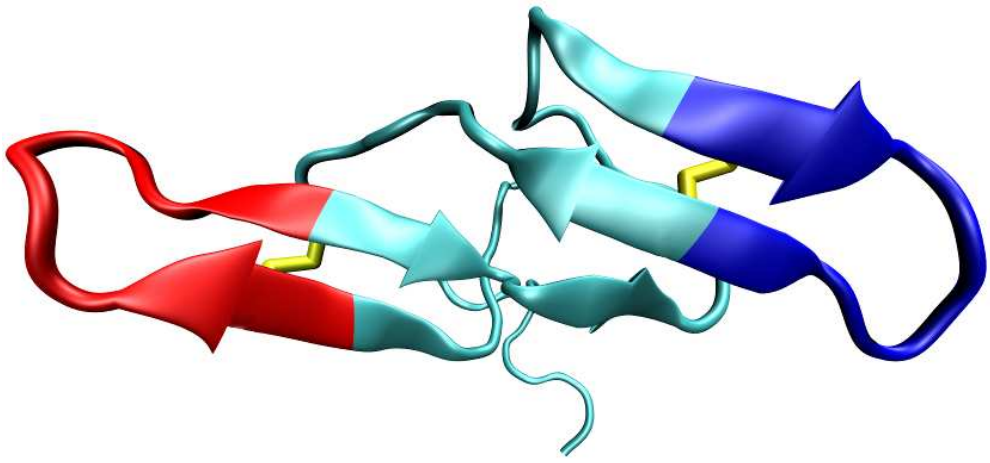

Figure 6.1. Three-dimensional structure of soybean trypsin/chymotrypsin Bowman-Birk inhibitor in solution (PDB code 1BBI [355]). Loop I is shown is red, loop II is blue and the disulphide bond is yellow.

6.2. Materials and methods

Herein it will be given a detailed description of some of the methods presented in the previous chapter. All other techniques were performed as described in Chapter II.

6.2.1. Materials

The Porcine Pancreatic Elastase (PPE), Human Neutrophil Elastase (HNE) and Elastatinal were purchase from Sigma, Spain. The peptides 1 (MGWCTASVPPQCYG, 1499.75 g/mol) and 2 (MGWCTASVPPQCYG$(GA)_7$, 2339.62 g/mol) were synthesized by JPT Peptide Technologies GmbH (Germany). The BJ5ta cell line (telomerase-immortalized human normal skin fibroblasts) was purchased from the European Collection of Cell Cultures (ECACC) and cultured according to ATCC recommendations. All other reagents, including those used in cell culture, were analytical grade and purchased from Sigma, Spain.

6.2.2. Collection of wound exudate

Wound exudate was collected from pressure wounds using a vacuum assisted closure system by the Medisch Spectrum in Twente. Wound fluid samples were weighed and 100 µL of phosphate buffer pH 7.0 were then added to 10 mg of wound fluid. Samples were incubated at room temperature for 1 h and then centrifuged at 2500 rpm for 20 min to remove cells and tissue-material. After centrifugation the wound exudate was sterilized using Oxy Fil Centrifugal Filter (0.2 µm membrane pore diameter). The samples were then ready for storage at -20 ℃ until further use. The total protein content in the wound exudate was determined by the Lowry method [450].

6.2.3. Determination of activity loss over time

The half-life times for HNE, exudate and PPE were determined following the incubation with different concentrations of inhibitor peptides (20-80 µM) at 25 ℃. The concentrations of HNE, exudate and PPE were 20 µg/mL, 2.4 µg/mL and

175 µg/mL respectively. At determined time points, aliquots were taken and the activity was determined against the synthetic substrates, 5 mM of N-Methoxysuccinyl-Ala-Ala-Pro-Val-*p*-nitroanilide for HNE and exudate. A stock solution of this substrate of 20 mM was prepared in DMSO (dimethyl sulfoxide). To prepare the 5 mM solution, the required amount of the stock solution was added to 0.1 M HEPES buffer, 0.5 M NaCl, pH 7.5. The substrate used for PPE was N-Succinyl-Ala-Ala-Ala-*p*-nitroanilide, 4.4 mM prepared in 0.1 M Tris-HCl buffer, pH 8.0. The absorbance was monitored for 5 min at 410 nm using a Heλios γ ThermoSpectronic spectrophotometer. Control assays were performed in the same conditions but without inhibitor. Measurements were recorded in triplicate and the results were expressed as mean value ± S.D. (standard deviation).

6.2.4. Inhibition kinetics

The inhibition kinetics of the peptides was determined by competitive binding studies [370, 374]. Briefly, 15 µL of proteases (HNE (20 µg/mL), exudate (2.4 µg/mL) and PPE (175 µg/mL)) were incubated with 15 µL of peptide inhibitors (20-80 µM) for 30 min at 25 ℃. The final volume of each sample was adjusted to 300 µL with 0.1 M HEPES buffer, 0.5 M NaCl, pH 7.5 (HNE and exudate) and 0.1 M Tris-HCl buffer, pH 8.0 (PPE). The reaction was initiated with the addition of an adequate volume of substrate to obtain a substrate concentration range of 100-3000 µM. The substrate for HNE and exudate is N-Methoxysuccinyl-Ala-Ala-Pro-Val-p-nitroanilide 5 mM and for PPE is N-Succinyl-Ala-Ala-Ala-*p*-nitroanilide 4.4 mM prepared in the respective buffer solutions. The residual activity was determined by the increase in the optical density at 410 nm over 10 min using a microplate reader (Varian). Control assays were performed in the same conditions without inhibitor peptides. All assays were done in triplicate and the results are expressed as the mean value ± S.D. K_i was determined by nonlinear regression analysis [451] using the GraphPad Prism software [431]

6.2.5. Determination of IC_{50} for proteases using synthetic substrates

To determine the IC_{50} values of the inhibitor peptides against proteases, 15 µL of proteases (HNE (20 µg/mL), exudate (2.4 µg/mL) and PPE (175 µg/mL)) were

incubated with 15 µL of peptide inhibitors (20-80 µM) for 30 min at 25 ℃. The volume was adjusted to 300 µL with respective buffer solutions. The reaction was started after the addition of 27 µL of 400 µM of N-Methoxysuccinyl-Ala-Ala-Pro-Val-*p*-nitroanilide (HNE and exudate) and N-Succinyl-Ala-Ala-Ala-*p*-nitroanilide (PPE). The increase in optical density at 410 nm was monitored over 10 min using a microplate reader (Varian). All assays were done in triplicate and the results are expressed as mean value ± S.D. IC_{50} was determined using the GraphPad Prism software, version 5.03 [431].

6.2.6. Determination of IC_{50} for HNE and exudate using insoluble elastin

The ability of the synthetic peptides to inhibit the hydrolysis of insoluble elastin by HNE was determined spectrophotometrically using elastin congo-red as a substrate according to the method previously described [452]. Briefly, elastin congo-red (2 mg/mL) and HLE (20 µg/mL) and exudate (2.4 µg/mL) were incubated with various concentrations of peptides (20-80 µM) in 1.5 mL of 0.1 M Tris-HCl buffer, pH 8.0 containing 0.2 M NaCl at 30 ℃ for 1 h. After incubation, the reaction was stopped by the addition of 1.5 mL of 0.1 M acetic acid and, the mixture was centrifuged at 3000 rpm for 10 min at room temperature. After centrifugation, the absorbance of the supernatant was measured at 495 nm using a Heλios γ ThermoSpectronic spectrophotometer. Triplicate measurements were made for each inhibitor concentration and the results are expressed as mean value ± S.D.

6.2.7. Silk fibroin films preparation and peptide incorporation

Silk fibroin films (SF) were prepared as described [326]. Briefly, SF solution 1% (w/v) was prepared by dissolving degummed silk fibers into a saturated solution of LiBr at 60 ℃ for 3 h. The solution was then filtered, and dialyzed against distilled water using, cellulose tubing (molecular-weight cut-off of 12000-14000 Da), until complete removal of salts. The peptides (40 µM) were mixed with the SF solution for 5 min at room temperature. After this time, solutions were cast in 24-well plates and dried overnight at room temperature. In order to induce the transition of SF from random coil to β-sheet structure and consequently

insolubility, the films were immersed in 90% (v/v) methanol solution for 30 minutes and then washed in distilled water and air dried. Films were incubated with HNE for 1 h at 25 ℃ and then aliquots were taken for the evaluation of HNE activity decrease as described above.

6.2.8. Cytotoxicity evaluation

The peptides were tested for cytotoxicity using the BJ5ta cell line (normal human skin fibroblasts) was used to determine the cytotoxicity of the peptides as described in Chapter II. Data are presented as average ± S.D. Non-parametric, Wilcoxon matched samples test was used, with statistically significant differences when $p < 0.05$. All calculations were performed using GraphPad Prism software, version 5.03 [431].

6.3. Results and discussion

In this study synthetic peptides based on the anti-trypic loop of the BBI protein were used for the design of new inhibitor peptides. Based on the nomenclature of Schechter and Berger [328], the primary contact region between the inhibitor and the enzyme is the scissile peptide bon P1-P1'. Therefore, the specificity of the inhibition is dictated by the P1 residue which typically reflects the substrate preference of the target enzyme [366, 367]. The peptide selected from the combinatorial library [362] has an alanine residue in the P1 position (Figure 6.2). This residue in this position is consistent with the substrate specificity of elastase for small alkyl side chains [335, 453, 454]. The stability and consequently the biological activity of the BBI-based peptides are supported by an extensive intramolecular hydrogen-bond network. The main-chain to main-chain hydrogen bond between P2 and P1' (Figure 6.2, dash lines) is responsible for projecting the P1 side-chain outwards for the primary interaction with the enzyme [356, 357]. The *cis*-Pro-*trans*-Pro motif in the P3'-P4' positions and, the disulphide bridge covalently linking the P3-P6' positions together with the hydrogen bond network guarantees the β-hairpin conformation typical of the BBI protein [359, 362, 455].
In this study, the 9-residue motif was maintained in the new peptides but, without generate de disulphide bond between P3-P6' positions. To this 9-residue motif,

modifications were made in the N-terminal, by the introduction of methionine (M) and glycine (G) (Peptide 2, MGWCTASVPPQCYG, Figure 6.2, light gray circles). This sequence was maintained and a glycine/alanine (GA) tail (n=7) was added to the C-terminal (Peptide 3, MGWCTASVPPQCYG(GA)7, Figure 2, dark gray circles).

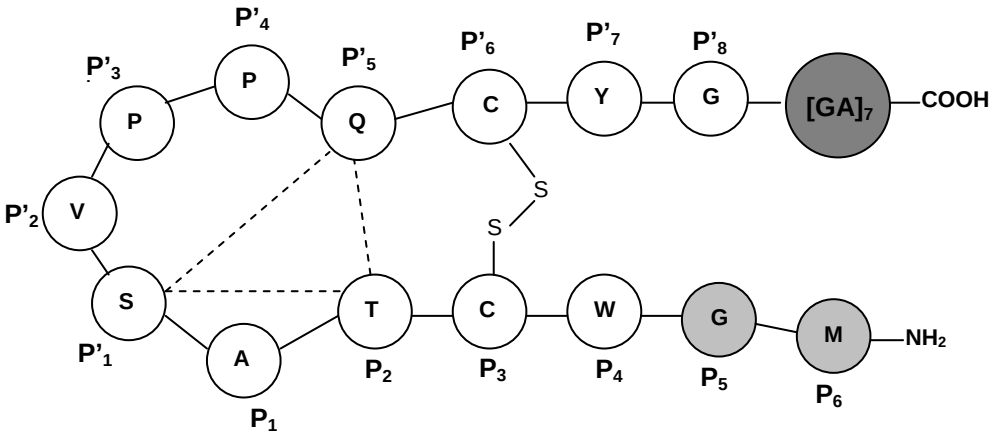

Figure 6.2. Representation of the peptide sequences mimicking the reactive site loop of the Bowman-Birk Inhibitor protein.

6.3.1. Activity loss over time

The time of incubation necessary to obtain a decrease in 50% of elastase activity, was determined by incubating the peptides with PPE, HNE and wound exudate and the decrease in activity was monitored over the time as described in experimental section. In our study, it was also used elastatinal, a small molecular weight elastase inhibitor, as a control.

Figure 6.3, represents the activity loss obtained with the lowest concentration of peptides used (20 µM) after 30 min of incubation. It can be observed that after 30 min it was obtained more than 50% of activity loss for all the peptides. Nevertheless, both peptide 3 and elastatinal present higher activity loss than peptide 2, especially for human elastase, indicating the higher inhibitory activity. The time of incubation determined (30 minutes) will be used in the further experiments.

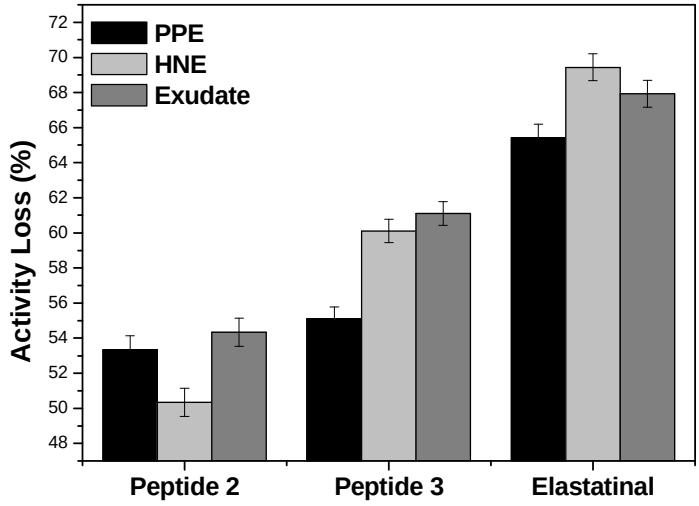

Figure 6.3. Activity loss obtained after 30 min of incubation at 25 ℃ of elastases with 20 µM of peptides 2, 3 or elastatinal. (Peptide 2 = MGWCTASVPPQCYG, peptide 3 = MGWCTASVPPQCYG$(GA)_7$)

6.3.2. Inhibition kinetics

In order to establish the inhibition mechanism, PPE, HNE and wound exudate were incubated with different peptide concentrations. To analyse the inhibition, Lineweaver-Burk plots, i.e. double-reciprocal plot for the hydrolysis of the synthetic substrates were determined for all the peptides and enzyme (Data not show for PPE and wound exudate). Figure 6.4 represents the progress curves for the inhibition of HNE by both peptides (Figures 6.4a) and 6.4b)) and the correspondent Lineweaver-Burk plot (Figures 6.4c) and 6.4d)). From the analysis of the last, it can be determined the mechanism of inhibition and from the results, peptide MGWCTASVPPQCYG and MGWCTASVPPQCYG$(GA)_7$ are competitive inhibitors for HNE, PPE and wound exudate. Then, non-linear regression was applied to determine the Michaelis-Menten constant (K_m) and V_{max} by equation 2.6., Chapter II.

The results also confirmed the type of inhibition present because V_{max} remains unchanged in the presence of different peptide concentrations and, there is an increase in the K_m. These values are higher for HNE in the presence of peptide MGWCTASVPPQCYG$(GA)_7$, indicating that this peptide causes higher inhibition.

The competitive inhibition exhibited for peptides MGWCTASVPPQCYG and MGWCTASVPPQCYG$(GA)_7$ may work through direct competition with the substrate by binding to the active site, or binding to a remote site and causing a conformational change in the enzyme.

Competitive inhibitors cause an apparent increases of K_m (i.e., the inhibitor interferes with substrate binding) without affecting V_{max} (inhibitor cannot bid to the complex enzyme-substrate). Therefore, inhibition constants (K_i) were determined by the modified Michaelis-Menten equation for competitive inhibition using the equation 2.7., Chapter II.

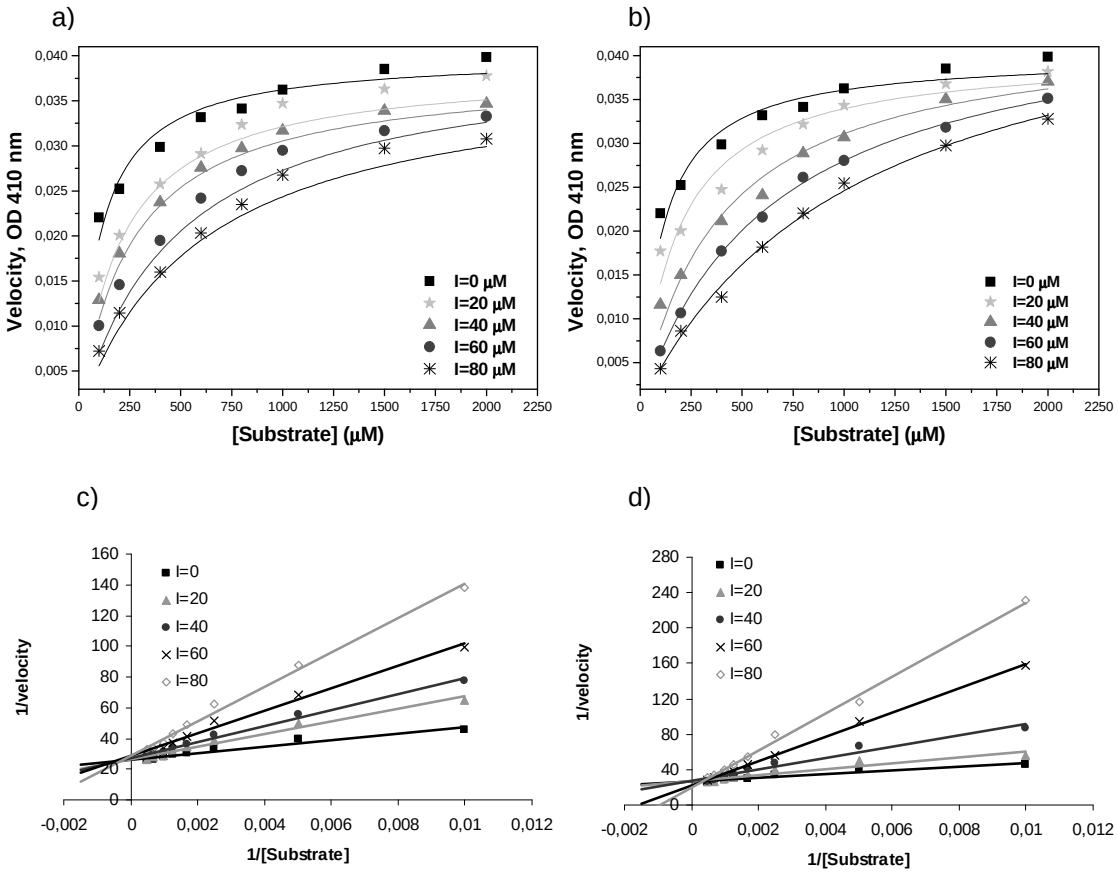

Figure 6.4. Progress curves for the inhibition of HNE by peptide 2 (a) and peptide 3 (b) for the hydrolysis of the synthetic substrate. The correspondent Lineweaver-Burk plots are represented in c) peptide 2 and d) peptide 3. (Peptide 2 = MGWCTASVPPQCYG, peptide 3 = MGWCTASVPPQCYG$(GA)_7$)

The inhibition constants (K_i) obtained for the peptides are presented in Table 6.1. It can be observed that the inhibition constants obtained for peptide MGWCTASVPPQCYG$(GA)_7$ presents the best results, especially for HNE. There is an improvement in K_i for HNE obtained for peptide WCTASVPPQCYG [363], when amino acid residues were added to both N- and C-terminals.

The K_i ratio presented shows the selectivity of the peptides for HNE. The results indicate that peptide MGWCTASVPPQCYG$(GA)_7$ presents higher specificity for HNE. Moreover, K_i values obtained for PPE, HNE and wound exudate with the peptides are comparable, and in some cases better (peptide MGWCTASVPPQCYG$(GA)_7$ for HNE), with the K_i obtained for elastatinal.

A very important result and approach of this study, is the use of a human wound exudate. The peptides MGWCTASVPPQCYG and MGWCTASVPPQCYG$(GA)_7$ present good inhibition constants and the differences obtained when compared with HNE (Sigma) might be related with the presence of other proteases present in the exudate that can interfere with the inhibition.

Table 6.1. Inhibition constants (K_i) obtained for the peptides against PPE, HNE and wound exudate. (*Values were obtained from the literature [363], Peptide 1 = WCTASVPPQCYG, peptide 2 = MGWCTASVPPQCYG, peptide 3 = MGWCTASVPPQCYG$(GA)_7$)

Peptide	Ki (μM)			K_iPPE/ K_iHNE
	PPE	HNE	Exudate	
Peptide 1*	13	2.77	-	-
Peptide 2	8.1 ± 1.6	6.3 ± 1.2	7.0 ± 1.8	1.3
Peptide 3	7.0 ± 2.0	0.4 ± 0.01	3.1 ± 0.9	17.5
Elastatinal	9.7 ± 1.4	6.7 ± 1.1	7.8 ± 1.2	1.2

6.3.3. IC_{50} for proteases

The inhibitory activity of peptides MGWCTASVPPQCYG and MGWCTASVPPQCYG$(GA)_7$ against PPE, HNE and wound exudate were evaluated using synthetic and natural substrates. The results were compared with the activity

of elastatinal inhibitor as control. IC_{50} values obtained for peptides MGWCTASVPPQCYG, MGWCTASVPPQCYG$(GA)_7$ and elastatinal, using synthetic substrates, are presented in Table 6.2 and are within the range of 11 – 19 µM. Once again peptide MGWCTASVPPQCYG$(GA)_7$ shows the lowest IC_{50} values which are the results of a higher inhibitory activity already demonstrated by the K_i values. The ability of peptides MGWCTASVPPQCYG and MGWCTASVPPQCYG$(GA)_7$ to inhibit the hydrolysis of insoluble elastin by HNE was also evaluated. Peptides MGWCTASVPPQCYG and MGWCTASVPPQCYG$(GA)_7$ present lower IC_{50} values in comparison with elastatinal under our assay conditions. Peptide MGWCTASVPPQCYG$(GA)_7$ presents higher inhibitory activity in the presence of a natural substrate.

Table 6.2. Inhibitory activity of peptides and elastatinal against PPE, HNE and wound exudate using synthetic and natural substrates. (Peptide 2 = MGWCTASVPPQCYG, peptide 3 = MGWCTASVPPQCYG$(GA)_7$)

Enzyme	IC_{50} (µM)		
	MGWCTASVPPQCYG	MGWCTASVPPQCYG$(GA)_7$	Elastatinal
PPE	18.7 ± 0.06	16.0 ± 0.06	13.8 ± 0.06
HNE	19.2 ± 0.07	11.5 ± 0.06	12.2 ± 0.05
Exudate	16.0 ± 0.09	13.1 ± 0.06	14.3 ± 0.07
HNE (insoluble elastin)	29.3 ± 0.1	25.3 ± 0.1	37.6 ± 0.09
Exudate (insoluble elastin)	31.8 ± 0.04	26.9 ± 0.05	41.9 ± 0.04

6.3.4. Peptides inhibitory activity after incorporation into SF films

The primary objective of adding the GA tail was to increase the affinity of this peptide to silk fibroin-based materials. In this way, SF-based wound dressings will be easily obtained with a specific biological activity: elastase inhibition [326]. Nevertheless the results presented indicated that this GA tail has a very important role in the HNE inhibition. Peptide MGWCTASVPPQCYG(GA)7, presented K_i and IC50 values for HNE of 0.4 µM and 11.5 µM respectively. The K_i was 7-fold lower

when compared with the peptide WCTASVPPQCYG [359] indicating a higher inhibitory activity. In contrast, the modifications introduced only at the N-terminal (peptide MGWCTASVPPQCYG) show a slightly improvement in the inhibition of pancreatic elastase (PPE), but a worst result for the inhibition of HNE when compared with peptide WCTASVPPQCYG. The better results obtained with peptide MGWCTASVPPQCYG$(GA)_7$ might be related with the increase in hydrophobicity resulting from the GA tail which corresponds to the preference of HNE for hydrophobic substrates. Although not possible, from the activity measurements, to quantify the exact number of binding sites, one might speculate that the potent binding between peptide MGWCTASVPPQCYG$(GA)_7$ and HNE might be due to the binding of this GA tail to the active centre or adjacent active sites of HNE. The differences in inhibitory activity between peptide MGWCTASVPPQCYG and MGWCTASVPPQCYG$(GA)_7$ might be related with the GA tail introduced in the C-terminal of peptide MGWCTASVPPQCYG$(GA)_7$. To test this hypothesis, peptides were incorporated in SF films prepared as described in the experimental section and, the decrease in activity was monitored after 1 h of incubation of SF films, containing peptide MGWCTASVPPQCYG, MGWCTASVPPQCYG$(GA)_7$ and elastatinal, with HNE. SF film without peptides was used as control. It can be seen from Figure 6.5 that the activity loss obtained for peptide MGWCTASVPPQCYG and MGWCTASVPPQCYG$(GA)_7$ is similar. The amino acid composition of silk fibroin (SF) consists primarily of glycine, alanine and serine amino acids which form typical -(-ala-gly-)n- repeating motifs [12]. In the fiber, fibroin chains are aligned along the fiber axis held together by a close network of interchain hydrogen bonds with adjacent -(-ala-gly-)n- sequences forming the well known β-sheets crystals [14, 456]. Therefore, peptide MGWCTASVPPQCYG$(GA)_7$ will have a high affinity towards SF films due to the GA tail. The activity loss of HNE obtained in the presence of SF films incorporating peptides indicated that the inhibitory activity of peptide MGWCTASVPPQCYG$(GA)_7$ decreases. The activity loss obtained was similar to the one obtained for peptide 2 (MGWCTASVPPQCYG) which is a less potent inhibitor already demonstrated by inhibition kinetics results. This fact clearly demonstrates the importance of GA tail on the inhibitory activity. The loss in activity verified for peptide MGWCTASVPPQCYG$(GA)_7$ is explained by the fact that after film crystallization a transition from random coil to β-sheet of SF films occurs

and the GA tail of peptide MGWCTASVPPQCYG$(GA)_7$ may thus become a part of these β-sheet crystals being unavailable for the inhibitory activity.

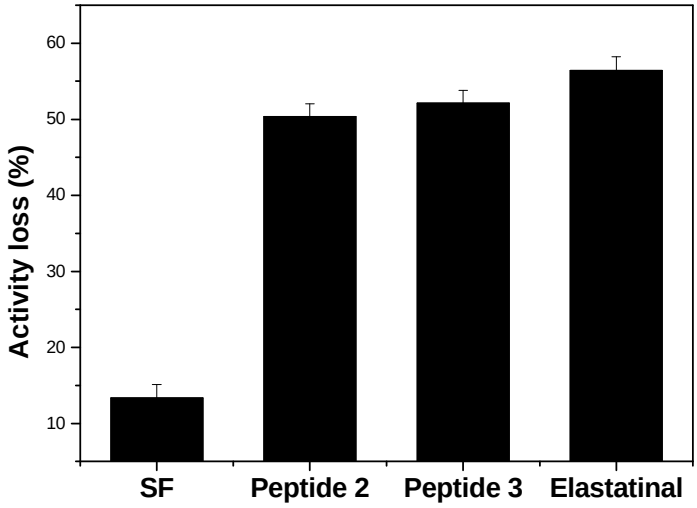

Figure 6.5. Activity loss of HNE after 1 h of incubation at 25 ℃ with SF films incorporating peptide 2, 3 and elastatinal. (Peptide 2 = MGWCTASVPPQCYG, Peptide 3 = MGWCTASVPPQCYG$(GA)_7$)

6.3.5. Molecular-docking analysis

Molecular-docking analysis was done in order to better understand the mechanism of HNE inhibition by the new peptides. Docking calculations were made using AutoDock Vina version 1.1.1 [457]. For the calculations we use the X-ray structure, PDB code 1B0F [332], after removing the ligand present in this structure. This structure was used as the receptor without flexible side chains. The ligands were made flexible turning all possible bonds rotatable. Cyclic and amide bonds were considered as non-rotatable. Considering these we get 37 torsions for peptide 1 (WCTASVPPQCYG), 44 torsions for peptide 2 (MGWCTASVPPQCYG) and 72 torsions for peptide 3 (MGWCTASVPPQCYG$(GA)_7$). For peptides 1 and 2 the grid size was chosen in order to included not only the known catalytic site of HNE but also all the surrounding area. The surface in the opposite side of the enzyme was not considered. For the peptide 3, and because this peptide is bigger, the grid was centred at the centre of the protein and big enough to include all the protein and peptide 3 interacting with any spot of the surface. This procedure allows us to

obtain the most favourable configuration representing the interaction between peptide 3 and HNE, without any kind of external impositions. Docking analysis indicated that the reactive site-loop of the BBI-peptides occupied most of the active site, inhibiting the HNE activity as already demonstrated by others [362, 368, 369, 458]. This also confirms the competitive inhibition obtained for BBI-peptides that was confirmed by our kinetic analysis. Nevertheless, modifications made on the C- and N-terminal of peptides had influence on the binding mode to the active site of HNE.

Peptide MGWCTASVPPQCYG had two more residues (MG) at the N-terminal, which increases the hydrophobic interactions between P-P' side-chains (methionine is hydrophobic) thereby closing the loop (Figure 6.6b)) when compared to peptide WCTASVPPQCYG (Figure 6.6a)). This might increase the distance of P1 (Ala) to the active centre decreasing the inhibition. On the other hand, the increase in hydrophobicity of peptide MGWCTASVPPQCYG$(GA)_7$, given by the GA tail at the C-terminal causes the opening of the loop (Figure 6.6c)). This peptide showed the best HNE inhibitory activity. Docking analysis suggested that the primary interaction with the active site is also made by the P1, as observed for the other two peptides. Nevertheless the interaction of peptide MGWCTASVPPQCYG$(GA)_7$ with the enzyme tends to be more favourable. The hydrophobic GA tail has the ability to interact with the remaining enzyme, leading to a stronger interaction between the two species (Figure 6.6c)). This is consistent with what others observed for this particular enzyme. It was shown that HNE activity increases with the length of the synthetic substrates indicating that HNE has an extended binding site [329, 336]. It is possible, as shown by docking analysis, that HNE accommodates the GA tail due to the high length and hydrophobicity leading to stronger interactions and, therefore, to higher inhibition rates.

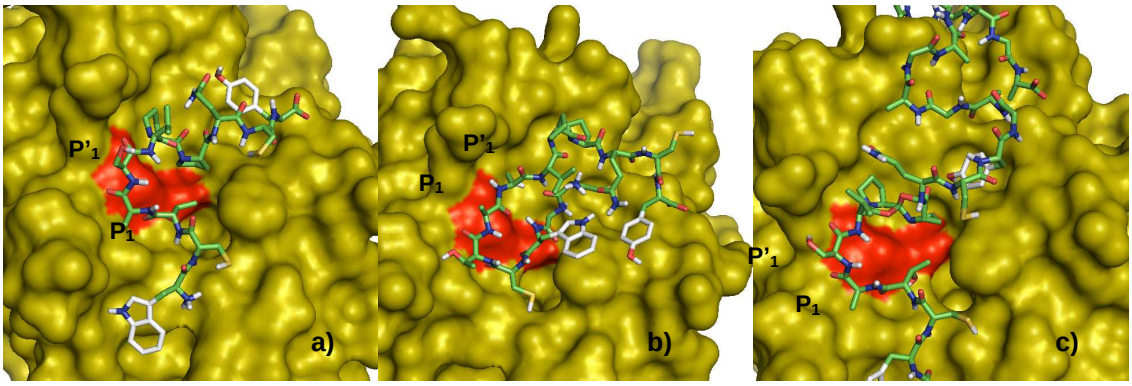

Figure 6.6. Docking images of the interactions between HNE and peptides 1 (a), 2 (b) and 3 (c). The catalytic triad is shown in red. (Peptide 2 = MGWCTASVPPQCYG, Peptide 3 = MGWCTASVPPQCYG$(GA)_7$)

6.3.6 Cytotoxicity evaluation

The biocompatibility of the designed peptides was assessed through the use of fibroblast cultures. A preliminary screening was made using murine embryonic fibroblasts cells (MEFs) as a measure of global cytotoxicity. In this study, a wide range of peptide concentrations (20-80 µM) used for inhibition assays was evaluated and no toxicity was observed (Data not shown). The results obtained with MEFs were then confirmed with human skin fibroblasts, testing the lowest and highest peptide concentrations were previously used and no additional damage to the cells was detected in any case. Figure 6.7 shows the cell viability of human skin fibroblasts after 24 h (a) and 48 h (b) of incubation with the various peptides. In all cases, the cell viability was close to 100% indicating that peptides MGWCTASVPPQCYG and MGWCTASVPPQCYG$(GA)_7$ can be safely applied to the skin at these concentrations.

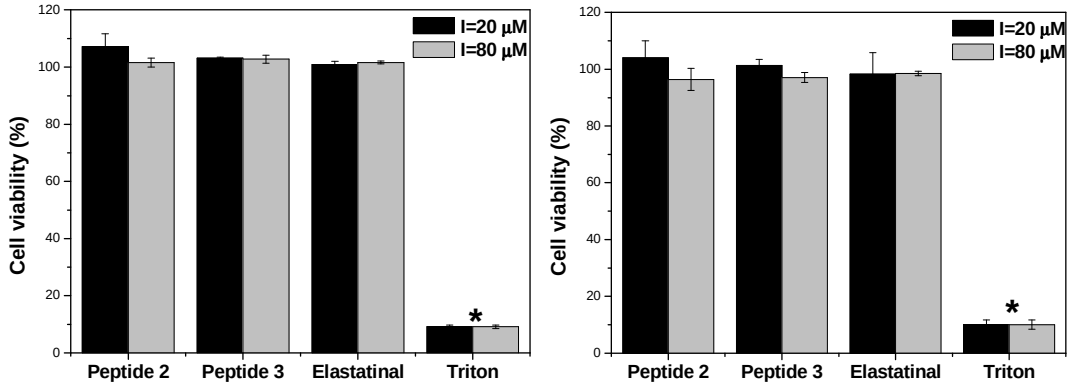

Figure 6.7. Viability of human normal skin fibroblasts after 24 h (left panel) and 48 h (right panel) of contact with peptides 2, 3 and elastatinal. Only the positive control (treatment with Triton detergent) revealed diminished cell viability. (* = significantly different from all the other tested conditions, $p<0.05$). (Peptide 2 = MGWCTASVPPQCYG, Peptide 3 = MGWCTASVPPQCYG$(GA)_7$)

6.4. Conclusion

The results presented in this study confirmed the ability of BBI-peptides to inhibit HNE. Peptide MGWCTASVPPQCYG and MGWCTASVPPQCYG$(GA)_7$ are competitive inhibitors of HNE being peptide MGWCTASVPPQCYG$(GA)_7$ the one that presents higher inhibitory activity. This is due to the presence of the GA tail that increases hydrophobicity. Consequently, the affinity for HNE increases because of the preference of this enzyme for hydrophobic residues. The importance of the GA tail in the inhibition HNE was confirmed by incorporating peptides in a silk fibroin matrix and by molecular-docking analysis. After incorporation and subsequent crystallization of SF films, the inhibitory activity was similar to that obtained for peptide MGWCTASVPPQCYG. This happens because the GA tail, upon crystallization, is no longer available for the inhibition.

Peptide MGWCTASVPPQCYG and MGWCTASVPPQCYG$(GA)_7$ were also able to inhibit HNE present on a chronic wound exudate. This fact, along with the cytocompatibility observed with human skin fibroblasts, indicates that these peptides, especially peptide MGWCTASVPPQCYG$(GA)_7$, are potential bioactive agents against deleterious HNE-derived inflammatory episodes such as chronic wounds.

CHAPTER VII

General Conclusions and Future Perspectives

CHAPTER VII

7.1. General conclusions

This thesis reports for the first time the use of protein blend systems as wound dressing materials. Herein a summary of the major achievements will be given.
This work can be divided into two parts: Development of new protein materials based on silk fibroin, keratin and elastin were developed for wound dressing applications; Use of innovative peptide sequences based on the reactive site-loop of the Bowman-Birk inhibitor (BBI) protein were used to control the high levels of human neutrophil elastase (HNE) found on chronic wounds.
The general conclusions of the research work produced in the present thesis, which extends from Chapter III to VI, are summarized as follows:

Development of new protein-based materials

Silk fibroin (SF), keratin (K) and elastin (EL) are proteins with distinctive properties such as mechanical strength, biodegradability, secondary structure and amino acid composition. This was determined for the three proteins; SF is characterized by a high content in glycine (44%), alanine (29%) and serine (12%) amino acid residues that are responsible for the formation of the β-sheet crystal that characterize the secondary structure of SF.
Keratin is distinct from the other studied proteins by the high content of cysteine (9%) residues responsible for the formation of disulfide bonds, which gives high strength to the keratin materials. Elastin is mainly composed of glycine (32%), alanine (24%), proline (12%) and valine (11%) that characterizes the hydrophobic regions of elastin in the human body.
Blending often allows modulating the final properties of the resulting materials, thus we used this approach to develop SF/K films and SF/EL porous scaffolds.
SF/K films were prepared by solvent casting and evaporation, by aqueous and formic acid-derived systems.
The two proteins were mixed in several ratios being 100% SF and 100% K the controls. Nevertheless, although native keratin materials present high mechanical strength, the same is not observed for regenerated keratin. Thus, the first conclusion observed during this study was that the maximum keratin that can be

used, in our test conditions, to obtain a handled film is 60%. In addition, the non linear trend obtained from FT-IR (intensity ratio of amide II bands of SF and K) and DSC analysis (energy for the decomposition of SF and K) indicated that SF and K are able to establish intermolecular interactions, most likely, hydrogen bonds.

Pure SF films obtained from regenerated SF solutions are prevalently amorphous/silk I. After methanol or formic acid treatment, the films underwent a β-sheet conformation, which confers a closed and compact structure to the materials giving high mechanical strength. In our study, addition of keratin that is highly polar, decreases the β-sheet content causing a more open and hydrophilic structure. This alters the properties of materials such as: decrease of tensile strength with the increase of keratin content; higher swelling ratio for higher keratin amounts; higher and faster degradation rates by trypsin and porcine pancreatic elastase (PPE): at low keratin contents (20%) the degradation is relatively slower but at high keratin amounts (60%), the degradation is fast and, after 7 days of incubation the film is completely disintegrated; the surface topography of the SF/K films also changes by the addition of the keratin, exhibiting a smoother surface which will affect the mechanical strength; the release rate of model compounds is also influenced by the presence of keratin: at low keratin content (20%) the release of FITC-BSA is modulated by Fickian diffusion, a high keratin content (60%) the release is totally controlled by the degradation of the film.

SF/EL porous scaffolds were prepared by lyophilization. 3D architectures are recognized to be important for cellular infiltration and proliferation. For the development of these scaffolds, soluble elastin was used. It is reported that soluble elastin enhances elastin synthesis *in vivo*. Nevertheless, the resulting materials often presented poor mechanical properties. To overcome this, SF and EL were fixed with a natural agent, genipin, due to its low toxicity. The proteins were successfully crosslinked with genipin after 6 h of reaction (maximum crosslinking degree). It was demonstrated that genipin induces conformational changes on SF, increasing the β-sheet content, and on EL, increases the amount of undefined conformations. It was also found that the thermal stability of SF and EL increased after genipin crosslinking.

For SF/EL scaffolds it was concluded that addition of elastin influences the physical and chemical properties of the materials. The morphology of the scaffolds after addition of EL is characterized by high pores with a loose and open network.

Even though, porous morphologies are required for cellular attachment and growth, such loose network might have negative effects on swelling, degradation and release rates as demonstrated by our results.

The swelling ratio was higher for samples with higher EL amounts (50%). It was found that the swelling ratio of SF/EL scaffolds was lower in acidic conditions, attributed to the formation of hydrogen bonds between SF and EL, becoming progressively higher at neutral and alkaline media, as a consequence of the electrostatic repulsion between the ionized acid groups.

Our ultimately goal is to use these protein materials as wound dressings therefore, the degradation was evaluated under a human wound exudate obtained from decubitus wounds. The results indicated that higher degradation rates are obtained for higher EL amounts. This was an expected result because in the human body, elastin is degraded by HNE. However, addition of EL to the sponges allows us to obtain biomaterials mimicking the extracellular matrix (ECM).

The genipin crosslinking changes the properties mentioned above: scaffolds with smaller pore sizes and compact structures are obtained; the swelling ratio decreased because the formation of covalent bonds hampers the mobility and relaxation of the macromolecular chains and, the biological degradation is decreased. The release of model compounds from SF/EL scaffolds (Trypan-blue and FITC-BSA) that was characterized by anomalous transport, influenced by swelling and degradation, becomes dominated by Fickian diffusion, with slower release rates, after genipin crosslinking.

The results presented in this thesis indicated that SF/K films and SF/EL scaffolds are degraded, which is an important feature if the materials have to be implanted *in vivo*; have the ability to swell maintaining a moist environment in the wound promoting the healing; present drug delivery options and showed no cytotoxicity with mouse and human skin fibroblasts cells. These are essential parameters that make the developed protein materials suitable candidates for wound dressings.

Control of human neutrophil elastase (HNE) activity

Chronic wound exudates presented high levels of tissue destructive proteases such as HNE. The activity of this enzyme, in an acute wound environment, is controlled by endogenous inhibitors, which are inactivated in the presence of high

levels of HNE. Therefore, the use of synthetic peptides is necessary to control the elastase-antielastase imbalance.

In this study, peptides based on the reactive site-loop of the BBI protein were used. These were removed from a combinatorial peptide library created to obtain peptide sequences that greatly inhibit HNE.

In a first approach, the peptide 5(6)-Carboxyfluorescein-YCQPPWSATCF-OH was used to inhibit PPE (used here as a model for HNE) in solution and after incorporation into the SF/K films. The results indicated that the peptide is able to inhibit PPE in solution and, that the inhibitory activity increases with the increase of peptide concentration. The highest peptide concentration used (80 µM) decreases the half-life time of PPE by 7-fold.

The peptide was further incorporated into SF/K films, before film casting, to determine if the peptide retained its inhibitory activity. This originates films with the peptide incorporated by physical entrapment. The results indicated that incorporation of the peptides in pure SF films and blend films with low keratin content (80/20 SF/K) increases the half-life time of PPE when compared with the peptide alone, indicating that the peptide is slowly released showing that SF/K films can act as mechanism-based wound dressings with a specific target: the control of HNE activity.

In a second approach, we used another BBI-based peptide with the sequence, WCTASVPPQCYG. For this, modifications were made at both N- and C-terminal: MGWCTASVPPQCYG and MGWCTASVPPQCYG$(GA)_7$. It was found that these peptides are competitive inhibitors for PPE and HNE, being peptide MGWCTASVPPQCYG$(GA)_7$ the one that presents higher inhibitory activity, with an inhibition constant, K_i, 7-fold lower when compared with the peptide WCTASVPPQCYG. This is due to the presence of the GA tail that increases hydrophobicity. As a consequence, the affinity for HNE increases because of the preference of this enzyme for hydrophobic residues, increasing the inhibitory activity. Furthermore, the peptides showed no cytotoxicity with human skin fibroblasts and, are also able to inhibit HNE present in a human chronic wound exudate. The results demonstrated that MGWCTASVPPQCYG$(GA)_7$, can be used as HNE inhibitor for chronic wounds.

As a final remark, one can say that the work described in the present thesis intends to give another positive contribute for the development of novel protein-based biomaterials. Each of the individual work performed addresses some of the needs in the treatment of chronic wounds. SF/K films and SF/EL scaffolds were developed and evaluated for the first time. Moreover, new HNE inhibitors were developed in order to obtain interactive wound dressings: tailor-made materials to target high levels of HNE elastase. The results obtained clearly indicate the suitability of the developed materials for wound dressings which is the main innovation coming from this thesis.

7.2. Future perspectives

The results presented in this thesis showed that SF/K films and SF/EL sponges are promising candidates for wound dressing materials. Following the same approaches, new morphologies can be developed with these three proteins and, their properties can be further modulated.

The materials developed should also be evaluated *in vivo* through the use of animal models. Important parameters such as inflammation, cellular proliferation and differentiation and elastin synthesis should be determined.

New analysis must be done to fully understand the mechanism of HNE inhibition by the designed peptides.

REFERENCES

References

1. Kaplan, D.L., et al., *Silk-biology, structure, properties and genetics.* ACS Symposium Series, 1994, 544: p. 2-16.
2. Kaplan, D.L., et al., *Silk*, in *Protein based materials*, K. McGrath, D.L., Editor. 1998, Birkhauser: Boston. p. 103-31.
3. Vollrath, F. and Knight, D.P., *Liquid crystalline spinning of spider silk.* Nature, 2001, 410(6828): p. 541-8.
4. Winkler, S. and Kaplan, D.L., *Molecular biology of spider silk.* Reviews in Molecular Biotechnology, 2000, 74(2): p. 85-93.
5. Wong Po Foo, C. and Kaplan, D.L., *Genetic engineering of fibrous proteins: spider dragline silk and collagen.* Advanced Drug Delivery Reviews, 2002, 54(8): p. 1131-1143.
6. Altman, G.H., et al., *Silk-based biomaterials.* Biomaterials, 2003, 24(3): p. 401-416.
7. Jin, H.-J. and Kaplan, D.L., *Mechanism of silk processing in insects and spiders.* Nature, 2003, 424(6952): p. 1057-1061.
8. Bini, E., Knight, D.P. and Kaplan, D.L., *Mapping Domain Structures in Silks from Insects and Spiders Related to Protein Assembly.* Journal of Molecular Biology, 2004, 335(1): p. 27-40.
9. Simmons, A., Ray, E. and Jelinski, L.W., *Solid-State ^{13}C NMR of Nephila clavipes Dragline Silk Establishes Structure and Identity of Crystalline Regions.* Macromolecules, 1994, 27(18): p. 5235-5237.
10. Simmons, A.H., Michal, C.A. and Jelinski, L.W., *Molecular Orientation and Two-Component Nature of the Crystalline Fraction of Spider Dragline Silk.* Science, 1996, 271(5245): p. 84-87.
11. Vollrath, F., *Spiders' webs.* Current Biology, 2005, 15(10): p. R364-R365.
12. Zhou, C.-Z., et al., *Fine organization of Bombyx mori fibroin heavy chain gene.* Nucleic Acids Research, 2000, 28(12): p. 2413-2419.
13. Yamaguchi, K., et al., *Primary structure of the silk fibroin light chain determined by cDNA sequencing and peptide analysis.* Journal of Molecular Biology, 1989, 210(1): p. 127-139.
14. Inoue, S., et al., *Silk Fibroin of Bombyx mori Is Secreted, Assembling a High Molecular Mass Elementary Unit Consisting of H-chain, L-chain, and P25, with a 6:6:1 Molar Ratio.* Journal of Biological Chemistry, 2000, 275(51): p. 40517-40528.
15. Vasconcelos, A., Freddi, G. and Cavaco-Paulo, A., *Biodegradable Materials Based on Silk Fibroin and Keratin.* Biomacromolecules, 2008, 9(4): p. 1299-1305.
16. Zhou, C.Z., et al., *Silk fibroin: structural implications of a remarkable amino acid sequence.* Proteins, 2001, 44(2): p. 119-22.
17. Motta, A., Fambri, L. and Migliaresi, C., *Regenerated silk fibroin films: Thermal and dynamic mechanical analysis.* Macromolecular Chemistry and Physics, 2002, 203(10-11): p. 1658-1665.
18. Huemmerich, D., Slotta, U. and Scheibel, T., *Processing and modification of films made from recombinant spider silk proteins.* Applied Physics A: Materials Science & Processing, 2006, 82(2): p. 219-222.
19. Zhang, Y.-Q., *Applications of natural silk protein sericin in biomaterials.* Biotechnology Advances, 2002, 20(2): p. 91-100.

20. Moy, L.R., Lee, A. and Zalka, A., *Commonly used suture materials in skin surgery.* American Family Physician, 1991, 44(6): p. 2123-8.
21. Panilaitis, B., et al., *Macrophage responses to silk.* Biomaterials, 2003, 24(18): p. 3079-3085.
22. Rossitch, E., Bullard, D.E. and Oakes, W.J., *Delayed foreign-body reaction to silk sutures in pediatric neurosurgical patients.* Child's Nervous System, 1987, 3(6): p. 375-378.
23. Hollander, D.H., *Interstitial cystitis and silk allergy.* Medical Hypotheses, 1994, 43(3): p. 155-156.
24. Mandal, B.B., Priya, A.S. and Kundu, S.C., *Novel silk sericin/gelatin 3-D scaffolds and 2-D films: Fabrication and characterization for potential tissue engineering applications.* Acta Biomaterialia, 2009, 5(8): p. 3007-3020.
25. House, M., et al., *Cervical Tissue Engineering Using Silk Scaffolds and Human Cervical Cells.* Tissue Engineering Part A, 2010, 16(6): p. 2101-2112.
26. Hu, X., et al., *Biomaterials derived from silk-tropoelastin protein systems.* Biomaterials, 2010, 31(32): p. 8121-8131.
27. Lu, Q., et al., *Green Process to Prepare Silk Fibroin/Gelatin Biomaterial Scaffolds.* Macromolecular Bioscience, 2009, 10(3): p. 289-298.
28. Marelli, B., et al., *Compliant electrospun silk fibroin tubes for small vessel bypass grafting.* Acta Biomaterialia, 2010, 6(10): p. 4019-4026.
29. Pritchard, E.M., et al., *Silk fibroin encapsulated powder reservoirs for sustained release of adenosine.* Journal of Controlled Release, 2010, 144(2): p. 159-167.
30. Wang, X., et al., *Silk nanospheres and microspheres from silk/PVA blend films for drug delivery.* Biomaterials, 2009, 31(6): p. 1025-1035.
31. Wang, Y., et al., *The synergistic effects of 3-D porous silk fibroin matrix scaffold properties and hydrodynamic environment in cartilage tissue regeneration.* Biomaterials, 2010, 31(17): p. 4672-4681.
32. Wang, Y., et al., *In vivo degradation of three-dimensional silk fibroin scaffolds.* Biomaterials, 2008, 29(24-25): p. 3415-3428.
33. Gotoh, Y., et al., *Synthesis of poly(ethylene glycol)-silk fibroin conjugates and surface interaction between L-929 cells and the conjugates.* Biomaterials, 1997, 18(3): p. 267-271.
34. Gotoh, Y., Tsukada, M. and Minoura, N., *Effect of the chemical modification of the arginyl residue in Bombyx mori silk fibroin on the attachment and growth of fibroblast cells.* Journal of Biomedical Materials Research, 1998, 39(3): p. 351-357.
35. Santin, M., et al., *In vitro evaluation of the inflammatory potential of the silk fibroin.* Journal of Biomedical Materials Research, 1999, 46(3): p. 382-389.
36. Unger, R.E., et al., *Growth of human cells on a non-woven silk fibroin net: a potential for use in tissue engineering.* Biomaterials, 2004, 25(6): p. 1069-1075.
37. Horan, R.L., et al., *In vitro degradation of silk fibroin.* Biomaterials, 2005, 26(17): p. 3385-3393.
38. Wang, X., et al., *Biomaterial Coatings by Stepwise Deposition of Silk Fibroin.* Langmuir, 2005, 21(24): p. 11335-11341.
39. Fuchs, S., et al., *Outgrowth endothelial cells isolated and expanded from human peripheral blood progenitor cells as a potential source of autologous*

cells for endothelialization of silk fibroin biomaterials. Biomaterials, 2006, 27(31): p. 5399-5408.
40. Hofmann, S., et al., *Silk fibroin as an organic polymer for controlled drug delivery.* Journal of Controlled Release, 2006, 111(1-2): p. 219-227.
41. Uebersax, L., et al., *Silk fibroin matrices for the controlled release of nerve growth factor (NGF).* Biomaterials, 2007, 28(30): p. 4449-4460.
42. Wang, X., et al., *Silk coatings on PLGA and alginate microspheres for protein delivery.* Biomaterials, 2007, 28(28): p. 4161-4169.
43. Bondar, B., et al., *Functionality of endothelial cells on silk fibroin nets: Comparative study of micro- and nanometric fibre size.* Biomaterials, 2008, 29(5): p. 561-572.
44. Silva, S.S., et al., *Genipin-Modified Silk-Fibroin Nanometric Nets.* Macromolecular Bioscience, 2008, 8(8): p. 766-774.
45. Silva, S.S., et al., *Novel Genipin-Cross-Linked Chitosan/Silk Fibroin Sponges for Cartilage Engineering Strategies.* Biomacromolecules, 2008, 9(10): p. 2764-2774.
46. Acharya, C., Ghosh, S.K. and Kundu, S.C., *Silk fibroin film from non-mulberry tropical tasar silkworms: A novel substrate for in vitro fibroblast culture.* Acta Biomaterialia, 2009, 5(1): p. 429-437.
47. Jones, G.L., et al., *Osteoblast: Osteoclast co-cultures on silk fibroin, chitosan and PLLA films.* Biomaterials, 2009, 30(29): p. 5376-5384.
48. Lu, S., et al., *Stabilization of Enzymes in Silk Films.* Biomacromolecules, 2009, 10(5): p. 1032-1042.
49. Mandal, B.B., Kapoor, S. and Kundu, S.C., *Silk fibroin/polyacrylamide semi-interpenetrating network hydrogels for controlled drug release.* Biomaterials, 2009, 30(14): p. 2826-2836.
50. Yang, M.-C., et al., *The cardiomyogenic differentiation of rat mesenchymal stem cells on silk fibroin-polysaccharide cardiac patches in vitro.* Biomaterials, 2009, 30(22): p. 3757-3765.
51. Um, I.C., et al., *Structural characteristics and properties of the regenerated silk fibroin prepared from formic acid.* International Journal of Biological Macromolecules, 2001, 29(2): p. 91-97.
52. Um, I.C., et al., *The role of formic acid in solution stability and crystallization of silk protein polymer.* International Journal of Biological Macromolecules, 2003, 33(4-5): p. 203-213.
53. Nazarov, R., Jin, H.-J. and Kaplan, D.L., *Porous 3-D Scaffolds from Regenerated Silk Fibroin.* Biomacromolecules, 2004, 5(3): p. 718-726.
54. Bayraktar, O., et al., *Silk fibroin as a novel coating material for controlled release of theophylline.* European Journal of Pharmaceutics and Biopharmaceutics, 2005, 60(3): p. 373-381.
55. Lu, Q., et al., *Cytocompatibility and blood compatibility of multifunctional fibroin/collagen/heparin scaffolds.* Biomaterials, 2007, 28(14): p. 2306-2313.
56. She, Z., et al., *Preparation and in vitro degradation of porous three-dimensional silk fibroin/chitosan scaffold.* Polymer Degradation and Stability, 2008, 93(7): p. 1316-1322.
57. Zoccola, M., et al., *Study on Cast Membranes and Electrospun Nanofibers Made from Keratin/Fibroin Blends.* Biomacromolecules, 2008, 9(10): p. 2819-2825.

58. Lu, Q., et al., *Growth of fibroblast and vascular smooth muscle cells in fibroin/collagen scaffold.* Materials Science and Engineering: C, 2009, 29(7): p. 2239-2245.
59. Niamsa, N., et al., *Preparation of nanocomposite chitosan/silk fibroin blend films containing nanopore structures.* Carbohydrate Polymers, 2009, 78(1): p. 60-65.
60. Sofia, S., et al., *Functionalized silk-based biomaterials for bone formation.* Journal of Biomedical Materials Research, 2001, 54(1): p. 139-148.
61. Kim, U.-J., et al., *Three-dimensional aqueous-derived biomaterial scaffolds from silk fibroin.* Biomaterials, 2005, 26(15): p. 2775-2785.
62. Meinel, L., et al., *The inflammatory responses to silk films in vitro and in vivo.* Biomaterials, 2005, 26(2): p. 147-155.
63. Min, B.-M., et al., *Formation of silk fibroin matrices with different texture and its cellular response to normal human keratinocytes.* International Journal of Biological Macromolecules, 2004, 34(5): p. 223-230.
64. Liu, Y., et al., *Thermal and crystalline behavior of silk fibroin/nylon 66 blend films.* Polymer, 2004, 45(22): p. 7705-7710.
65. Gil, E.S., et al., *Mixed Protein Blends Composed of Gelatin and Bombyx mori Silk Fibroin: Effects of Solvent-Induced Crystallization and Composition.* Biomacromolecules, 2006, 7(3): p. 728-735.
66. Gupta, M.K., et al., *Patterned Silk Films Cast from Ionic Liquid Solubilized Fibroin as Scaffolds for Cell Growth.* Langmuir, 2006, 23(3): p. 1315-1319.
67. Mandal, B.B., Mann, J.K. and Kundu, S.C., *Silk fibroin/gelatin multilayered films as a model system for controlled drug release.* European Journal of Pharmaceutical Sciences, 2009, 37(2): p. 160-171.
68. Tamada, Y., *New Process to Form a Silk Fibroin Porous 3-D Structure.* Biomacromolecules, 2005, 6(6): p. 3100-3106.
69. Liu, H., et al., *The interaction between a combined knitted silk scaffold and microporous silk sponge with human mesenchymal stem cells for ligament tissue engineering.* Biomaterials, 2008, 29(6): p. 662-674.
70. Mandal, B.B. and Kundu, S.C., *Calcium alginate beads embedded in silk fibroin as 3D dual drug releasing scaffolds.* Biomaterials, 2009, 30(28): p. 5170-5177.
71. Mandal, B.B. and Kundu, S.C., *Cell proliferation and migration in silk fibroin 3D scaffolds.* Biomaterials, 2009, 30(15): p. 2956-2965.
72. Kundu, J., et al., *Silk fibroin nanoparticles for cellular uptake and control release.* International Journal of Pharmaceutics, 2010, 388(1-2): p. 242-250.
73. Lammel, A.S., et al., *Controlling silk fibroin particle features for drug deliver* Biomaterials, 2010, 31(16): p. 4583-4591.
74. Hino, T., Tanimoto, M. and Shimabayashi, S., *Change in secondary structure of silk fibroin during preparation of its microspheres by spray-drying and exposure to humid atmosphere.* Journal of Colloid and Interface Science, 2003, 266(1): p. 68-73.
75. Yeo, J.-H., et al., *Simple preparation and characteristics of silk fibroin microsphere.* European Polymer Journal, 2003, 39(6): p. 1195-1199.
76. Wang, X., et al., *Silk microspheres for encapsulation and controlled release.* Journal of Controlled Release, 2007, 117(3): p. 360-370.

77. Drummy, L.F., et al., *Thermally Induced α-Helix to β-Sheet Transition in Regenerated Silk Fibers and Films.* Biomacromolecules, 2005, 6(6): p. 3328-3333.
78. Hu, X., Kaplan, D.L. and Cebe, P., *Determining Beta-Sheet Crystallinity in Fibrous Proteins by Thermal Analysis and Infrared Spectroscopy.* Macromolecules, 2006, 39(18): p. 6161-6170.
79. Lu, Q., et al., *Water-insoluble silk films with silk I structure.* Acta Biomaterialia, 2009, 6(4): p. 1380-1387.
80. Jin, H.J., et al., *Water-Stable Silk Films with Reduced β-Sheet Content.* Advanced Functional Materials, 2005, 15(8): p. 1241-1247.
81. Lee, K.Y., et al., *Effect of surface properties on the antithrombogenicity of silk fibroin/S-carboxymethyl kerateine blend films.* Journal of Biomaterials Science - Polymer Edition, 1998, 9: p. 905-914.
82. Garcia-Fuentes, M., et al., *The effect of hyaluronic acid on silk fibroin conformation.* Biomaterials, 2008, 29(6): p. 633-642.
83. Vepari, C. and D.L. Kaplan, *Silk as a biomaterial.* Progress in Polymer Science, 2007, 32(8-9): p. 991-1007.
84. Dal Pra, I., et al., *De novo engineering of reticular connective tissue in vivo by silk fibroin nonwoven materials.* Biomaterials, 2005, 26(14): p. 1987-1999.
85. Li, C., et al., *Electrospun silk-BMP-2 scaffolds for bone tissue engineering.* Biomaterials, 2006, 27(16): p. 3115-3124.
86. Rammensee, S., et al., *Rheological characterization of hydrogels formed by recombinantly produced spider silk.* Applied Physics A, 2006, 82: p. 261-264.
87. Jin, H.-J., et al., *Biomaterial Films of Bombyx Mori Silk Fibroin with Poly(ethylene oxide).* Biomacromolecules, 2004, 5(3): p. 711-717.
88. Minoura, N., Tsukada, M. and Nagura, M., *Fine structure and oxygen permeability of silk fibroin membrane treated with methanol.* Polymer, 1990, 31(2): p. 265-269.
89. Minoura, N., Tsukada, M. and Nagura, M., *Physico-chemical properties of silk fibroin membrane as a biomaterial.* Biomaterials, 1990, 11(6): p. 430-434.
90. Uebersax, L., et al., *The support of adenosine release from adenosine kinase deficient ES cells by silk substrates.* Biomaterials, 2006, 27(26): p. 4599-4607.
91. Szybala, C., et al., *Antiepileptic effects of silk-polymer based adenosine release in kindled rats.* Experimental Neurology, 2009, 219(1): p. 126-135.
92. Chen, J., et al., *Human bone marrow stromal cell and ligament fibroblast responses on RGD-modified silk fibers.* Journal of Biomedical Materials Research Part A, 2003, 67A(2): p. 559-570.
93. Karageorgiou, V., et al., *Bone morphogenetic protein-2 decorated silk fibroin films induce osteogenic differentiation of human bone marrow stromal cells.* Journal of Biomedical Materials Research Part A, 2004, 71A(3): p. 528-537.
94. Gotoh, Y., et al., *Physical properties and structure of poly(ethylene glycol)-silk fibroin conjugate films.* Polymer, 1997, 38(2): p. 487-490.
95. Kweon, H.Y., et al., *Preparation of semi-interpenetrating polymer networks composed of silk fibroin and poly(ethylene glycol) macromer* Journal of Applied Polymer Science, 2001, 80(10): p. 1848-1853.

96. Freddi, G., Tsukada, M. and Beretta, S., *Structure and physical properties of silk fibroin/polyacrylamide blend films.* Journal of Applied Polymer Science, 1999, 71(10): p. 1563-1571.
97. Freddi, G., et al., *Silk fibroin/cellulose blend films: Preparation, structure, and physical properties.* Journal of Applied Polymer Science, 1995, 56(12): p. 1537-1545.
98. Yang, G., Zhang, L. and Liu, Y., *Structure and microporous formation of cellulose/silk fibroin blend membranes: I. Effect of coagulants.* Journal of Membrane Science, 2000, 177(1-2): p. 153-161.
99. Arai, T., et al., *Preparation of silk fibroin and polyallylamine composites.* Journal of Applied Polymer Science, 2002, 84(11): p. 1963-1970.
100. Chen, X., Li, W. and Yu, T., *Conformation Transition of Silk Fibroin Induced by Blending Chitosan.* Journal of Polymer Science: Part B: Polymer Physics, 1997, 35: p. 2293–2296.
101. Chen, X., et al., *pH sensitivity and ion sensitivity of hydrogels based on complex-forming chitosan/silk fibroin interpenetrating polymer network.* Journal of Applied Polymer Science, 1997, 65(11): p. 2257-2262.
102. Hu, K., et al., *Biocompatible Fibroin Blended Films with Recombinant Human-like Collagen for Hepatic Tissue Engineering.* Journal of Bioactive and Compatible Polymers, 2006, 21(1): p. 23-37.
103. Chiarini, A., et al., *Silk fibroin/poly(carbonate)-urethane as a substrate for cell growth: in vitro interactions with human cells.* Biomaterials, 2003, 24(5): p. 789-799.
104. Dal Pra, I., et al., *Silk Fibroin-Coated Three-Dimensional Polyurethane Scaffolds for Tissue Engineering: Interactions with Normal Human Fibroblasts.* Tissue Engineering, 2003, 9(6): p. 1113-1121.
105. Cai, K., et al., *Poly(,-lactic acid) surfaces modified by silk fibroin: effects on the culture of osteoblast in vitro.* Biomaterials, 2002, 23(4): p. 1153-1160.
106. Cai, K., et al., *Influence of different surface modification treatments on poly(,-lactic acid) with silk fibroin and their effects on the culture of osteoblast in vitro.* Biomaterials, 2002, 23(7): p. 1603-1611.
107. Wang, X., et al., *Nanolayer biomaterial coatings of silk fibroin for controlled release.* Journal of Controlled Release, 2007, 121(3): p. 190-199.
108. Li, M., Ogiso, M. and Minoura, N., *Enzymatic degradation behavior of porous silk fibroin sheets.* Biomaterials, 2003, 24(2): p. 357-365.
109. Meinel, L., et al., *Bone Tissue Engineering Using Human Mesenchymal Stem Cells: Effects of Scaffold Material and Medium Flow.* Annals of Biomedical Engineering, 2004, 32(1): p. 112-122.
110. Meinel, L., et al., *Silk implants for the healing of critical size bone defects.* Bone, 2005, 37(5): p. 688-698.
111. Kim, H.J., et al., *Influence of macroporous protein scaffolds on bone tissue engineering from bone marrow stem cells.* Biomaterials, 2005, 26(21): p. 4442-4452.
112. Wang, Y., et al., *Cartilage tissue engineering with silk scaffolds and human articular chondrocytes.* Biomaterials, 2006, 27(25): p. 4434-4442.
113. Morita, Y., et al., *Frictional properties of regenerated cartilage in vitro.* Journal of biomechanics, 2006, 39(1): p. 103-109.
114. Mandal, B., Das, T. and Kundu, S., *Non-bioengineered silk gland fibroin micromolded matrices to study cell-surface interactions.* Biomedical Microdevices, 2009, 11(2): p. 467-476.

115. Vepari, C.P. and Kaplan, D.L., *Covalently immobilized enzyme gradients within three-dimensional porous scaffolds.* Biotechnology and Bioengineering, 2006, 93(6): p. 1130-1137.
116. Karageorgiou, V., et al., *Porous silk fibroin 3-D scaffolds for delivery of bone morphogenetic protein-2 in vitro and in vivo.* Journal of Biomedical Materials Research Part A, 2006, 78A(2): p. 324-334.
117. Uebersax, L., Merkle, H.P. and Meinel, L., *Insulin-like growth factor I releasing silk fibroin scaffolds induce chondrogenic differentiation of human mesenchymal stem cells.* Journal of Controlled Release, 2008, 127(1): p. 12-21.
118. Wilz, A., et al., *Silk polymer-based adenosine release: Therapeutic potential for epilepsy.* Biomaterials, 2008, 29(26): p. 3609-3616.
119. Li, T., et al., *Human mesenchymal stem cell grafts engineered to release adenosine reduce chronic seizures in a mouse model of CA3-selective epileptogenesis.* Epilepsy research, 2009, 84(2): p. 238-241.
120. Gobin, A.S., Froude, V.E. and Mathur, A.B., *Structural and mechanical characteristics of silk fibroin and chitosan blend scaffolds for tissue regeneration.* Journal of Biomedical Materials Research Part A, 2005, 74A(3): p. 465-473.
121. Yeo, J.H., et al., *The effects of PVA/chitosan/fibroin (PCF)-blended spongy sheets on wound healing in rats*. Biological & Pharmaceutical Bulletin, 2000, 23. p. 1220-3.
122. Sugihara, A., et al., *Promotive Effects of a Silk Film on Epidermal Recovery from Full-Thickness Skin Wounds.* Proceedings of the Society for Experimental Biology and Medicine, 2000, 225(1): p. 58-64.
123. Roh, D.-H., et al., *Wound healing effect of silk fibroin/alginate-blended sponge in full thickness skin defect of rat.* Journal of Materials Science: Materials in Medicine, 2006, 17(6): p. 547-552.
124. Okabayashi, R., et al., *Efficacy of polarized hydroxyapatite and silk fibroin composite dressing gel on epidermal recovery from full-thickness skin wounds.* Journal of Biomedical Materials Research Part B: Applied Biomaterials, 2009, 90B(2): p. 641-646.
125. Tsubouchi, K., *Wound dressing material containing silk fibroin and sericin as main component and method for preparing the same*, US Patent 6175053, 2001.
126. Mcdevitt, J.P. and Tyrrell, D.J., *Removal of targeted proteases with proteinaceous wound dressings*. US Patent 0156437, 2002.
127. Wharram, S.E., et al., *Electrospun Silk Material Systems for Wound Healing.* Macromolecular Bioscience, 2010, 10(3): p. 246-257.
128. Schneider, A., et al., *Biofunctionalized electrospun silk mats as a topical bioactive dressing for accelerated wound healing.* Acta Biomaterialia, 2009, 5(7): p. 2570-2578.
129. Altman, A.M., et al., *IFATS Collection: Human Adipose-Derived Stem Cells Seeded on a Silk Fibroin-Chitosan Scaffold Enhance Wound Repair in a Murine Soft Tissue Injury Model.* STEM CELLS, 2009, 27(1): p. 250-258.
130. Liu, T., et al., *Cytocompatibility of regenerated silk fibroin film: a medical biomaterial applicable to wound healing.* Journal of Zhejiang University SCIENCE B, 2010, 11(1): p. 10-6.

131. Feughelmann, M., *Keratin*, in *Encyclopedia of Polymer Science and Engineering, 2nd Edition, Wiley*, J.I. Kroschwitz, Editor. 1985, Wiley: New York. p. 566-600.
132. Hardy, M.H., *The secret life of the hair follicle.* Trends in Genetics, 1992, 8(2): p. 55-61.
133. Blessing, M., et al., *Transgenic mice as a model to study the role of TGF-beta-related molecules in hair follicles.* Genes & Development, 1993, 7(2): p. 204-215.
134. Stenn, K.S., Prouty, S.M. and Seiberg, M., *Molecules of the cycling hair follicle-a tabulated review.* Journal of Dermatological Science, 1994, 7(Supplement 1): p. S109-S124.
135. Panteleyev, A.A., Jahoda, C.A.B. and Christiano, A.M., *Hair follicle predetermination.* Journal of Cell Science, 2001, 114(19): p. 3419-3431.
136. Rogers G.E., *Hair follicle differentiation and regulation.* International Journal of Developmental Biology 2004, 48(2-3): p. 163-170.
137. Rippon, J.A., ed. *The structure of wool* in Wool dyeing, ed. D.M. Lewis. 1992, Society of Dyers and Colourists. Bradford, England. 1-51.
138. Makinson, K.R., *Shrinkproofing of wool*. 1979, Marcel Dekker Inc.: New York, Basel. p. 373p.
139. Negri, A.P., Cornell, H.J. and Rivett, D.E., *A Model for the Surface of Keratin Fibers.* Textile Research Journal, 1993, 63(2): p. 109-115.
140. Feughelman, M., *Introduction to the physical properties of wool, hair & other α–keratin fibres*, in *Mechanical properties and structure of alpha-keratin fibres: wool, human hair and related fibres*. UNSW Press, 1997, p. 1-14.
141. Plowman, J.E., *Proteomic database of wool components.* Journal of Chromatography B, 2003, 787(1): p. 63-76.
142. Speakman, P.T., *Wool fibres*, in *Fibre Chemistry Handbook of Fibre Science and Technology*, M.a.P. Lewin, E.M Editor. 1984, M. Dekker: New York. p. 589-646.
143. Naik, S., *Study of naturally crosslinked protein from wool, including membrane protein*. 1994, University of Leeds, Leeds.
144. Heine, E. and Höcker, H., *Enzyme treatments for wool and cotton.* Review of Progress in Coloration and Related Topics, 1995, 25(1): p. 57-70.
145. Astbury, W.T. and Street, P.A., *X-ray studies of the structures of hair, wool and related fibres. I. General.* Philosophical Transactions of the Royal Society 1931, 230: p. 75-101.
146. Pauling, L. and Corey, R., *Configuration of Polypeptide Chains.* Nature, 1951, 168: p. 550-551.
147. Pauling, L. and Corey, R., *Compound Helical Configurations of Polypeptide Chains: Structure of Proteins of the alpha-Keratin Type.* Nature, 1953, 171: p. 59-61.
148. Parry, D.A.D. and Steinert, P.M., *Intermediate filament structure.* Current Opinion in Cell Biology, 1992, 4(1): p. 94-98.
149. Crewther, W.G., et al., *The chemistry of keratins*, in *Advances in protein chemistry*, J.C.B. Anfinsen, Anson, M.L., Edsall, J.T., Richards, F.M., Editor. 1965, Academic Press: New York. p. 191-346.
150. Hill, P., Brantleya, H. and Van Dyke, M., *Some properties of keratin biomaterials: Kerateines* Biomaterials, 2010, 31(4): p. 585-593.

151. Breinl, F. and Baudisch, O., *The oxidative breaking up of keratin through treatment with hydrogen peroxide.* Hoppe Seylers Z Physiol Chem, 1907, 52: p. 158-169.
152. Earland, C. and Knight, C.S., *Structure of Keratin II: amino acid content of fractions isolated from oxidized wool.* Biochimica et Biophysica Acta, 1956, 22: p. 405-411.
153. Buchanan, J.H., *A cystine-rich protein fraction from oxidized alpha-keratin.* Biochemical Journal, 1977, 167(2): p. 489-491.
154. Goddard, D.R. and Michaelis, L., *A STUDY ON KERATIN.* Journal of Biological Chemistry, 1934, 106(2): p. 605-614.
155. Maclaren, J.A., *The extent of reduction of wool proteins by thiols.* Australian Journal of Chemistry, 1962, 15(4): p. 824-831.
156. O'Donnell, I.J. and Thompson, E.O.P., *Studies on reduced wool IV: the isolation of a major component.* Australian Journal of Biological Sciences, 1964, 17: p. 973-989.
157. Zahn, H., *Progress report on hair keratin research.* International Journal of Cosmetic Science, 2002, 24(3): p. 163-169.
158. Katoh, K., et al., *Preparation and physicochemical properties of compression-molded keratin films.* Biomaterials, 2004, 25(12): p. 2265-2272.
159. Katoh, K., Tanabe, T. and Yamauchi, K., *Novel approach to fabricate keratin sponge scaffolds with controlled pore size and porosity.* Biomaterials, 2004, 25(18): p. 4255-4262.
160. Tonin, C., et al., *Thermal and structural characterization of poly(ethylene-oxide)/keratin blend films.* Journal of Thermal Analysis and Calorimetry, 2007, 89(2): p. 601-608.
161. Steinert, P.M. and Gullino, M.I., *Bovine epidermal keratin filament assembly.* Biochemical and Biophysical Research Communications, 1976, 70(1): p. 221-227.
162. Thomas, H., et al., *In vitro reconstitution of wool intermediate filaments.* International Journal of Biological Macromolecules, 1986, 8(5): p. 258-264.
163. van de Löcht, M., *Reconstitution of microfibrils fom wool and filaments from epidermis proteins.* Melliand Textilberichte, 1987, 10: p. 221-227.
164. Ikkai, F. and Naito, S., *Dynamic Light Scattering and Circular Dichroism Studies on Heat-Induced Gelation of Hard-Keratin Protein Aqueous Solutions.* Biomacromolecules, 2002, 3(3): p. 482-487.
165. Tachibana, A., et al., *Fabrication of wool keratin sponge scaffolds for long-term cell cultivation.* Journal of Biotechnology, 2002, 93(2): p. 165-170.
166. Vipin, V. et al., *Preparation of scaffolds from human hair proteins for tissue-engineering applications.* Biomedical Materials, 2008, 3(2): p. 025007.
167. Humphries, M.J., et al., *Identification of two distinct regions of the type III connecting segment of human plasma fibronectin that promote cell type-specific adhesion.* Journal of Biological Chemistry, 1987, 262(14): p. 6886-6892.
168. Hamasaki, S., et al., *Fabrication of highly porous keratin sponges by freeze-drying in the presence of calcium alginate beads.* Materials Science and Engineering: C, 2008, 28(8): p. 1250-1254.
169. Anker, C.A., *Method of preparing keratin-containing films and coatings*. US patent 3642498, 1972.

170. Kawano, Y., Okamoto, S., *Film and gel of keratin.* Kagaku to Seibutsu, 1975, 13(5): p. 291-292.
171. Okamoto, S., *Formation of films from some proteins.* Nippon Shokuhin Kogyo Gakkaishi, 1977. 24(1): p. 40-50.
172. Noishiki Y., et al., *Application of denaturated wool keratin derivatives to an antithrombogenic biomaterial: vascular graft coated with heparinized keratin derivative.* Kobunshi Ronbunshi, 1982, 39(4): p. 221-227.
173. Blanchard, C.R., Smith, R.A. and Siller-Jackson, A., *Keratinous protein material for wound healing applications and method*. US Patent 6274163, 2001.
174. Blanchard, C.R., Timmons, S.F. and Smith, R.A., *Keratin-based hydrogel for biomedical applications and method of production*. US patent 5932552, 1999.
175. Van Dyke, M., Blanchard, C.R., Siller-Jackson, A., *Soluble keratin peptides*. US patent 6270791, 2001.
176. Blanchard, C.R., et al. *Absorbent keratin wound dressing,* US patent 6270793, 2001.
177. Cowsar, D.R., *Bioactive keratin peptides*. US patent 7501485, 2009.
178. Van Dyke, M., *Wound healing compositions containing keratin biomaterials*. WO patent 130607, 2008.
179. Tachibana, A., et al., *Rapid fabrication of keratin-hydroxyapatite hybrid sponges toward osteoblast cultivation and differentiation.* Biomaterials, 2005, 26(3): p. 297-302.
180. Aboushwareb, T., et al., *A keratin biomaterial gel hemostat derived from human hair: Evaluation in a rabbit model of lethal liver injury.* Journal of Biomedical Materials Research Part B: Applied Biomaterials, 2009, 90B(1): p. 45-54.
181. Apel, P.J., et al., *Peripheral Nerve Regeneration Using a Keratin-Based Scaffold: Long-Term Functional and Histological Outcomes in a Mouse Model.* The Journal of Hand Surgery, 2008, 33(9): p. 1541-1547.
182. Sierpinski, P., et al., *The use of keratin biomaterials derived from human hair for the promotion of rapid regeneration of peripheral nerves.* Biomaterials, 2008, 29(1): p. 118-128.
183. Yamauchi, K., et al., *Preparation of stable aqueous solution of keratins, and physiochemical and biodegradational properties of films.* Journal of Biomedical Materials Research, 1996, 31(4): p. 439-444.
184. Yamauchi, K., Maniwa, M. and Mori, T., *Cultivation of fibroblasts cells on keratin-coated substrata.* Journal of Biomaterials Science - Polymer Edition, 1998, 9(2): p. 259-270.
185. Fujii, T., Ogiwara, D. and Arimoto, M., *Convenient Procedures for Human Hair Protein Films and Properties of Alkaline Phosphatase Incorporated in the Film.* Biological & Pharmaceutical Bulletin, 2004, 27(1): p. 89-93.
186. Fujii, T. and Ide, Y., *Preparation of Translucent and Flexible Human Hair Protein Films and Their Properties.* Biological & Pharmaceutical Bulletin, 2004, 27(9): p. 1433-1436.
187. Lee, K.Y. and Ha, W.S., *DSC studies on bound water in silk fibroin/S-carboxymethyl kerateine blend films.* Polymer, 1999, 40(14): p. 4131-4134.
188. Lee, K., *Characterization of silk fibroin/S-carboxymethyl kerateine surfaces: Evaluation of biocompatibility by contact angle measurements.* Fibers and Polymers, 2001, 2(2): p. 71-74.

189. Tanabe, T., et al., *Preparation and characterization of keratin-chitosan composite film.* Biomaterials, 2002, 23(3): p. 817-825.
190. Yamauchi, K., et al., *Enhanced cell adhesion on RGDS-carrying keratin film.* Materials Science and Engineering: C, 2003, 23(4): p. 467-472.
191. Zoccola, M., et al., *Electrospinning of polyamide 6/modified-keratin blends.* E-Polymers, 2007, 27: p. 1433-1436.
192. Tanabe, T., Okitsu, N. and Yamauchi, K., *Fabrication and characterization of chemically crosslinked keratin films.* Materials Science and Engineering: C, 2004, 24(3): p. 441-446.
193. Yang, X., et al., *Wool keratin: A novel building block for layer-by-layer self-assembly.* Journal of Colloid and Interface Science, 2009, 336(2): p. 756-760.
194. Reichl, S., *Films based on human hair keratin as substrates for cell culture and tissue engineering.* Biomaterials, 2009, 30(36): p. 6854-6866.
195. Kurimoto, A., et al., *Keratin sponge: Immobilization of lysozyme.* Journal of Bioscience and Bioengineering, 2003. 96(3): p. 307-309.
196. Tachibana, A., et al., *Modified keratin sponge: Binding of bone morphogenetic protein-2 and osteoblast differentiation.* Journal of Bioscience and Bioengineering, 2006, 102(5): p. 425-429.
197. Peplow, P.V. and Dias, G.J., *A study of the relationship between mass and physical strength of keratin bars in vivo.* Journal of Materials Science: Materials in Medicine, 2004, 15(11): p. 1217-1220.
198. Chen, Y.H., et al., *Preparation and bioactivity of human hair keratin-collagen sponge, a new type of dermal analogue.* Journal of Southern Medical University, 2006, 26(2): p. 131-138.
199. Chen, Y.H., et al., *Biological dressing with human hair keratin-collagen sponge-poly 2-hydroxyethyl methacrylate composite promotes burn wound healing in SD rats.* Journal of Southern Medical University, 2007, 27(11): p. 1621-1626.
200. Thilagar, S., et al., *Effect of keratin-gelatin and bFGF-gelatin composite film as a sandwich layer for full-thickness skin mesh graft in experimental dogs.* Journal of Biomedical Materials Research Part B: Applied Biomaterials, 2009, 88B(1): p. 12-16.
201. Ide, Y. and Fijii, T., *Immunogenicity of hair proteins containing hard keratins.* Journal of Society Fiber Science and Technology Japan, 2004, 60(9).
202. Dias, G.J., et al., *Biocompatibility and osseointegration of reconstituted keratin in an ovine model.* Journal of Biomedical Materials Research Part A, 2010, 92A(2): p. 513-520.
203. Pasquali-Ronchetti, I. and Baccarani-Contri, M., *Elastic fiber during development and aging.* Microscopy Research and Technique, 1997, 38(4): p. 428-435.
204. Martyn, C. and Greenwald, S., *A Hypothesis About A Mechanism For The Programming Of Blood Pressure And Vascular Disease In Early Life.* Clinical and Experimental Pharmacology and Physiology, 2001, 28(11): p. 948-951.
205. Faury, G., *Function-structure relationship of elastic arteries in evolution: from microfibrils to elastin and elastic fibres.* Pathologie-Biologie, 2001 49(4): p. 310-25.

206. Ayad, S., et al., *The extracellular matrix facts book*. 1994, London: G Academic Press.
207. Madsen, K., et al., *Synthesis of proteoglycans, collagen, and elastin by cultures of rabbit auricular chondrocytes--Relation to age of the donor.* Developmental Biology, 1983, 96(1): p. 63-73.
208. Mecham, R.P., et al., *Elastin production by cultured calf pulmonary artery endothelial cells.* Journal of Cellular Physiology, 1983, 116(3): p. 282-288.
209. Long, J.L. and Tranquillo, R.T., *Elastic fiber production in cardiovascular tissue-equivalents.* Matrix Biology, 2003, 22(4): p. 339-350.
210. Narayanan, A.S., et al., *The smooth muscle cell. III. Elastin synthesis in arterial smooth muscle cell culture.* The Journal of Cell Biology, 1976, 68(3): p. 411-419.
211. Fornieri, C., et al., *Lysyl oxidase activity and elastin/glycosaminoglycan interactions in growing chick and rat aortas.* The Journal of Cell Biology, 1987, 105(3): p. 1463-1469.
212. Ross, R. and Bornstein, P., *THE ELASTIC FIBER.* The Journal of Cell Biology, 1969, 40(2): p. 366-381.
213. Hinek, A., et al., *The elastin receptor: a galactoside-binding protein.* Science, 1988, 239(4847): p. 1539-1541.
214. Rosenbloom, J., Abrams, W.R. and Mecham, R., *Extracellular matrix 4: the elastic fiber.* FASEB Journal, 1993, 7(13): p. 1208-1218.
215. Hinek, A. and Rabinovitch, M., *67-kD elastin-binding protein is a protective "companion" of extracellular insoluble elastin and intracellular tropoelastin.* The Journal of Cell Biology, 1994, 126(2): p. 563-74.
216. Debelle, L. and Alix, A.J.P., *The structures of elastins and their function.* Biochimie, 1999, 81(10): p. 981-994.
217. Li, B. and Daggett, V., *Molecular basis for the extensibility of elastin.* Journal of Muscle Research and Cell Motility, 2002, 23(5): p. 561-573.
218. Urry, D.W. and Parker, T.M., *Section: Extracellular matrix proteins; Mechanics of elastin: molecular mechanism of biological elasticity and its relationship to contraction.* Journal of Muscle Research and Cell Motility, 2002, 23(5): p. 543-559.
219. Gosline, J., et al., *Elastic proteins: biological roles and mechanical properties.* Philosophical Transactions of the Royal Society of London. Series B: Biological Sciences, 2002, 357(1418): p. 121-132.
220. Vrhovski, B. and Weiss, A.S., *Biochemistry of tropoelastin.* European Journal of Biochemistry, 1998, 258(1): p. 1-18.
221. Hoeve, C.A.J. and Flory, P.J., *The elastic properties of elastin.* Biopolymers, 1974, 13(4): p. 677-686.
222. Urry, D.W. and Venkatachalam, C.M., *Conformation in Biology*, ed. R. Srinivasan, Sarma, R.H., Ramachandran, G.N. 1982, USA: Adenine Press.
223. Villani, V. and Tamburro, A.M., *Conformational Chaos of an Elastin-Related Peptide in Aqueous Solution.* Annals of the New York Academy of Sciences, 1999, 879(1): p. 284-287.
224. Kakivaya, S.R. and Hoeve, C.A., *The glass point of elastin.* Proceedings of the National Academy of Sciences of the United States of America, 1975, 72(9): p. 3505-3507.
225. Lillie, M.A. and Gosline, J.M., *The effects of hydration on the dynamic mechanical properties of elastin.* Biopolymers, 1990, 29(8-9): p. 1147-1160.

226. Samouillan, V., et al., *Effect of Water on the Molecular Mobility of Elastin.* Biomacromolecules, 2004, 5(3): p. 958-964.
227. Bungenberg de Jong, H.G., *Crystallization-coacervation-flocculation*. Colloid Science, ed. H.R. Kruyt. 1949, New York: Elsevier.
228. Urry, D.W. et al., *Characterization of soluble peptides of elastin by physical techniques*, in *Methods in Enzymology*. 1982, Academic Press. p. 673-716.
229. Vrhovski, B., Jensen, S. and Weiss, A.S., *Coacervation Characteristics of Recombinant Human Tropoelastin.* European Journal of Biochemistry, 1997, 250(1): p. 92-98.
230. van Hest, J.C.M. and Tirrell, D. A., *Protein-based materials, toward a new level of structural control.* Chemical Communications, 2001, 19: p. 1897-1904.
231. Urry, D.W., *On the molecular mechanisms of elastin coacervation and coacervate calcification.* Faraday Discuss Chemical Society, 1976, 61: p. 205-12.
232. Keeley, F.W., Bellingham, C.M. and Woodhouse, K.A., *Elastin as a self organizing biomaterial: use of recombinantly expressed human elastin polypeptides as a model for investigations of structure and self-assembly of elastin.* Philosophical Transactions of the Royal Society of London. Series B: Biological Sciences, 2002, 357(1418): p. 185-189.
233. Urry, D.W., et al., *Temperature of polypeptide inverse temperature transition depends on mean residue hydrophobicity.* Journal of the American Chemical Society, 1991, 113(11): p. 4346-4348.
234. Kaibara, K., et al., *α-Elastin coacervate as a protein liquid membrane: Effect of pH on transmembrane potential responses.* Biopolymers, 1992, 32(9): p. 1173-1180.
235. Bellingham, C.M., et al., *Self-aggregation characteristics of recombinantly expressed human elastin polypeptides.* Biochimica et Biophysica Acta (BBA) - Protein Structure and Molecular Enzymology, 2001, 1550(1): p. 6-19.
236. Urry, D.W., et al., *The synthetic polypentapeptide of elastin coacervates and forms filamentous aggregates.* Biochimica et Biophysica Acta (BBA) - Protein Structure, 1974, 371(2): p. 597-602.
237. Tamburro, A.M., De Stradis, A. and Alessio, L. *Fractal aspects of elastin supramolecular organization*. Journal of biomolecular structure & dynamics, 1995, 12. p. 1161-72.
238. Bressan, G.M., et al., *Relevance of aggregation properties of tropoelastin to the assembly and structure of elastic fibers.* Journal of Ultrastructure and Molecular Structure Research, 1986, 94(3): p. 209-216.
239. Partridge, S.M., et al., *The chemistry of connective tissues. 2. Soluble proteins derived from partial hydrolysis of elastin.* Biochemical Journal, 1955, 61(1): p. 11–21. .
240. Jacob, M.P. and Robert, L., *Isolation, characterization and biochemical properties of elastin*. Elastin and Elastases, ed. L. Robert, Hornebeck, W. 1989, Florida: CRC Press.
241. Duca, L., et al., *Elastin as a matrikine.* Critical reviews in oncology/hematology, 2004, 49(3): p. 235-244.
242. Wright, E., et al., *Thermoplastic Elastomer Hydrogels via Self-Assembly of an Elastin-Mimetic Triblock Polypeptide.* Advanced Functional Materials, 2002, 12(2): p. 149-154.

243. Mithieux, S.M., J.E.J. Rasko, and A.S.A.S. Weiss, *Synthetic elastin hydrogels derived from massive elastic assemblies of self-organized human protein monomers.* Biomaterials, 2004. 25(20): p. 4921-4927.
244. Daamen, W.F., et al., *Elastin as a biomaterial for tissue engineering.* Biomaterials, 2007, 28(30): p. 4378-4398.
245. Herrero-Vanrell, R., et al., *Self-assembled particles of an elastin-like polymer as vehicles for controlled drug release.* Journal of Controlled Release, 2005, 102(1): p. 113-122.
246. Bellingham, C.M., et al., *Recombinant human elastin polypeptides self-assemble into biomaterials with elastin-like properties.* Biopolymers, 2003, 70(4): p. 445-455.
247. Reguera, J., et al., *Nanopore Formation by Self-Assembly of the Model Genetically Engineered Elastin-like Polymer [(VPGVG)2(VPGEG)(VPGVG)2]15.* Journal of the American Chemical Society, 2004, 126(41): p. 13212-13213.
248. Dutoya, S., et al., *Elastin-derived protein coating onto poly(ethylene terephthalate). Technical, microstructural and biological studies.* Biomaterials, 2000, 21(15): p. 1521-1529.
249. Jordan, S.W., et al., *The effect of a recombinant elastin-mimetic coating of an ePTFE prosthesis on acute thrombogenicity in a baboon arteriovenous shunt.* Biomaterials, 2007, 28(6): p. 1191-1197.
250. Nowatzki, P.J. and Tirrell, D.A., *Physical properties of artificial extracellular matrix protein films prepared by isocyanate crosslinking.* Biomaterials, 2004, 25(7-8): p. 1261-1267.
251. Leach, J.B., et al., *Crosslinked [alpha]-elastin biomaterials: towards a processable elastin mimetic scaffold.* Acta Biomaterialia, 2005, 1(2): p. 155-164.
252. Annabi, N., et al., *Synthesis of highly porous crosslinked elastin hydrogels and their interaction with fibroblasts in vitro.* Biomaterials, 2009, 30(27): p. 4550-4557.
253. Annabi, N., et al., *The fabrication of elastin-based hydrogels using high pressure CO_2.* Biomaterials, 2009, 30(1): p. 1-7.
254. Annabi, N., et al., *Cross-linked open-pore elastic hydrogels based on tropoelastin, elastin and high pressure CO_2.* Biomaterials, 31(7): p. 1655-1665.
255. Urry, D.W., *Physical Chemistry of Biological Free Energy Transduction As Demonstrated by Elastic Protein-Based Polymers.* The Journal of Physical Chemistry B, 1997, 101(51): p. 11007-11028.
256. Wood, S.A., et al., *In vitro calcification and in vivo biocompatibility of the cross-linked polypentapeptide of elastin.* Journal of Biomedical Materials Research, 1986, 20(3): p. 315-335.
257. Lee, J., Macosko, C.W. and Urry, D.W., *Elastomeric Polypentapeptides Cross-Linked into Matrixes and Fibers.* Biomacromolecules, 2001, 2(1): p. 170-179.
258. Lee, J., Macosko, C.W. and Urry, D.W., *Mechanical Properties of Cross-Linked Synthetic Elastomeric Polypentapeptides.* Macromolecules, 2001, 34(17): p. 5968-5974.
259. Alkalay, R.N., et al., *Prevention of Postlaminectomy Epidural Fibrosis Using Bioelastic Materials.* Spine, 2003, 28(15): p. 1659-1665.
260. Urry, D.W., *Elastic molecular machines in metabolism and soft-tissue restoration.* Trends in Biotechnology, 1999, 17(6): p. 249-257.

261. Urry, D.W., *Free energy transduction in polypeptides and proteins based on inverse temperature transitions.* Progress in Biophysics and Molecular Biology, 1992, 57(1): p. 23-57.
262. Bidwell Iii, G.L., et al., *Development of elastin-like polypeptide for thermally targeted delivery of doxorubicin.* Biochemical Pharmacology, 2007, 73(5): p. 620-631.
263. Vieth, S., et al., *Microstructural and tensile properties of elastin-based polypeptides crosslinked with Genipin and pyrroloquinoline quinone.* Biopolymers, 2007, 85(3): p. 199-206.
264. Cappello, J., et al., *Genetic engineering of structural protein polymers.* Biotechnology Progress, 1990, 6(3): p. 198-202.
265. Megeed, Z., Cappello, J. and Ghandehari, H., *Genetically engineered silk-elastinlike protein polymers for controlled drug delivery.* Advanced Drug Delivery Reviews, 2002, 54(8): p. 1075-1091.
266. Cappello, J., et al., *In-situ self-assembling protein polymer gel systems for administration, delivery, and release of drugs.* Journal of Controlled Release, 1998, 53(1-3): p. 105-117.
267. Megeed, Z., et al., *In vitro and in vivo evaluation of recombinant silk-elastinlike hydrogels for cancer gene therapy.* Journal of Controlled Release, 2004, 94(2-3): p. 433-445.
268. Haider, M., et al., *Molecular Engineering of Silk-Elastinlike Polymers for Matrix-Mediated Gene Delivery: Biosynthesis and Characterization.* Molecular Pharmaceutics, 2005, 2(2): p. 139-150.
269. Bonzon, N., et al., *New artificial connective matrix made of fibrin monomers, elastin peptides and type I + III collagens: structural study, biocompatibility and use as tympanic membranes in rabbit.* Biomaterials, 1995, 16(11): p. 881-885.
270. San-Galli, F., et al., *Use of a biodegradable elastin--fibrin material, Neuroplast®, as a dural substitute.* Biomaterials, 1996, 17(11): p. 1081-1085.
271. Takahashi, K., et al., *Improvement of the Physical Properties of Pepsin-Solubilized Elastin-Collagen Film by Crosslinking.* Bioscience, Biotechnology, and Biochemistry, 1999, 63(12): p. 2144-2149.
272. Hafemann, B., et al., *Cross-linking by 1-ethyl-3- (3-dimethylaminopropyl)-carbodiimide (EDC) of a collagen/elastin membrane meant to be used as a dermal substitute: effects on physical, biochemical and biological features in vitro.* Journal of Materials Science: Materials in Medicine, 2001, 12(5): p. 437-446.
273. Daamen, W.F., et al., *Preparation and evaluation of molecularly-defined collagen-elastin-glycosaminoglycan scaffolds for tissue engineering.* Biomaterials, 2003, 24(22): p. 4001-4009.
274. Berglund, J.D., Nerem, R.M. and Sambanis, A., *Incorporation of Intact Elastin Scaffolds in Tissue-Engineered Collagen-Based Vascular Grafts.* Tissue Engineering, 2004, 10(9-10): p. 1526-1535.
275. Skopinska-Wisniewska, J., et al., *Surface characterization of collagen/elastin based biomaterials for tissue regeneration.* Applied Surface Science, 2009, 255(19): p. 8286-8292.
276. Daamen, W.F., et al., *Tissue response of defined collagen-elastin scaffolds in young and adult rats with special attention to calcification.* Biomaterials, 2005, 26(1): p. 81-92.

277. Daamen, W.F., et al., *A Biomaterial Composed of Collagen and Solubilized Elastin Enhances Angiogenesis and Elastic Fiber Formation Without Calcification.* Tissue Engineering Part A, 2008, 14(3): p. 349-360.
278. Buttafoco, L., et al., *Electrospinning of collagen and elastin for tissue engineering applications.* Biomaterials, 2006, 27(5): p. 724-734.
279. Li, M., et al., *Electrospun protein fibers as matrices for tissue engineering.* Biomaterials, 2005, 26(30): p. 5999-6008.
280. Li, M., et al., *Co-electrospun poly(lactide-co-glycolide), gelatin, and elastin blends for tissue engineering scaffolds.* Journal of Biomedical Materials Research Part A, 2006, 79A(4): p. 963-973.
281. McClure, M.J., et al., *Cross-linking Electrospun Polydioxanone-Soluble Elastin Blends: Material Characterization.* Journal of Engineered Fibers and Fabrics, 2008, 3(1): p. 1-9.
282. Smith, M.J., et al., *In vitro evaluations of innate and acquired immune responses to electrospun polydioxanone-elastin blends.* Biomaterials, 2009, 30(2): p. 149-159.
283. De Vries, H., et al., *Reduced wound contraction and scar formation in punch biopsy wounds. Native collagen dermal substitutes. A clinical study.* British Journal of Dermatology, 1995, 132(5): p. 690-697.
284. Lamme, E.N., et al., *Extracellular matrix characterization during healing of full-thickness wounds treated with a collagen/elastin dermal substitute shows improved skin regeneration in pigs.* Journal of Histochemistry and Cytochemistry, 1996, 44(11): p. 1311-1322.
285. Lamme, E., et al., *Living skin substitutes: survival and function of fibroblasts seeded in a dermal substitute in experimental wounds.* Journal of Investigative Dermatology, 1998, 111(6): p. 989-95.
286. Hafemann, B., et al., *Use of a collagen/elastin-membrane for the tissue engineering of dermis.* Burns, 1999, 25(5): p. 373-384
287. Cullen, B., et al., *The role of oxidized regenerated cellulose/collagen in chronic wound repair and its potential mechanism of action.* The International Journal of Biochemistry & Cell Biology, 2002, 34(12): p. 1544-1556.
288. Hinek, A., et al., *Proteolytic digest derived from bovine Ligamentum Nuchae stimulates deposition of new elastin-enriched matrix in cultures and transplants of human dermal fibroblasts.* Journal of Dermatological Science, 2005, 39(3): p. 155-166.
289. van Zuijlen, P.P.M., et al., Esther *Long-term results of a clinical trial on dermal substitution. A light microscopy and Fourier analysis based evaluation* Burns, 2002, 28(2): p. 151-160.
290. Klein, B., et al., *Inflammatory response to a porcine membrane composed of fibrous collagen and elastin as dermal substitute.* Journal of Materials Science: Materials in Medicine, 2001, 12(5): p. 419-424.
291. Hashimoto, T., et al., *Development of alginate wound dressings linked with hybrid peptides derived from laminin and elastin.* Biomaterials, 2004, 25(7-8): p. 1407-1414.
292. Haslik, W., et al., *First experiences with the collagen-elastin matrix Matriderm as a dermal substitute in severe burn injuries of the hand.* Burns, 2007, 33(3): p. 364-8.
293. Haslik, W., et al., *Management of full-thickness skin defects in the hand and wrist region: first long-term experiences with the dermal matrix Matriderm®.*

Journal of plastic, reconstructive & aesthetic surgery, 2010, 63(2): p. 360-364.
294. Vasconcelos, A., A.C. Gomes, and A. Cavaco-Paulo, *Novel silk fibroin/elastin sponges crosslinked with genipin for wound dressings. Submitted*
295. Lazarus, G.S., et al., *Definitions and Guidelines for Assessment of Wounds and Evaluation of Healing.* Archives of Dermatology, 1994, 130(4): p. 489-493.
296. Nicholas, J.P., *Classification of Wounds and their Management.* Surgery (Oxford), 2002, 20(5): p. 114-117.
297. Martin, C.R., *WOUND INFECTION: A Failure of Wound Healing Caused by an Imbalance of Bacteria.* The Surgical clinics of North America, 1997, 77(3): p. 637-650.
298. Stadelmann, W.K., Digenis, A.G. and Tobin, G.R., *Physiology and healing dynamics of chronic cutaneous wounds.* The American Journal of Surgery, 1998, 176(2, Supplement 1): p. 26S-38S.
299. Harding, K.G., Morris, H.L. and Patel, G.K., *Healing chronic wounds.* British Medical Journal, 2002, 324(7330): p. 160-163.
300. Eaglstein, W.H. and Falanga, V., *Chronic wounds.* Surgical Clinics of North America, 1997, 77: p. 689 - 700.
301. Moore, K., et al., *Prediction and monitoring the therapeutic response of chronic dermal wounds.* International Wound Journal, 2006, 3(2): p. 89-98.
302. Strodtbeck, F., *Physiology of wound healing.* Newborn and Infant Nursing Reviews, 2001, 1(1): p. 43-52.
303. Enoch, S. and Leaper, D.J., *Basic science of wound healing.* Surgery (Oxford), 2008, 26(2): p. 31-37.
304. Beanes, S.R., et al., *The phases of cutaneous wound healing.* Expert Reviews in Molecular Medicine, 2003, 5: p. 1-22.
305. Gray, D. and White, R.J., *The wound exudate continuum: an aid to wound assessment.* Wounds UK: Applied wound management suppl., 2004, p. 19 - 21.
306. Cutting, K.F. and White, R.J., *Maceration of the skin and wound bed 1: its nature and causes* Journal of Wound Care, 2002, 11(7): p. 275 - 278.
307. Chen, W.Y.J., Rogers, A.A. and Lydon, M.J., *Characterization of Biologic Properties of Wound Fluid Collected During Early Stages of Wound Healing.* Journal of Investigative Dermatology, 1992, 99(5): p. 559-564.
308. Stacey, M.C., et al., *Tissue and urokinase plasminogen activators in the environs of venous and ischaemic leg ulcers.* British Journal of Surgery, 1993, 80(5): p. 596-599.
309. Yager, D.R., et al., *Ability of chronic wound fluids to degrade peptide growth factors is associated with increased levels of elastase activity and diminished levels of proteinase inhibitors.* Wound Repair and Regeneration, 1997, 5(1): p. 23-32.
310. Inngjerdingen, K., et al., *An ethnopharmacological survey of plants used for wound healing in Dogonland, Mali, West Africa.* Journal of Ethnopharmacology, 2004, 92(2-3): p. 233-244.
311. Mensah, A.Y., et al., *In Vitro evaluation of effects of two ghanaian plants relevant to wound healing.* Phytotherapy Research, 2006, 20(11): p. 941-944.

312. Sai K, P. and Babu, M., *Collagen based dressings-a review.* Burns, 2000, 26(1): p. 54-62.
313. Thomas, S., *Wound and wound healing*, in *Wound management and dressings*. 2004, Pharmaceutical Press: London.
314. Queen, D., et al., *A dressing history.* International Wound Journal, 2004, 1(1): p. 59-77.
315. Falabella, A.F., *Debridement and wound bed preparation.* Dermatologic Therapy, 2006, 19(6): p. 317-325.
316. Nigam, Y., et al., *Maggot Therapy: The Science and Implication for CAM Part I-History and Bacterial Resistance.* eCAM, 2006, 3(2): p. 223-227.
317. Vachon, D.J. and Yager, D.R., *Novel sulfonated hydrogel composite with the ability to inhibit proteases and bacterial growth.* Journal of Biomedical Materials Research Part A, 2006, 76A(1): p. 35-43.
318. Edwards, J.V., et al., *Inhibition of elastase by a synthetic cotton-bound serine protease inhibitor: in vitro kinetics and inhibitor release.* Wound Repair and Regeneration, 1999, 7(2): p. 106-118.
319. Edwards, J.V., Howley, P. and Cohen, I.K., *In vitro inhibition of human neutrophil elastase by oleic acid albumin formulations from derivatized cotton wound dressings.* International Journal of Pharmaceutics, 2004, 284(1-2): p. 1-12.
320. Edwards, J.V., et al., *Human neutrophil elastase inhibition with a novel cotton-alginate wound dressing formulation.* Journal of Biomedical Materials Research Part A, 2003, 66A(3): p. 433-440.
321. Edwards, J.V. and Howley, P.S., *Human neutrophil elastase and collagenase sequestration with phosphorylated cotton wound dressings.* Journal of Biomedical Materials Research Part A, 2007, 83A(2): p. 446-454.
322. Edwards, J.V., et al., *Modified cotton gauze dressings that selectively absorb neutrophil elastase activity in solution.* Wound Repair and Regeneration, 2001, 9(1): p. 50-58.
323. Schönfelder, U., et al., *Influence of selected wound dressings on PMN elastase in chronic wound fluid and their antioxidative potential in vitro.* Biomaterials, 2005, 26(33): p. 6664-6673.
324. Cullen, B., et al., *Mechanism of action of PROMOGRAN, a protease modulating matrix, for the treatment of diabetic foot ulcers.* Wound Repair and Regeneration, 2002, 10(1): p. 16-25.
325. Edwards, J.V., et al., *Synthesis and activity of NH2- and COOH-terminal elastase recognition sequences on cotton.* The Journal of Peptide Research, 1999, 54(6): p. 536-543.
326. Vasconcelos, A., et al., *Protein Matrices for Improved Wound Healing: Elastase Inhibition by a Synthetic Peptide Model.* Biomacromolecules, 2010, 11: p. 2213-2220.
327. Rao, M.B., et al., *Molecular and Biotechnological Aspects of Microbial Proteases.* Microbiology and Molecular Biology Reviews, 1998, 62(3): p. 597-635.
328. Schechter, I. and Berger, A., *On the size of the active site in proteases. I. Papain.* Biochemical and Biophysical Research Communications, 1967, 27(2): p. 157-162.
329. Bode, W., et al., *X-ray crystal structure of the complex of human leukocyte elastase (PMN elastase) and the third domain of the turkey ovomucoid inhibitor.* EMBO Journal, 1986, 5: p. 2453-2458.

330. An-Zhi, W., Mayr, I. and Bode, W., *The refined 2.3 Å crystal structure of human leukocyte elastase in a complex with a valine chloromethyl ketone inhibitor.* FEBS Letters, 1988, 234(2): p. 367-373.
331. Navia, M.A., et al., *Structure of human neutrophil elastase in complex with a peptide chloromethyl ketone inhibitor at 1.84-A resolution.* Proceedings of the National Academy of Sciences of the United States of America, 1989, 86(1): p. 7-11.
332. Cregge, R.J., et al., *Inhibition of Human Neutrophil Elastase. 4. Design, Synthesis, X-ray Crystallographic Analysis, and Structure Activity Relationships for a Series of P2-Modified, Orally Active Peptidyl Pentafluoroethyl Ketones.* Journal of Medicinal Chemistry, 1998, 41(14): p. 2461-2480.
333. Macdonald, S.J.F., et al., *Discovery of Further Pyrrolidine trans-Lactams as Inhibitors of Human Neutrophil Elastase (HNE) with Potential as Development Candidates and the Crystal Structure of HNE Complexed with an Inhibitor (GW475151).* Journal of Medicinal Chemistry, 2002, 45(18): p. 3878-3890.
334. Zimmerman, M. and Ashe, B.M., *Substrate specificity of the elastase and the chymotrypsin-like enzyme of the human granulocyte.* Biochimica et Biophysica Acta, 1977, 480: p. 241-245.
335. McRae, B., et al., *Studies on reactivity of human leukocyte elastase, cathepsin G, and porcine pancreatic elastase toward peptides including sequences related to the reactive site of .alpha.1-protease inhibitor (.alpha.1-antitrypsin).* Biochemistry, 1980, 19(17): p. 3973-3978.
336. Lestienne, P. and Bieth, J.G., *Activation of human leukocyte elastase activity by excess substrate, hydrophobic solvents, and ionic strength.* Journal of Biological Chemistry, 1980, 255(19): p. 9289-9294.
337. Wagner, J.G. and Roth, R.A., *Neutrophil migration during endotoxemia.* Journal of Leukocyte Biology, 1999, 66(1): p. 10-24.
338. Sandholm, L., *Proteases and their inhibitors in chronic inflammatory periodontal disease.* Journal of Clinical Periodontology, 1986, 13(1): p. 19-26.
339. Anderson, B.O., Brown, J.M. and Harken, A.H., *Mechanisms of neutrophil-mediated tissue injury.* Journal of Surgical Research, 1991, 51(2): p. 170-179.
340. Dallegri, F. and Ottonello, L., *Tissue injury in neutrophilic inflammation.* Inflammation Research, 1997, 46(10): p. 382-391.
341. Harris, I.R., et al., *Cytokine and protease levels in healing and non-healing chronic venous leg ulcers.* Experimental Dermatology, 1995, 4(6): p. 342-349.
342. Wlaschek, M., et al., *Protease inhibitors protect growth factor activity in chronic wounds.* British Journal of Dermatology, 1997, 137(4): p. 646-663.
343. Porteu, F., et al., *Human neutrophil elastase releases a ligand-binding fragment from the 75-kDa tumor necrosis factor (TNF) receptor. Comparison with the proteolytic activity responsible for shedding of TNF receptors from stimulated neutrophils.* Journal of Biological Chemistry, 1991, 266(28): p. 18846-18853.
344. Doring, G., et al., *Cleavage of lymphocyte surface antigens CD2, CD4, and CD8 by polymorphonuclear leukocyte elastase and cathepsin G in patients with cystic fibrosis.* Journal of Immunology, 1995, 154(9): p. 4842-4850.

345. Hamacher, J., et al., *Soluble complement receptor type 1 (CD35) in bronchoalveolar lavage of inflammatory lung diseases.* European Respiratory Journal, 1998, 11(1): p. 112-119.
346. Padrines, M., et al., *Interleukin-8 processing by neutrophil elastase, cathepsin G and proteinase-3.* FEBS Letters, 1994, 352(2): p. 231-235.
347. Owen, C.A. and Campbell, E.J., *The cell biology of leukocyte-mediated proteolysis.* J Leukocyte Biology, 1999, 65(2): p. 137-150.
348. Potempa, J., Korzus, E. and Travis, J., *The serpin superfamily of proteinase inhibitors: structure, function, and regulation.* Journal of Biological Chemistry, 1994, 269(23): p. 15957-15960.
349. Silverman, G.A., et al., *The Serpins Are an Expanding Superfamily of Structurally Similar but Functionally Diverse Proteins.* Journal of Biological Chemistry, 2001, 276(36): p. 33293-33296.
350. Edwards, P.D. and Bernstein, P.R., *Synthetic Inhibitors of Elastase.* Medicinal Research Reviews, 1994, 14(2): p. 127-194.
351. Norioka, S. and Ikenaka, T., *Amino Acid Sequences of Trypsin-Chymotrypsin Inhibitors (A-I, A-II, B-I, and B-II) from Peanut (Arachis hypogaea)1: A Discussion on the Molecular Evolution of Legume Bowman-Birk Type Inhibitors.* Journal of Biochemistry, 1983, 94(2): p. 589-598.
352. Bowman, D.E., *Differentiation of soybean antitryptic factors.* Proceedings of the Society for Experimental Biology and Medicine, 1946, 63: p. 547-550.
353. Birk, Y., Gertler, A. and Khalef, S., *A Pure Trypsin Inhibitor from. Soya Beans.* Biochemical Journal, 1963, 87: p. 281-284.
354. Chen, P., et al., *Reactive sites of an anticarcinogenic Bowman-Birk proteinase inhibitor are similar to other trypsin inhibitors.* Journal of Biological Chemistry, 1992, 267(3): p. 1990-1994.
355. Werner, M.H. and Wemmer, D.E., *Three-dimensional structure of soybean trypsin/chymotrypsin Bowman-Birk inhibitor in solution.* Biochemistry, 1992, 31(4): p. 999-1010.
356. Lin, G., et al., *The 0.25-nm X-ray structure of the Bowman-Birk-type inhibitor from mung bean in ternary complex with porcine trypsin.* European Journal of Biochemistry, 1993, 212(2): p. 549-555.
357. Voss, R.-H., et al., *Crystal Structure of the Bifunctional Soybean Bowman-Birk Inhibitor at 0.28-nm Resolution.* European Journal of Biochemistry, 1996, 242(1): p. 122-131.
358. Birk, Y., *The Bowman-Birk inhibitor. Trypsin-and chymotrypsin-inhibitor from soybeans.* International Journal of Peptide and Protein Research, 1985, 25(2): p. 113-131.
359. McBride, J.D. and Leatherbarrow, R.J., *Synthetic Peptide Mimics of the Bowman-Birk Inhibitor Protein.* Current Medicinal Chemistry, 2001, 8(8): p. 909-917.
360. Jensen, B., et al., *Proteolytic cleavage of soybean Bowman-Birk inhibitor monitored by means of high-performance capillary electrophoresis. Implications for the mechanism of proteinase inhibitors.* Journal of Biochemical and Biophysical Methods, 1996, 33(3): p. 171-185.
361. Larionova, N.I., Gladysheva, I.P., and Gladyshev, D.P., *Human leukocyte elastase inhibition by Bowman-Birk soybean inhibitor: Discrimination of the inhibition mechanisms.* FEBS Letters, 1997, 404(2-3): p. 245-248.
362. Mcbride, J.D., Freeman, H.N.M. and Leatherbarrow, R.J., *Selection of human elastase inhibitors from a conformationally constrained*

combinatorial peptide library. European Journal of Biochemistry, 1999, 226: p. 403 - 412.
363. McBride, J.D., et al., *Peptide mimics of the Bowman–Birk inhibitor reactive site loop.* Peptide Science, 2002, 66(2): p. 79-92.
364. Laskowski, M. and Kato, I., *Protein Inhibitors of Proteinases.* Annual Review of Biochemistry, 1980, 49(1): p. 593-626.
365. Bode, W. and Huber, R., *Natural protein proteinase inhibitors and their interaction with proteinases.* European Journal of Biochemistry, 1992, 204(2): p. 433-451.
366. Lu, W., et al., *Binding of amino acid side-chains to S1 cavities of serine proteinases.* Journal of Molecular Biology, 1997, 266(2): p. 441-461.
367. Qasim, M.A., et al., *Interscaffolding Additivity. Association of P1 Variants of Eglin c and of Turkey Ovomucoid Third Domain with Serine Proteinases.* Biochemistry, 1997, 36(7): p. 1598-1607.
368. Nishino, N., et al., *Studies on the Synthesis of Proteinase Inhibitors.* Journal of Biochemistry, 1977, 82(3): p. 901-909.
369. Terada, S., et al., *Inhibitory properties of nonapeptide loop structures related to reactive sites of soybean Bowman-Birk inhibitor.* FEBS Letters, 1978, 90(1): p. 89-92.
370. Domingo, G.J., et al., *Synthesis of a mixture of cyclic peptides based on the Bowman-Birk reactive site loop to screen for serine protease inhibitors.* International Journal of Peptide and Protein Research, 1995, 46(1): p. 79-87.
371. McBride, J.D., et al., *The role of threonine in the P2 position of bowman-birk proteinase inhibitors: studies on P2 variation in cyclic peptides encompassing the reactive site loop.* Journal of Molecular Biology, 1998, 282(2): p. 447-457.
372. Nishino, N. and Izumiya, N., *Anti-tryptic activity of a synthetic bicyclic fragment of soybean bowman-birk inhibitor.* Biochimica et Biophysica Acta (BBA)-Protein Structure and Molecular Enzymology, 1982, 708(2): p. 233-235.
373. Gariani, T. and Leatherbarrow, R.J., *Stability of protease inhibitors based on the Bowman-Birk reactive site loop to hydrolysis by proteases.* Journal of Peptide Research, 1997, 49(6): p. 467-475.
374. Gariani, T., McBride, J.D. and Leatherbarrow, R.J., *The role of the P2' position of Bowman-Birk proteinase inhibitor in the inhibition of trypsin: Studies on P2' variation in cyclic peptides encompassing the reactive site loop.* Biochimica et Biophysica Acta (BBA)-Protein Structure and Molecular Enzymology, 1999, 1431(1): p. 232-237.
375. Fujikawa, S., Nakamura, S. and Koga, K., *Genipin, a New Type of Protein Crosslinking Reagent from Gardenia Fruits.* Agricultural and Biological Chemistry, 1988, 52(3): p. 869-870.
376. Avila, M.Y. and Navia, J.L., *Effect of genipin collagen crosslinking on porcine corneas.* Journal of Cataract & Refractive Surgery, 2010, 36(4): p. 659-664.
377. Bigi, A., et al., *Stabilization of gelatin films by crosslinking with genipin.* Biomaterials, 2002, 23(24): p. 4827-4832.
378. Muzzarelli, R.A.A., *Genipin-crosslinked chitosan hydrogels as biomedical and pharmaceutical aids.* Carbohydrate Polymers, 2009, 77(1): p. 1-9.

379. Chang, Y., et al., *Reconstruction of the right ventricular outflow tract with a bovine jugular vein graft fixed with a naturally occurring crosslinking agent (genipin) in a canine model.* Journal of Thoracic and Cardiovascular Surgery, 2001, 122(6): p. 1208-1218.
380. Butler, M.F., Ng, Y.F. and Pudney, P.D.A., *Mechanism and kinetics of the crosslinking reaction between biopolymers containing primary amine groups and genipin.* Journal of Polymer Science Part A: Polymer Chemistry, 2003, 41(24): p. 3941-3953.
381. Sung, H.W., et al., *Feasibility study of a natural crosslinking reagent for biological tissue fixation.* Journal of Biomedical Materials Research, 1998, 42(4): p. 560-567.
382. Liang, H.C., et al., *Crosslinking structures of gelatin hydrogels crosslinked with genipin or a water-soluble carbodiimide.* Journal of Applied Polymer Science, 2004, 91(6): p. 4017-4026.
383. Friedman, M., *Applications of the Ninhydrin Reaction for Analysis of Amino Acids, Peptides, and Proteins to Agricultural and Biomedical Sciences.* Journal of Agricultural and Food Chemistry, 2004, 52(3): p. 385-406.
384. Yuan, Y., et al., *The effect of cross-linking of chitosan microspheres with genipin on protein release.* Carbohydrate Polymers, 2007, 68(3): p. 561-567.
385. Laemmli, U.K., *Cleavage of structural proteins during assembly of head of bacteriofage-T4.* Nature, 1970, 227: p. 680–685.
386. Ritger, P.L. and Peppas, N.A., *A simple equation for description of solute release II. Fickian and anomalous release from swellable devices.* Journal of Controlled Release, 1987, 5(1): p. 37-42.
387. Tanaka, H., et al., *A sensitive and specific assay for granulocyte elastase in inflammatory tissue fluid using L-pyroglutamyl-L-prolyl-L-valine-p-nitroanilide.* Clinica Chimica Acta, 1990, 187(2): p. 173-180.
388. Cotter, T.G. and Robinson, G.B., *Purification and characterization of an "elastase-like" enzyme from rabbit polymorphonuclear leucocytes.* Biochimica et Biophysica Acta (BBA)-Enzymology, 1980, 615(2): p. 414-425.
389. Yung-Chi, C. and Prusoff, W.H., *Relationship between the inhibition constant (KI) and the concentration of inhibitor which causes 50 per cent inhibition (I50) of an enzymatic reaction.* Biochemical Pharmacology, 1973, 22(23): p. 3099-3108.
390. Dowling, L.M., Crewther, W.G. and Parry, D.A., *Secondary structure of component 8c-1 of alpha-keratin. An analysis of the amino acid sequence.* Biochemical Journal, 1986, 236(3): p. 705-712.
391. Alemdar, A., Iridag, Y. and Kazanci, M., *Flow behavior of regenerated wool-keratin proteins in different mediums.* International Journal of Biological Macromolecules, 2005, 35(3-4): p. 151-153.
392. Lotz, B. and Colonna Cesari, F., *The chemical structure and the crystalline structures of Bombyx mori silk fibroin.* Biochimie, 1979, 61(2): p. 205-214.
393. Tamada, Y., et al., *Ca-adsorption and apatite deposition on silk fabrics modified with phosphate polymer chains.* Journal Biomaterial Science: Polymer Edition, 1999, 10: p. 787–793.
394. Altman, G.H., et al., *Silk matrix for tissue engineered anterior cruciate ligaments.* Biomaterials, 2002, 23(20): p. 4131-4141.

395. Furuzono, T., et al., *Chemical modification of silk fibroin with 2-methacryloyloxyethyl phosphorylcholine. II. Graft-polymerization onto fabric through 2-methacryloyloxyethyl isocyanate and interaction between fabric and platelets.* Biomaterials, 2000, 21(4): p. 327-333.
396. Minoura, N., et al., *Attachment and Growth of Fibroblast Cells on Silk Fibroin.* Biochemical and Biophysical Research Communications, 1995, 208(2): p. 511-516.
397. Inouye, K., et al., *Use of Bombyx mori silk fibroin as a substratum for cultivation of animal cells.* Journal of Biochemical and Biophysical Methods, 1998, 37(3): p. 159-164.
398. Amiya, T., et al., *Conformational studies of the [alpha]-helical proteins from wool keratin by c.d.* International Journal of Biological Macromolecules, 1982, 4(3): p. 165-172.
399. Yamada, H., et al., *Preparation of undegraded native molecular fibroin solution from silkworm cocoons.* Materials Science and Engineering: C, 2001, 14(1-2): p. 41-46.
400. Bhat, N.V. and Ahirrao, S.M., *Investigation of the structure of silk film regenerated with lithium thiocyanate solution.* Journal of Polymer Science: Polymer Chemistry Edition, 1983, 21(5): p. 1273-1280.
401. Tsukada, M., et al., *Structural changes of silk fibroin membranes induced by immersion in methanol aqueous solutions.* Journal of Polymer Science Part B: Polymer Physics, 1994, 32(5): p. 961-968.
402. Wojciechowska, E., Wlochowicz, A. and Weselucha-Birczynska, A., *Application of Fourier-transform infrared and Raman spectroscopy to study degradation of the wool fiber keratin.* Journal of Molecular Structure, 1999, 511-512: p. 307-318.
403. Ha, S.-W., Tonelli, A.E. and Hudson, S.M., *Structural Studies of Bombyx mori Silk Fibroin during Regeneration from Solutions and Wet Fiber Spinning.* Biomacromolecules, 2005, 6(3): p. 1722-1731.
404. Berli, C.L.A., Deiber, J.A. and Anon, M.C., *Heat-Induced Phenomena in Soy Protein Suspensions. Rheometric Data and Theoretical Interpretation.* Journal of Agricultural and Food Chemistry, 1999, 47(3): p. 893-900.
405. Pielesz, A., et al., *Assessing secondary structure of a dyed wool fibre by means of FTIR and FTR spectroscopies.* Journal of Molecular Structure, 2003, 651-653: p. 405-418.
406. Lyman, D.J., Murray-Wijelath, J. and Feughelman, M., *Effect of Temperature on the Conformation of Extended α-Keratin* Applied Spectroscopy, 2001, 55(5): p. 552-554.
407. Barone, J.R. and Schmidt, W.F., *Effect of formic acid exposure on keratin fiber derived from poultry feather biomass.* Bioresource Technology, 2006, 97(2): p. 233-242.
408. Aluigi, A., et al., *Study on the structure and properties of wool keratin regenerated from formic acid.* International Journal of Biological Macromolecules, 2007, 41(3): p. 266-273.
409. Dong, A., Huang, P. and Caughey, W.S., *Protein secondary structures in water from second-derivative amide I infrared spectra.* Biochemistry, 1990, 29(13): p. 3303-3308.
410. Goormaghtigh, E., Cabiaux, V. and Ruysschaert, J.-M., *Secondary structure and dosage of soluble and membrane proteins by attenuated total*

reflection Fourier-transform infrared spectroscopy on hydrated films. European Journal of Biochemistry, 1990, 193(2): p. 409-420.
411. Jung, C., *Insight into protein structure and protein–ligand recognition by Fourier transform infrared spectroscopy.* Journal of Molecular Recognition, 2000, 13(6): p. 325-351.
412. Taddei, P. and Monti, P., *Vibrational infrared conformational studies of model peptides representing the semicrystalline domains of Bombyx mori silk fibroin.* Biopolymers, 2005, 78(5): p. 249-258.
413. Tsukada, M., *Structural changes induced in tussah silk (Antheraea pernyi) fibroin films by immersion in methanol.* Journal of Polymer Science Part B: Polymer Physics, 1986, 24(6): p. 1227-1232.
414. Cutting K, W.R., *Maceration of the skin and wound bed 1: Its nature and causes.* Journal of Wound care, 2002, 11: p. 275 - 278.
415. Wolfram, B. and Robert, H., *Natural protein proteinase inhibitors and their interaction with proteinases.* European Journal of Biochemistry, 1992, 204(2): p. 433-451.
416. Laskowski, M. and Qasim, M.A., *What can the structures of enzyme-inhibitor complexes tell us about the structures of enzyme substrate complexes?* Biochimica et Biophysica Acta (BBA)-Protein Structure and Molecular Enzymology, 2000, 1477(1-2): p. 324-337.
417. Yamauchi, K., Maniwa, M. and Mori, T., *Cultivation of fibroblast cells on keratin-coated substrata.* Journal of Biomaterials Science, Polymer Edition, 1998, 9: p. 259-270.
418. Shudong, W., et al., *Electrospun polylactide/silk fibroin-gelatin composite tubular scaffolds for small-diameter tissue engineering blood vessels.* Journal of Applied Polymer Science, 2009, 113(4): p. 2675-2682.
419. Motta, A., et al., *Fibroin hydrogels for biomedical applications: preparation, characterization and in vitro cell culture studies.* Journal of Biomaterials Science, Polymer Edition, 2004, 15(7): p. 851-864.
420. Huang, Y., Yu, H. and Xiao, C., *pH-sensitive cationic guar gum/poly (acrylic acid) polyelectrolyte hydrogels: Swelling and in vitro drug release.* Carbohydrate Polymers, 2007, 69(4): p. 774-783.
421. Lazarous, GS, et al., *Definitions and guidelines for assessment of wounds and evaluation of healing.* Archives of Dermatology, 1994, 130: p. 489-493.
422. Park, J.E. and Barbul, A., *Understanding the role of imune regulation in wound healing.* The American Journal of Surgery, 2004, 187: p. S11-S16.
423. McHale, M.K., Setton, L.A. and Chilkoti, A., *Synthesis and in Vitro Evaluation of Enzymatically Cross-Linked Elastin-Like Polypeptide Gels for Cartilaginous Tissue Repair.* Tissue Engineering, 2005, 11(11-12): p. 1768-1779.
424. Nagapudi, K., et al., *Protein-Based Thermoplastic Elastomers.* Macromolecules, 2004, 38(2): p. 345-354.
425. Nagapudi, K., et al., *Viscoelastic and mechanical behavior of recombinant protein elastomers.* Biomaterials, 2005,26(23): p. 4695-4706.
426. Mithieux, S.M., et al., *In situ polymerization of tropoelastin in the absence of chemical cross-linking.* Biomaterials, 2009, 30(4): p. 431-435.
427. Sung, H.W., et al., *Evaluation of gelatin hydrogel crosslinked with various crosslinking agents as bioadhesives: In vitro study.* Journal of Biomedical Materials Research, 1999, 46(4): p. 520-530.

428. Chang, Y., et al., *In vivo evaluation of cellular and acellular bovine pericardia fixed with a naturally occurring crosslinking agent (genipin).* Biomaterials, 2002, 23(12): p. 2447-2457.
429. Sung, H.W., et al., *Stability of a biological tissue fixed with a naturally occurring crosslinking agent (genipin).* Journal of Biomedical Materials Research, 2001, 55(4): p. 538-546.
430. Chen, H., et al., *Reaction of chitosan with genipin and its fluorogenic attributes for potential microcapsule membrane characterization.* Journal of Biomedical Materials Research Part A, 2005, 75A(4): p. 917-927.
431. GraphPad Software, I. 2010: USA.
432. Mi, F.L., Sung, H.W. and Shyu, S.S., *Synthesis and characterization of a novel chitosan-based network prepared using naturally occurring crosslinker.* Journal of Polymer Science Part A: Polymer Chemistry, 2000, 38(15): p. 2804-2814.
433. Sung, H.W., et al., *Fixation of biological tissues with a naturally occurring crosslinking agent: Fixation rate and effects of pH, temperature, and initial fixative concentration.* Journal of Biomedical Materials Research, 2000, 52(1): p. 77-87.
434. Hu, X., et al., *Microphase Separation Controlled β-Sheet Crystallization Kinetics in Fibrous Proteins.* Macromolecules, 2009, 42(6): p. 2079-2087.
435. Wise, S.G., et al., *Engineered Tropoelastin and Elastin-Based Biomaterials*, in *Advances in Protein Chemistry and Structural Biology*. 2009, Academic Press. p. 1-24.
436. Wise, S.G. and Weiss, A.S., *Tropoelastin.* The International Journal of Biochemistry & Cell Biology, 2009, 41(3): p. 494-497.
437. Chittur, K.K., *FTIR/ATR for protein adsorption to biomaterial surfaces.* Biomaterials, 1998, 19(4-5): p. 357-369.
438. Wilson, D., Valluzzi, R. and Kaplan, D.L., *Conformational Transitions in Model Silk Peptides.* Biophysical Journal, 2000, 78(5): p. 2690-2701.
439. Debelle, L., et al., *The secondary structure and architecture of human elastin.* European Journal of Biochemistry, 1998, 258(2): p. 533-539.
440. Rokhade, A.P., Patil, S.A. and Aminabhavi, T.M., *Synthesis and characterization of semi-interpenetrating polymer network microspheres of acrylamide grafted dextran and chitosan for controlled release of acyclovir.* Carbohydrate Polymers, 2007, 67(4): p. 605-613.
441. Bajpai, A.K. and Giri, A., *Water sorption behavior of highly swelling (carboxy methylcellulose-g-polyacrylamide) hydrogels and release of potassium nitrate as agrochemical.* Carbohydrate Polymers, 2003, 53(3): p. 271-279.
442. Havemann, K. and Gramse, M., *Physiology and pathology of neutral proteinases of human granurocytes.* Advances in Experimental Medicine and Biology, 1984, 164: p. 1-20.
443. Owen, C.A., et al., *Cell surface-bound elastase and cathepsin G on human neutrophils: a novel, non-oxidative mechanism by which neutrophils focus and preserve catalytic activity of serine proteinases.* The Journal of Cell Biology, 1995, 131(3): p. 775-789.
444. Siedle, B., et al., *The effect of sesquiterpene lactones on the release of human neutrophil elastase.* Biochemical Pharmacology, 2003, 65(5): p. 897-903.

445. Lamme, E.N., et al., *Living Skin Substitutes: Survival and Function of Fibroblasts Seeded in a Dermal Substitute in Experimental Wounds.* Journal of Investigative Dermatology, 1998, 111(6): p. 989-995.
446. Ferrero, C., Massuelle, D. and Doelker, E., *Towards elucidation of the drug release mechanism from compressed hydrophilic matrices made of cellulose ethers. II. Evaluation of a possible swelling-controlled drug release mechanism using dimensionless analysis.* Journal of Controlled Release 2010, 141(2): p. 223-233.
447. Korsmeyer, R.W. and Peppas, N.A., *Effect of the morphology of hydrophilic polymeric matrices on the diffusion and release of water soluble drugs.* Journal of Membrane Science, 1981, 9(3): p. 211-227.
448. Shinguh, Y., et al., *Biochemical and pharmacological characterization of FK706, a novel elastase inhibitor.* European Journal of Pharmacology, 1997, 337(1): p. 63-71.
449. Grinnell, F. and Zhu, M., *Identification of Neutrophil Elastase as the Proteinase in Burn Wound Fluid Responsible for Degradation of Fibronectin.* Journal of Investigative Dermatology, 1994, 103(2): p. 155-161.
450. Lowry, O.H., et al., *Protein measurement with the folin phenol reagent.* The Journal of Biological Chemistry, 1951, 193: p. 265-75.
451. Leatherbarrow, R.J., *Using linear and non-linear regression to fit biochemical data.* Trends in Biochemical Sciences, 1990, 15(12): p. 455-458.
452. Naughton, M.A. and Sanger, F., *Purification and specificity of pancreatic elastase.* Biochemical Journal, 1961, 78: p. 156-163.
453. Harper, J.W., et al., *Active site mapping of the serine proteases human leukocyte elastase, cathepsin G, porcine pancreatic elastase, rat mast cell proteases I and II, bovine chymotrypsin A. alpha., and Staphylococcus aureus protease V-8 using tripeptide thiobenzyl ester substrates.* Biochemistry, 1984, 23(13): p. 2995-3002.
454. Stein, R.L., et al., *Neutrophil Elastase*, in *Annual Reports in Medicinal Chemistry*. 1985, Academic Press. p. 237-246.
455. Brauer, A.B.E., et al., *The Bowman-Birk inhibitor reactive site loop sequence represents an independent structural β-hairpin motif.* Journal of Molecular Biology, 2001, 306(4): p. 799-807.
456. Arai, T., et al., *Absorption of metal cations by modified B. mori silk and preparation of fabrics with antimicrobial activity.* Journal of Applied Polymer Science, 2001, 80(2): p. 297-303.
457. Trott, O. and Olson, A.J., *AutoDock Vina: Improving the speed and accuracy of docking with a new scoring function, efficient optimization, and multithreading.* Journal of Computational Chemistry, 2010, 31(2): p. 455-461.
458. Odani, S. and Ikenaka, T., *Scission of Soybean Bowman-Birk Proteinase Inhibitor into Two Small Fragments Having Either Trypsin or Chymotrypsin Inhibitory Activity.* Journal of Biochemistry, 1973, 74(4): p. 857-860.